



Insight into a rift volcanism with the petrogenesis of ultramafic enclaves and the host basalts: Kula Volcanic Field, Western Anatolia, Turkey

Erdal Şen, Erkan Aydar, Pınar Şen, Alain Gourgaud

► To cite this version:

Erdal Şen, Erkan Aydar, Pınar Şen, Alain Gourgaud. Insight into a rift volcanism with the petrogenesis of ultramafic enclaves and the host basalts: Kula Volcanic Field, Western Anatolia, Turkey. *Italian Journal of Geosciences*, 2023, 142 (2), pp.291-315. 10.3301/IJG.2023.16 . hal-04148854

HAL Id: hal-04148854

<https://uca.hal.science/hal-04148854v1>

Submitted on 13 Nov 2023

HAL is a multi-disciplinary open access archive for the deposit and dissemination of scientific research documents, whether they are published or not. The documents may come from teaching and research institutions in France or abroad, or from public or private research centers.

L'archive ouverte pluridisciplinaire **HAL**, est destinée au dépôt et à la diffusion de documents scientifiques de niveau recherche, publiés ou non, émanant des établissements d'enseignement et de recherche français ou étrangers, des laboratoires publics ou privés.

Insight into a rift volcanism with the petrogenesis of ultramafic enclaves and the host basalts: Kula Volcanic Field, Western Anatolia, Turkey

Journal:	<i>Italian Journal of Geosciences</i>
Manuscript ID	IJG-2022-1058.R2
Manuscript Type:	Original Article
Date Submitted by the Author:	n/a
Complete List of Authors:	Şen, Erdal; Hacettepe University, Geological Engineering Aydar, Erkan; Hacettepe University, Geological Engineering Şen, Pınar; General Directorate of Mineral Research and Exploration Gourgaud, Alain; Université Blaise-Pascal
Keywords:	Alkaline basalt, ultramafic enclaves, fractional crystallisation, partial melting, uplift

SCHOLARONE™
Manuscripts

Insight into a rift volcanism with the petrogenesis of ultramafic enclaves and the host basalts: Kula Volcanic Field, Western Anatolia, Turkey

Erdal Şen^{1*}, Erkan Aydar¹, Pınar Şen² & Alain Gourgaud³

¹Hacettepe University, Dept. of Geological Engineering, Beytepe, Ankara, Turkey, 06800

²General Directorate of Mineral Research and Exploration, Mineral Research and Exploration Department, 06800, Çankaya/Ankara, Turkey

³Université Blaise-Pascal, UMR-CNRS 6524, Campus Universitaire des Cézeaux, 6 Avenue Blaise Pascal, TSA 60026 - CS 60026- 63178, Aubiere Cedex, France

 EŞ, 0000-0002-9172-9926; EA, 0000-0002-6550-0714; PŞ, 0000-0002-2457-7280

*Corresponding author e-mail: erdals@hacettepe.edu.tr

ABSTRACT

The Quaternary Kula Volcanic Field (KVF), located on an E-W trending Plio-Quaternary horst, consists of at least 80 scoria cones, associated fissural lava flows and maars. Volcanic activity is divided into three main stages as BI (ca. 2-0.9 Ma), BII (ca. 300-50 ka) and BIII (ca. 10-0.7 ka). The volcanic products of BII and BIII contain ultramafic enclaves. They are generally spherical or elliptical varying in size from <1 to <48 cm and some samples bear vesicles and glass. Based on modal mineralogy, the dominant enclave types are hornblendite, Cpx-hornblendite, while Phl-clinopyroxenite, wehrlite, plagioclase-bearing Cpx-hornblendite and Hbl-gabbro are subordinate. They occasionally represent adcumulate and/or mesocumulate textures. The alkaline host rocks are basanite, phonotephrite, trachybasalt, picrobasalt, and foidite in composition.

LILE (Rb, Ba, Sr, and Pb) and HFSE (Nb, Ta) concentrations of host rocks indicate an Enriched Within Plate Mantle source. Additionally, they have high Nb/La (>1.3), Nb/Y (>1.7), and Nb/U (>31) ratios, reflecting that crustal contamination is insignificant. Petrogenetic modelling shows that Kula enclaves and host rocks are probably originating from 3-5% partial melting of garnet and spinel-peridotite mantle source mixtures. Rb/Sr (0.03-0.10) and slightly high Ba/Rb (9.5-23) ratios for host rocks demonstrate the presence of amphibole and phlogopite in their source, while low Rb/Sr (0.01-0.09) and high Ba/Rb (18-115) reveal

1
2
3 33 that amphibole is present in the source. Estimated T/P conditions of early crystallizations
4
5 34 are between 19.5–9.5 kbar, 63–31 km, and 1260–1130 °C for host rocks and 18.3–11.1
6
7 35 kbar, 59–36 km, and 1324–1208 °C for the enclaves, which suggests that the crystallization
8
9 36 might have taken place in the lithospheric mantle.
10
11

12 37 **KEYWORDS:** Alkaline basalt, ultramafic enclaves, fractional crystallisation, partial melting,
13
14 38 uplift
15
16
17 39
18
19 40
20
21 41
22
23
24 42
25
26 43
27
28
29
30
31
32
33
34
35
36
37
38
39
40
41
42
43
44
45
46
47
48
49
50
51
52
53
54
55
56
57
58
59
60

1 2 3 44 1. INTRODUCTION 4 5

6 Anatolia is located in the collision zone between African-Arabian and Eurasian plates. The
7 convergence began in the Late Cretaceous–Eocene and ended with the continental collision
8 in the middle Miocene ([Şengör & Yılmaz, 1981](#); [Yılmaz et al., 1987](#); [Ring & Layer, 2003](#);
9 [Okay. et al., 2010](#)). This collision led to the Anatolian plate moving westwards via the North
10 Anatolian and East Anatolian faults ([Fig. 1a](#)) ([Dewey & Şengör, 1979](#); [Şengör, 1979](#); [Şengör](#)
11 & [Yılmaz, 1981](#); [Pasquare et al., 1988](#); [McKenzie, 2020](#); [Şengör & Yazıcı, 2020](#); [Seyitoğlu](#)
12 [et al., 2022](#)). The combined effects of the westward Anatolian migration, back-arc extension
13 of Hellenic arc and the retreat of the trench are the main controls on subsequent expansion
14 ([Seyitoğlu & Scott, 1991, 1992](#); [Seyitoğlu et al., 2002](#); [Sözbilir, 2002](#); [Westaway et al., 2005](#);
15 [Koçyiğit, 2005](#); [Bozkurt & Mittwede, 2005](#); [Ersoy & Helvacı, 2007](#); [Jolivet et al., 2013](#);
16 [Gessner et al., 2013, 2018](#); [Seyitoğlu et al., 2022](#)). After crustal extension, metamorphic
17 basement rocks of the Menderes Massif exhumed by a combination of west-east strike-slip
18 faulting and successive north-south detachment faults ([Bozkurt & Park, 1997](#); [Bozkurt, 2001](#);
19 [Seyitoğlu, 1997](#); [Lips et al., 2001](#); [Gessner et al., 2001](#); [Ring & Layer, 2003](#); [İşık et al., 2004](#);
20 [Sözbilir, 2005](#); [Bozkurt & Rojay, 2005](#); [Ersoy et al., 2011, 2012](#)). [Gessner et al. \(2013, 2018\)](#)
21 divide the exhumation of the Menderes Massif into two stages as a resulting from of
22 asthenospheric flow below western Anatolia. The rapid tectonic denudation was due to
23 differential footwall uplift during the early Miocene, and the formation of the Central
24 Menderes Metamorphic Core Complex (CMCC; ‘inner’ axial zone) by late Miocene to recent
25 detachment fault and normal fault systems, located between northern and southern (Çine)
26 segments of the complex ([Fig. 1b](#)). The Menderes Massif includes the NE-SW trending
27 Miocene Gördes, Demirci, Selendi, and Uşak-Güre basins in its northern part ([Seyitoğlu &](#)
28 [Scott, 1991](#); [Seyitoğlu & Scott, 1994](#); [Helvacı, 1995](#); [Helvacı & Yağmurlu, 1995](#); [Seyitoğlu,](#)
29 [1997](#); [Yılmaz et al., 2000](#); [Bozkurt, 2003](#); [Purvis & Robertson, 2004](#); [Westaway et al., 2004](#);
30 [Erkül et al., 2005](#); [Ersoy & Helvacı, 2007](#); [Ersoy et al., 2010](#); [Karaoğlu et al., 2010](#); [Ersoy et](#)

1
2
3 70 al., 2011, 2012). These basins were cut by seismically active E–W-trending oblique-normal
4
5 71 faults, resulting in the formation of the Simav and Gediz grabens under the late Miocene to
6
7 72 recent N-S rift-type extensional tectonics (Seyitoğlu, 1997; Cohen et al., 1995; Bozkurt &
8
9 73 Sözbilir, 2004; Rojay et al., 2005; Emre & Sözbilir, 2007; Çiftçi & Bozkurt, 2009; Ersoy et al.,
10
11 74 2010, 2011, 2012; Hakyemez et al., 2013; Hetzel et al., 2013) (Fig 1b).

14
15 75 Volcanism in NE-SW trending basins has been associated with lithospheric thinning, and
16
17 76 the volcanic products show geochemical variations during Miocene, including high-K calc-
18
19 77 alkaline felsic and shoshonitic, ultrapotassic-lamproitic rocks (early Miocene); high-K calc-
20
21 78 alkaline intermediate and high-Mg shoshonitic to ultrapotassic rocks (middle Miocene); and
22
23 79 K-trachybasaltic rocks (late Miocene) (Yılmaz, 1989, 1990; Seyitoğlu, 1997; Bunbury et al.,
24
25 80 2001; Erkül et al., 2005; Innocenti et al., 2005; Westaway et al., 2006; Ersoy et al., 2008;
26
27 81 Karaoğlu et al., 2010; Çoban et al., 2012; Prelevic et al., 2012). The Kula Volcanism (KVF),
28
29 82 located within the Selendi Basin, began with eruptions of plateau lavas ~1.5-2 Ma ago and
30
31 83 continued until prehistoric time as monogenetic volcanoes (Bunbury, 1996; Bunbury et al.,
32
33 84 2001; Innocenti et al., 2005; Westaway et al., 2004, 2006). The KVF is characterized by
34
35 85 high-Na alkaline volcanics in the rift-mode extension regime (Bunbury et al., 2001; Alıcı et
36
37 86 al., 2002; Bozkurt & Sözbilir, 2004; Innocenti et al., 2005).

41
42 87 The KVF comprises 92 Quaternary monogenic volcanic centres (scoria cones, spatter
43
44 88 cones, maars) and covers an area of around 350 km². The volcanic products contain
45
46 89 ultramafic and mafic enclaves, which were previously studied by Hollnes et al. (2005),
47
48 90 Hollnes & Bunbury (2006) and Grützner et al. (2013). Their previous studies mainly focused
50
51 91 on hornblendite and clinopyroxenite samples. In this study, we also examine olivine-rich
52
53 92 clinopyroxenite and wehrlite samples to demonstrate the origin of those co-genetic
54
55 93 inclusions in the host basaltic rocks and their petrological importance.

56
57 94
58
59 95 **2. CRUSTAL EXTENSION AND UPLIFT**

1
2
3 96 It is generally accepted that Western Anatolian crust has experienced extension since the
4
5 97 late Miocene to Pliocene (e.g. [Angelier et al., 1981](#)). Geophysical studies indicate that the
6
7 98 crust's thickness in the west, near recent Kula alkaline basaltic volcanic area, is
8
9 approximately 30 km, increasing to 34-38 km eastwards ([Saunders et al., 1998](#); [Zhu et al.,](#)
10 99 [2006](#); [Mahatsente et al., 2017](#)). The active faults point out an extending subcrustal
11 100 lithosphere as a result of mantle uplift in the region ([Saunders et al., 1998](#)). Basin
12 101 sedimentation characteristics constrain uplift rates to 0.1 mm/year, for a period 2-0.2 Ma,
13
14 102 followed by 3.5 mm/year (since 0.2 Ma) ([Bunbury et al., 2001](#)). Alternatively, erosion is
15 103 estimated to be 0.1 mm/year, with a total amount of uplift ~ 410 m since 3.1 Ma ([Westaway](#)
16
17 104 [et al., 2006](#)). In addition, [Bunbury et al. \(2001\)](#) suggest that the presence of the Hbl-dominant
18
19 105 mafic-ultramafic enclaves in the BII Kula lavas is a magmatic evidence supporting the "uplift"
20
21 106 model. [Doglioni et al. \(2002\)](#) proposed that the last activity of the KVF rapidly erupted in a
22
23 107 strongly extensional regime during neotectonic period due to the "horizontal windows"
24
25 108 resulting from the tearing of the Aegean and Cyprus slabs ~20 Ma ago, which allowed the
26
27 109 asthenospheric inflow into the lithosphere. However, the interaction of the asthenospheric
28
29 110 mantle upwelling with the lithosphere is controversial. Two hypotheses have been proposed
30
31 111 to explain lithospheric thinning and its relation to adiabatic upwelling of the asthenosphere.
32
33 112 The first one is the transformation of the lower parts of the lithosphere into asthenosphere
34
35 113 (asthenospherisation), resulting in the reconstruction of the paleo-depth of the Menderes
36
37 114 lithospheric root ([Prelevic et al., 2012](#)). The second hypothesis is the delamination of
38
39 115 lithospheric mantle by loss of material owing to gravitational collapse ([Seyitoğlu & Scott,](#)
40
41 116 [1996](#); [Aldanmaz et al., 2000](#); [Ersoy et al., 2008, 2011](#); [Karaoğlu et al., 2010](#)). Geophysical
42
43 117 studies support a lithospheric thinning in western Anatolia around Menderes Massif. A low-
44
45 118 velocity zone (ca. 80 km depth) underlying a thin lithosphere has been found near the KVF
46
47 119 ([Salaün et al., 2012](#); [Mahatsente et al., 2017](#)). Most of the western Anatolia has an
48
49 120 anomalously thin (50-80 km) and hot lithosphere that is possibly thinned to the crust (ca. 60
50
51 121

1
2
3 122 km, i.e. ~30 km below from the Moho) corresponding to the depth of basaltic magma
4
5 123 generation ([Artemieva & Shulgin, 2019](#)).
6
7
8 124
9
10 125

3. GEOLOGICAL BACKGROUND

11
12 126 The bedrocks underlying the KVF comprise Palaeozoic-Triassic metamorphic units (schist,
13 gneiss, and serpentinite), Cretaceous ophiolite mélange (ultramafic rocks, listvenite), and
14
15 127 800 m thick Miocene-Pliocene sedimentary rocks (claystone, siltstone, sandstone,
16
17 128 conglomerate and lacustrine limestone) ([Ercan et al., 1978](#)).
18
19 129
20
21 130 Ercan et al. (1983) proposed three volcanic stages, while Bunbury (1996) and Bunbury et
22
23
24 131 al. (2001) identified four episodes of the KVF. In this study, we divided the KVF into three
25
26 132 volcanic stages: BI, BII, and BIII, based on the stratigraphical, morphological and
27
28 133 chronological data ([Fig. 2](#)).
29
30
31 134
32
33 135

3.1. First Stage (BI):

34
35 136 The BI volcanics outcrop in the eastern part of the study area. K-Ar and Ar-Ar radiometric
36
37 137 data plot between $0.99 \pm 0.11 - 1.94 \pm 0.16$ Ma ([Fig. 2: Bunbury et al., 2001; Westaway et](#)
38
39
40 138 al., 2004, 2006; Maddy et al., 2015). The stage is primarily effusive, and its lavas flow over
41
42 139 the Neogene sediments. They form a flat hat in the topographic heights, and the erosion of
43
44 140 the concerned sediments, particularly in Gediz River gorge, formed spectacular earth pillars
45
46 141 or fairy chimneys. Those lava flows cover an area of about 35 km^2 , and their thickness
47
48 142 ranges from 5 to 25 m.
49
50
51 143
52
53
54 144

3.2. Second Stage (BII):

55
56 145 This stage comprehends the predominant volcanic activities of the KVF, represented by 49
57
58 146 cinder cones and associated lava flows, 3 tuff rings and 1 maar. K-Ar and Ar-Ar radiometric
59
60 147 data of the BII basalts have ages ranging from 50 ± 9 to 300 ± 3 ka ([Fig. 2: Bunbury et al.,](#)

1
2
3 148 2001; Westaway et al., 2004, 2006). They outcrop in topographically lowlands compared to
4
5 149 BI and are more altered than BI lava flows. Onion-skin alterations are commonly observed
6
7 150 at the lava fronts. We encountered evidence of hydromagmatic activities only in this stage.
8
9 151 The base surge deposits surrounding the crater comprise ash and lapilli layers, dune, anti-
10
11 152 dune structures and bomb sags (Fig. 3a). Kızıl Tepe tuff ring (M3) deposits contain ultramafic
12
13 153 enclaves.
14
15 154
16
17 155
18
19 156 **3.3. Third Stage (BIII):**
20
21 156 There are 31 cinder cones associated with at least 28 individual lava flows. In the west of
22
23 157 the study area, lavas flowed down southwestward about 17 km (Fig. 2). BIII lava flows are
24
25 158 a'a type and distinct with their fresh black-coloured appearance, sharp-edged blocks, and
26
27 159 unvegetated cover. BIII cinder cones can also easily be distinguished from BII cinder cones
28
29 159 due to their lower erosion, steeper slopes, clearly visible craters and lack of soil covers. We
30
31 160 also distinguished 16 small cinder cones (without crater) forming a cluster at the north of
32
33 161 Divlit Tepe near Kula, where there is the source area for the BIII lavas reaching the Gediz
34
35 162 River (Fig. 2, 3b). Most of the cinder cones are breached by lava flows, as shown in Figure
36
37 163 3c. Fissures and fractures are occasionally well-expressed by the spatter cones and tumuli.
38
39 164 The volcanic products of BIII are the youngest of the KVF eruptions, with radiometric ages
40
41 165 spanning between 0.7 ± 0.4 and 10.6 ± 1.9 ka (Westaway et al., 2004, 2006; Heineke et al.,
42
43 166 2016; Ulusoy et al., 2019). Human footprints are well known on the basaltic base surge
44
45 167 deposits near the Lake of Demirköprü Dam, and Ulusoy et al. (2019) have determined an
46
47 168 age of 4.7 ± 0.5 ka for these footprints using cosmogenic ^{36}Cl and combined U-Pb and (U-
48
49 169 Th)/He zircon double-dating methods.
50
51
52 170
53
54 171 **4. ENCLAVES**
55
56
57
58 172 The lavas and cinder projections contain mafic and ultramafic enclaves varying in size from
59
60 173 <1 to 48 cm. They are absent in the BI lava flows, but they are generally observed within the

1
2
3 174 ejecta of cinder cones, maars ([Fig. 3a, d](#)) and rare lava flows of the latest stage (BIII). The
4
5 175 lava flows originating from the breached Bağ Tepe cinder cone are rich in enclaves ([Fig. 3e,](#)
6
7 176 [f](#)). The most characteristic feature of Kula enclaves is the presence of vesicular glass ([Fig.](#)
8
9 177 [3g](#)). Most of the enclaves are rounded and sub-rounded with a smooth surface. Apart from
10
11 178 these enclaves, foliated metamorphic (mica schist and mica gneiss etc.) and magmatic
12
13 179 xenoliths are also present in the ejecta. In contrast to magmatic enclaves, they have an
14
15 180 angular shapes and irregular surfaces.
16
17
18
19 181
20
21 182 **5. ANALYTICAL TECHNIQUES**
22
23
24 183 Electron microprobe analyses of the cores and rims of phenocrysts, microcrysts, microlites
25
26 184 and glass were performed by Cameca SX100 instrument at the Blaise-Pascal University,
27
28 185 France. Operating conditions were: 15 kV accelerating voltage, 10–12 nA current and 10 s
29
30 186 counting time for each element.
31
32
33 187 Bulk-rock major and trace element analyses were performed at the Geological Engineering
34
35 188 Department of Hacettepe University, Turkey, using a Philips PW 1480 X-Ray Fluorescence
36
37 189 spectrometer, from fused glass tablets and pressed powdered samples. [Alici et al. \(1998\)](#)
38
39
40 190 gave a detailed explanation of sample preparation. The spectrometer was calibrated using
41
42 191 international standards (USGS and GEOSTANDARTS) to ensure accurate data. The X-ray
43
44 192 Fluorescence spectrometer was calibrated by using USGS and Geostandards to ensure
45
46 193 accurate data. Rare earth element (REE) analyses were performed by a JY701 inductively
47
48 194 coupled plasma emission spectrometer at the Blaise Pascal University in Clermont-Ferrand,
49
50 195 France.
51
52 196
53
54 197 **6. PETROGRAPHY**
55
56
57
58 198
59
60 199 **6.1. Host rock**

1
2
3 200 Lava samples from the KVF are typically porphyritic, with groundmass textures ranging from
4 intergranular to intersertal. Many lavas show obvious petrographic evidence of
5 disequilibrium, including strongly resorbed phenocrysts, reaction rims, zoned minerals,
6
7 202 disequilibrium mineral assemblage, and compositions. The main phenocryst phases are
8
9 203 olivine, clinopyroxene and hornblende, with plagioclase, leucite, and nepheline being less
10
11 204 abundant than mafic minerals. Mineral abbreviations are from [Whitney & Evans \(2010\)](#).
12
13 205
14
15 206 *Olivine* (Ol) is the most abundant phenocryst phase in BI basalt, ranging from 4 to 10 vol.%
16
17 207 of the rock. Olivines occasionally exhibit strongly skeletal texture in the BI and BIII basalts
18
19 208 and are frequently euhedral, sub-rounded ([Fig. 4a-c](#)). The iddingsite sparsely replaced
20
21 209 olivine in the groundmass of BI basalt.
22
23
24 209
25
26 210 *Clinopyroxene* (Cpx) is the most dominant mineral in all stages. They are euhedral,
27
28 211 subhedral, rounded, and strongly zoned ([Fig. 4c](#)). Some clinopyroxenes exhibit zoning,
29
30
31 212 especially in BI and BII basalts. The core zone, green in colour, is usually resorbed and
32
33 213 surrounded by colourless outer rim ([Fig. 4e](#)).
34
35 214 *Hornblende* (Hbl) is present only in the BII and BIII stages. They are prismatic, locally
36
37 215 resorbed (BIII), and generally rimmed by opaque oxides (BII) ([Fig. 4c-d](#)). We observed a
38
39 216 cumulate texture consisting of hornblende assemblage in BIII basalt ([Fig 4f](#)).
40
41
42 217 *Plagioclase* (Pl) is microlitic commonly with rare phenocrysts in all stages. They show some
43
44 218 disequilibrium features, such as honeycomb texture with numerous glass inclusions, fresh
45
46 219 core with dusty zone rims, and resorption.
47
48
49 220 *Nepheline* is commonly present as microlite in the groundmass of the BIII basalt. *Leucite* is
50
51 221 abundant in the lavas of the BIII, with a high modal percentage (up to %19), and sporadically
52
53 222 represented in the crystal aggregates ([Fig. 4c](#)).
54
55
56 223 *Fe-Ti Oxides* exist in the groundmass as titanomagnetite and spinel microphenocrysts in
57
58 224 BIII stage. It is also observed in the form of inclusions in olivine, clinopyroxene and leucite
59
60 225 ([Fig. 4b, d](#)).

1
2
3 226
4
5

6 227 **6.2. Enclaves**

7
8 228 Ultramafic and mafic enclaves are observed in BII and BIII stages. Modal results are as
9
10 229 follows: Cpx-hornblendite (12), hornblendite (8), Pl bearing Cpx-hornblendite (6), wehrlite
11
12 230 (6), Ol-Hbl-clinopyroxenite (5), Hbl-gabbro (4) and phlogopite (Phl) clinopyroxenite (1) (Fig.
13
14 231 5). Glass and vesicle abundances are highly variable among the enclaves (Suppl. Table 1),
15
16
17 232 reaching up to 48%. Enclaves are observed not only as hand specimens, but also as micro-
18
19 233 enclaves, including interstitial glass in thin sections (Fig. 4f-h).

20 234
21
22
23

24 235 **6.2.1. Hornblendites: Cpx-Hornblendite (BII), Hornblendite (BII, BIII), Pl-Bearing Cpx-**
25
26 236 **Hornblendite (BIII)**

27
28 237 Cpx-hornblendites and hornblendites generally exhibit porphyritic texture. The relationships
29
30 among grains are largely intergranular and sub-ophitic with interstitial vesicular glass (Fig.
31 238 6a-c). They are essentially composed of long prismatic hornblendes (Fig. 6i). One of the
32
33 239 Cpx-hornblendites contains pale blue hauyne minerals in a pocket of vesicular glass (Fig.
34
35 240 6d). Hornblendes commonly have fresh cores but altered rims. Some of them are resorbed
36
37 241 and contain glass inclusions.

38
39 242
40
41
42 243 Apart from the porphyritic texture, plagioclase-bearing Cpx-hornblendites occasionally
43
44 244 present adcumulate and/or mesocumulate textures with sporadically pegmatitic
45
46 appearance. They bear glass, resorbed hornblende, rounded clinopyroxene, ragged
47 245 phlogopite and resorbed plagioclase. Some plagioclase and apatite minerals also contain
48
49 246 glass inclusions (Fig. 6e).

50
51 247
52
53
54 248
55

56 249 **6.2.2. Clinopyroxenites: Phl-Clinopyroxenite (BIII) and Ol-Hbl-Clinopyroxenite (BII)**

57
58 250 We have only one Phl-clinopyroxenite sample. It consists of strongly resorbed phlogopite
59
60 251 (<12 mm, vol.38.5% modal) and subhedral resorbed clinopyroxene (vol.33% modal) with

1
2
3 252 interstitial vesicular glass (vol.25% modal). This enclave exhibits well developed embayment
4
5 253 textures of phlogopite ([Fig. 6f](#)).
6
7 254 Ol-Hbl-clinopyroxenite enclaves (up to 7% Ol, 21% Hbl) show well-defined adcumulate
8
9 255 texture ([Fig. 6j](#)). They mainly consist of subhedral, sub-rounded pale green coloured
10
11 256 clinopyroxene and reddish-brown-coloured hornblende with intercumulus resorbed
12
13 257 phlogopite and apatite ([Fig. 6j](#)). Several samples contain coarse-grained clinopyroxene (ca.
14
15 258 1-14 mm) replaced by hornblende along cleavage planes ([Fig. 6k](#)). Olivine is sub-rounded
16
17 259 and iddingsite is observed along its cracks ([Fig. 6k](#)).
18
19 259
20
21 260
22
23
24 261 **6.2.3. Hbl-Gabbro (BIII)**
25
26 262 These are represented by fine grained (<1 mm), resorbed, prismatic, greenish-brown and
27
28 263 acicular hornblende, minor embayed olivine and dusty-rimmed plagioclase ([Fig. 6l-m](#)).
29
30
31 264 Phlogopite only occurs around olivine ([Fig. 6m](#)).
32
33 265
34
35 266 **6.2.4. Wehrlite (BII)**
36
37 267 Wehrlite enclaves have poikilitic textures of strongly resorbed hornblende and sub-rounded,
38
39 268 partially resorbed olivine (1-7 mm) in clinopyroxene (<14 mm) oikocrysts ([Fig. 6g, h](#)). Some
40
41 269 have orthocumulate textures comprised of euhedral-subhedral olivine (62–68%), interstitial
42
43 269 subhedral clinopyroxene ([Fig. 6n](#)). Minor phlogopite grains formed around olivine and
44
45 270 hornblende in contact with glass. Apatite is accessory and only found in glass. Additionally,
46
47 271 euhedral Cr-spinel is found in olivine as inclusions ([Fig. 6g](#)).
48
49 272
50
51 273
52
53
54 274 **7. MINERAL COMPOSITIONS**
55
56 275 **7.1. Olivine**
57
58 276 Phenocryst and microcryst are variable in composition (Fo₇₀₋₈₇) ([Suppl. Table 2](#)).
59
60 277 Compositional zoning is more pronounced in enclaves (especially in wehrlite) than in the

1
2
3 278 host rock, but some grains are slightly richer in Fe. In contrast to wehrlite, the olivine gabbro
4
5 279 Mg number (Mg#) values range from 80 to 85.
6
7
8 280
9
10 281

7.2. Clinopyroxene

11
12 282 Selected analyses are listed in [Supplementary Table 3](#). Endmember plots in [Figure 7](#)
13
14 283 ([Morimoto, 1988](#)) for host rock and enclave minerals show that all pyroxene is diopsitic
15
16 284 (Wo_{46-57} , En_{20-45} , Fs_{6-30}), except two clinopyroxene analyses in host rock. One of them has
17
18 285 spongy texture, and the other is reversely zoned with hedenbergitic composition. The Mg#
19
20 286 of clinopyroxene slightly decrease from phenocryst (92) to microcryst (55) in the host rocks.
21
22 287 The compositional range is wide and noticeable variations in Mg#, Al_2O_3 and TiO_2 content
23
24 288 have been detected, particularly in BII and BIII basalt. In contrast to BII and BIII, BI
25
26 289 clinopyroxenes have lower Al (<6%) and Ti content (<2%).
27
28 290
29
30
31 291

7.3. Amphibole

32
33 292 The chemical composition of hornblendes is summarised in [Supplementary Table 4](#). They
34
35 293 are conspicuously rich in TiO_2 . According to [Leake et al. \(1997\)](#), the host rock amphiboles
36
37 294 are mostly kaersutite with rare pargasite. Pargasites contain lower K_2O , TiO_2 , Mg# and
38
39 295 higher CaO content than the kaersutite composition. Some reversely zoned hornblendes
40
41 296 exist in GIII basalt with Mg enrichment at the rim of phenocrysts.
42
43 297 Amphiboles in the enclaves are pargasitic and kaersutitic. The Mg#s range between 57 and
44
45 298 77. Some microcrysts in the glass and inclusions have lower Mg# (52-62). Amphiboles in
46
47 299 the enclaves are generally Mg-rich in their core, except those in wehrlite. Moreover,
48
49 300 amphiboles in the Hbl-Gabbro have lower Mg# compared to those of the other enclaves.
50
51
52 301
53
54 302

7.4. Phlogopite

1
2
3 303 Phlogopite is only seen in Hbl-gabbro, Phl-clinopyroxenite and rarely in wehrlite. Analyses
4
5 304 are listed in [Supplementary Table 5](#), with Fe# ranging from 0.17 to 0.29 ([Rieder et al., 1998](#),
6
7 305 Fe# < 0.3). Phlogopite in Phl-clinopyroxenite has higher Fe, Al, Ti and lower Na content
8
9 306 compared to phlogopite in Hbl-gabbro.
10
11
12 307
13
14
15 308 **7.5. Plagioclase**
16
17 309 The selected analyses are presented in [Supplementary Table 6](#). In the host rock,
18
19 310 plagioclases (An_{46_64}) are mostly andesine, with rare labradorite. Some microlites exhibit
20
21 311 higher An content than the unstable phenocrysts (anal. #2b). In Hbl-gabbro, the plagioclase
22
23 312 composition is relatively andesine (An₄₃₋₄₇), but in Cpx-hornblendite, they represent an
24
25 313 extensive compositional variation (An₆₀₋₉₄), ranging from labradorite to pure anortite. Some
26
27 314 plagioclases in Cpx-hornblendite are resorbed and contain glass inclusions.
28
29
30
31 315
32
33 316 **7.6. Feldspathoids**
34
35 317 The representative analyses are given in [Supplementary Table 7](#). The *nepheline* of the BII
36
37 318 stage has slightly higher Al₂O₃, FeO, CaO and lower Na₂O than the nepheline of the BIII. In
38
39 319 the enclave, nepheline is only observed in Hbl-clinopyroxenite (BII) and exhibits
40
41 320 compositional similarity with those of the BII stage.
42
43
44 321 *Hauyne* occurs exclusively in the Cpx-hornblendite ([Fig. 6d](#), BII), with K₂O and Na₂O content
45
46 322 changing from 4.3 to 6.3% and from 7.3 to 10.3%, respectively.
47
48
49 323
50
51 324 **7.7. Oxides**
52
53
54 325 *Ti-magnetite* is present as microcrysts in groundmass and inclusion phases in all the three
55
56 326 generations of the basalt. The chemical composition of Ti-magnetite is very homogeneous,
57
58 327 containing approximately 22-23% TiO₂ ([Suppl. Table 8](#)).
59
60

1
2
3 328 *Al-spinels* have bimodal distribution in the host rock BIII, occurring as euhedral
4 microphenocrysts and inclusion in olivine and leucite phenocrysts. The microphenocryst Al-
5 spinel is more evolved, with a lower Mg# than the inclusions.
6
7 330
8
9
10 331 *Cr-spinel* is observed as inclusion and is only present in wehrlite sample, with the Cr#
11
12 332 (Cr/(Cr+Al)) changing from 25 to 36.
13
14
15 333 *Mg-ilmenite* is only observed in Cpx-hornblendite samples, containing 7-8% MgO, 33-34%
16
17 334 FeO and 53-54% TiO₂.
18
19 335
20
21 336 **7.8. Vesicular Glass**

22
23
24 337 The ratio of the glass and vesicles within the enclaves is highly variable ([Suppl. Table 1](#)).
25
26 338 The glass in the enclaves of the BII stage varies in volume from 0.3 to 19%, while those of
27
28 339 BIII range from 9 to 29%. The glass exhibits a variety of colours ranging from light brown,
29
30
31 340 reddish dark brown to black, but the glass in the Hbl-gabbro is commonly colourless. Two
32
33 341 types of glasses, similar to those identified by [Yaxley et al., \(1997\)](#), have been observed in
34
35 342 the enclaves, namely “glass pocket” (Gp), and “glass associated with intergranular minerals”
36
37 (Gim). The Gp is occasionally observed in the enclaves of the BII stage, which modally
38 343 comprise less than 15 vol.% of the glass. In some of the OI-Hbl-clinopyroxenite and wehrlite
39
40 344 samples, the Gps are frequently connected with a glass film, forming a network system ([Fig.](#)
41
42 345 [6j, n](#)). However, the Gim is commonly found in the hornblendite, Cpx-hornblendite, and Phl-
43
44 346 clinopyroxenite samples, mostly belonging to BIII stage ([Fig. 6a-d, f, i](#)). In several enclaves,
45
46 347 the Gp consists of disequilibrium mineral assemblage, such as resorbed minerals
47
48 348 (hornblende, olivine, phlogopite, apatite and hauyne) ([Fig. 6d, f-h](#)). Some minerals have
49
50 349 reacted with glass, resulting in a dark-coloured contact surface between mineral and melt,
51
52 350 observed in both the glass veins and glass pockets ([Fig. 6g-j](#)). Relict fragments of
53
54 351 phlogopite, completely surrounded by the glass, are optically continuous with larger primary
55
56 352 phlogopite ([Fig. 6f](#)). The glass in the coarse-grained enclaves, especially hornblendites,
57
58 353

1
2
3 354 comprise euhedral and prismatic apatites (Fig. 6b-e, h, j). They are observed as both
4
5 355 isolated crystals and inclusions in hornblende and clinopyroxene.
6
7
8 356 The glass contains a high concentration of vesicles, with the abundance of the vesicles
9
10 357 occasionally surpassing that of the glass content. The vesicles typically increase in size
11
12 358 from the Gim (<0.1 mm) to Gp (<1.5 mm). They are mostly spherical to elliptical in the Gp,
13
14 359 in contrast to those in the Gim. Some vesicle walls in the glass are collapsed or probably
15
16 360 plucked out during thin-section preparation (Fig. 6c).
17
18
19 361 The chemical composition of the glasses is given in Supplementary Table 9. The glasses
20
21 362 are intermediate to basic (44–56 wt.% SiO₂), and are commonly foiditic, phonotephritic, and
22
23 363 rarely tephriphonolitic and basanitic (Fig. 8). The glass in the enclaves relatively comprises
24
25 364 higher SiO₂ and total alkaline content than their bulk rock. The glasses with the lowest SiO₂
26
27 365 content (44–47%) occur in wehrlite, Phl-clinopyroxenite, and a Cpx-hornblendite. Although
28
29 366 the enclaves have different mineralogy and chemistry, Figure 9 shows that the composition
30
31 367 of the glass from wehrlite to Hbl-gabbro samples exhibits evident trends on the plots of SiO₂
32
33 368 versus major oxides. Some glass composition within Phl-clinopyroxenite does not conform
34
35 369 to the general trends. Glass adjacent to phlogopite is commonly rich in K₂O, Na₂O and Al₂O₃
36
37 370 and poor in MgO and CaO.
38
39
40 370
41
42 371
43
44 372
45 372 **8. GEOCHEMISTRY**
46
47 373 Major oxides, trace, and rare element compositions of representative samples from Kula
48
49 374 lava flows and their enclaves are listed in Supplementary Table 10. All samples exhibit an
50
51 375 alkaline trend (Fig. 8). The *B1* lava flows range in composition from basanite, trachybasalt
52
53 376 and phonotephrite. While the majority of the samples from *BII* host rocks are basanite with
54
55 377 lesser amount of phonotephrite, *BIII* host rocks are phonotephrite in composition. Besides,
56
57 378 although enclaves are mantle rocks and should not be shown on the TAS diagram with host
58
59 379 volcanics, they are plotted on the same diagram to show similarities or variations in chemical

1
2
3 380 compositions. Enclaves are definitely ultrabasic in character, with SiO₂ (39-45%) and
4
5 381 K₂O+Na₂O (1-7.5 %) values, lower than their host rocks.
6
7
8 382 Plots of SiO₂ versus selected major oxides are shown in [Figure 9](#). Increasing SiO₂ is well
9
10 383 correlated with; i) decreasing Fe₂O₃, MgO, CaO, P₂O₅ and TiO₂ in both host rocks and their
11
12 384 enclaves; ii) increasing Al₂O₃, Na₂O and K₂O in host rocks. However, Al₂O₃, Na₂O and K₂O
13
14 385 contents of enclaves vary within a narrow range with no systematic variation ([Fig. 9](#)). The
15
16 386 decrease in Fe₂O₃, MgO, CaO, P₂O₅, and TiO₂ is coherent with crystallisation of olivine,
17
18 387 clinopyroxene, plagioclase, Fe-Ti oxides, and apatite.
19
20
21 388 The variations of Al₂O₃ and Na₂O in host rocks are notably different from those in their
22
23 389 enclaves. As shown in [Figure 9](#), while the Al₂O₃ and Na₂O contents of the host rocks
24
25 390 increase with increasing SiO₂, the values of these elements decrease with increasing SiO₂
26
27 391 content in enclaves. This indicates that the Al₂O₃ contents increase from ultrabasic enclaves
28
29 392 to basic host rocks, which may be linked to the plagioclase fractionation.
30
31
32 393 Trace element data are reported in [Supplementary Table 10](#) and plotted against SiO₂ in
33
34 394 [Figure 9](#). The best correlation is represented by Co, V, Rb, and Sr. Ba, Nb, Y, and Zr show
35
36 395 no systematic variation. The contents of Co and V regularly decrease with increasing SiO₂,
37
38 396 possibly indicating the fractionation of olivine, spinel/clinopyroxene and V-bearing Fe-Ti
39
40 397 oxides. On the other hand, Rb and Nb contents increase with increasing SiO₂.
41
42
43 398 MORB-normalised ([Pearce, 1983](#)) spider diagrams are shown in ([Fig. 10](#)). All samples from
44
45 399 host rocks exhibit typical within-plate patterns (humped-patterns) enriched in large ion
46
47 400 lithophile elements (LILE, e.g. Sr, K, Rb, Ba and Th), light rare earth elements (LREE), and
48
49 401 high field strength elements (HFSE, e.g. Nb, Ta and Ti) relative to the MORB ([Fig. 10a](#)).
50
51
52 402 The trace element abundances of enclaves are characterized by significant depletion in Rb,
53
54 403 K and Th with respect to HFS elements ([Fig. 10b](#)). The Kula enclaves are strongly depleted
55
56 404 in Rb and Th compared to their host rocks. As expected, the enclave of Phl-clinopyroxenite
57
58 405 (K97-70a2) show anomalously high K, Rb and Ba peaks.

1
2
3 406 REE data of both Kula host rocks and enclaves are summarized on a chondrite-normalised
4
5 407 (Nakamura, 1974) diagrams. Both suites exhibit light LREE enrichment relative to chondrite
6
7 408 (i.e. La= 70 to 250 times) and also show clear fractionation between LREE and HREE.
8
9 409 All samples for Kula host rocks have flat patterns from Er to Lu with respect to LREE (Fig.
10
11 410 10c). While the abundances of LREE are variable, the HREE are relatively constant.
12
13 411 Herewith, LREE/HREE ratios are also variable, and the (La/Yb)n ratios of Kula host rocks
14
15 412 range from 13.36 to 24.56.
16
17
18
19 413 Enclaves of Phl-clinopyroxenite (K97-70a2), Cpx-hornblendite (K97-30a, K97-48a2),
20
21 414 hornblendite (K97-14a, K97-17a2) and plagioclase bearing Cpx-hornblendite (K97-46a)
22
23
24 415 have almost similar patterns identical to those of host rocks (Fig. 10d). They are also
25
26 416 characterized by LREE enrichment relative to chondrite (i.e. La= 70-250 times chondrite).
27
28 417 However, they have more fractionated nature relative to their host rocks with (La/Yb)n ratios
29
30
31 418 varying from 9.27 to 33.83. The wherlite sample (K97-10a2) also exhibits REE pattern
32
33 419 similar to other enclaves but has considerably lower REE contents.
34
35
36
37
38 421 **9. DISCUSSION AND CONCLUSION**
39
40
41
42
43
44
45 423 **9.1. Source Characteristics and Partial Melting Modeling**
46
47
48
49
50
51
52
53
54
55
56
57
58
59
60
61
62
63
64
65
66
67
68
69
70
71
72
73
74
75
76
77
78
79
80
81
82
83
84
85
86
87
88
89
90
91
92
93
94
95
96
97
98
99
100
101
102
103
104
105
106
107
108
109
110
111
112
113
114
115
116
117
118
119
120
121
122
123
124
125
126
127
128
129
130
131
132
133
134
135
136
137
138
139
140
141
142
143
144
145
146
147
148
149
150
151
152
153
154
155
156
157
158
159
160
161
162
163
164
165
166
167
168
169
170
171
172
173
174
175
176
177
178
179
180
181
182
183
184
185
186
187
188
189
190
191
192
193
194
195
196
197
198
199
200
201
202
203
204
205
206
207
208
209
210
211
212
213
214
215
216
217
218
219
220
221
222
223
224
225
226
227
228
229
230
231
232
233
234
235
236
237
238
239
240
241
242
243
244
245
246
247
248
249
250
251
252
253
254
255
256
257
258
259
260
261
262
263
264
265
266
267
268
269
270
271
272
273
274
275
276
277
278
279
280
281
282
283
284
285
286
287
288
289
290
291
292
293
294
295
296
297
298
299
300
301
302
303
304
305
306
307
308
309
310
311
312
313
314
315
316
317
318
319
320
321
322
323
324
325
326
327
328
329
330
331
332
333
334
335
336
337
338
339
340
341
342
343
344
345
346
347
348
349
350
351
352
353
354
355
356
357
358
359
360
361
362
363
364
365
366
367
368
369
370
371
372
373
374
375
376
377
378
379
380
381
382
383
384
385
386
387
388
389
390
391
392
393
394
395
396
397
398
399
400
401
402
403
404
405
406
407
408
409
410
411
412
413
414
415
416
417
418
419
420
421
422
423
424
425
426
427
428
429
430
431

1
2
3 432 apatite could form (Watson, 1980). Rb and Ba, both are compatible with phlogopite (Kd_{Rb}
4
5 433 and Kd_{Ba} are 3.06 and 1.090, respectively), whereas amphibole does not retain Rb, Sr and
6
7 434 Ba ($Kd_{Rb} = 0.29$; $Kd_{Ba}=0.42$ and $Kd_{Sr}=0.46$) (Furman & Graham, 1999; Rollinson, 1993).
8
9 435 Ionov & Hofmann (1995) have also indicated from the mantle xenoliths that amphibole has
10
11 436 very low Rb concentrations while phlogopite is rich in Rb. According to these criteria, melting
12
13 437 of an amphibole-bearing mantle source can reveal lower Rb/Sr and higher Ba/Rb ratios.
14
15 438 Conversely, melts from phlogopite-bearing mantle sources (amphibole-free) may have
16
17 439 higher Rb/Sr (>0.1) and lower Ba/Rb (<20) ratios than those formed from amphibole-bearing
18
19 440 sources (Furman & Graham, 1999).
20
21 441 The alkaline host rocks have generally relatively low Rb/Sr (0.03-0.10) and high Ba/Rb
22
23 442 (9.48-23.24) ratios (Fig. 11a), suggesting the presence of mostly amphibole with lesser
24
25 443 amount of phlogopite in their source region. They also plot close to the trend line of
26
27 444 amphibole and phlogopite. At the same time, the Rb/Sr and Ba/Rb ratios of Kula enclaves
28
29 445 show wide variation and range from 0.01 to 0.09 and 17.57 to 114, respectively. The majority
30
31 446 of the samples are clearly plotted on the amphibole trend line. As expected, the enclave of
32
33 447 K97-70a2 (Phl-clinopyroxenite) is shifted towards the phlogopite trend line due to its
34
35 448 relatively high Rb/Sr and low Ba/Rb ratios.
36
37 449 Furthermore, the high Na_2O/K_2O ratios (>1.27) of both Kula host rocks and enclaves (except
38
39 450 sample no: K97-70a2, Phl-clinopyroxenite) further support the above arguments, as melting
40
41 451 of amphibole bearing phases can account for $Na_2O/K_2O>1$ (Foley et al., 1999; Moufti et al.,
42
43 452 2012).
44
45 453 To specify the source mineralogy and melting depth of Kula enclaves and their host rocks,
46
47 454 partial melting modelling using REE ratios was calculated. The modelling uses the non-
48
49 455 modal batch melting equations of Shaw (1970), partition coefficients from McKenzie &
50
51 456 O'Nions (1991) and Rollinson (1993). Partial melting calculations were carried out by the
52
53 457 "PETROMODELER" program of Ersoy (2013). In the calculations, LREE-enriched

1
2
3 458 compositions from McDonough (1990) were regarded as initial source composition. Spinel
4
5 459 and garnet mineral modes were used to make an assessment of the melting depth (Baker
6
7 460 et al., 1997; Shaw et al., 2003). LREE/HREE variations are good proxies for the depth/extent
8
9 461 of melting and the residual garnet in the source. Garnet retains the HREE, and garnet-facies
10 462 melts are represented by higher LREE/HREE ratios relative to spinel-facies. Figures 11b-d
11
12 463 display Sm/Yb versus La/Yb variations for Kula host rocks and enclaves with non-modal
13
14 464 batch melting curves of spinel and garnet peridotite sources. As expressed in Figure 11b,
15
16 465 the genesis of Kula host rocks cannot be explained by variable degrees of melting from a
17 466 single garnet or spinel peridotitic source. Thus, binary mixing calculations of Langmuir et al.
18
19 467 (1978) were performed between spinel and garnet peridotite. Kula host basalts clearly plot
20
21 468 on the lines obtained by binary mixing between 3-5% spinel and garnet peridotite melts. The
22
23 469 mixing proportions extend between 40%-60% melt of spinel peridotite and 30%-70% melt of
24
25 470 garnet. On the other hand, enclaves shifted towards the melting curve of garnet-facies.
26
27
28 471 Figure 11c illustrates the $(\text{Tb}/\text{Yb})_n$ versus $(\text{La}/\text{Yb})_n$ variations in Kula host rocks and
29
30 472 enclaves with the horizontal line separating the garnet and spinel peridotite melting fields
31
32 473 (Wang et al., 2002; 2004; Furman et al., 2004; Moufti et al., 2012). The $(\text{Tb}/\text{Yb})_n$ ratios of
33
34 474 Kula host rocks (1.50-2.03) are generally clustered on the horizontal line, indicating that
35
36 475 melts originate from both garnet and spinel bearing sources, and extend along the mixing
37
38 476 lines between 3% and 5% melt of garnet and 5% melt of spinel-peridotite. Calculations
39
40 477 further support that the mixing of melts derived from both garnet and spinel peridotite
41
42 478 sources accounts for the generation of Kula volcanism. AICI et al. (2002) have also
43
44 479 suggested a mixture of asthenospheric and lithospheric mantle sources. Grützner et al.
45
46 480 (2013) mention Mg-rich and green-core Mg-poor clinopyroxene in lava flows and enclaves
47
48 481 indicating two different melt sources. In addition, Nikogosian et al. (2018) note that the
49
50 482 compositional diversity of the Kula volcanism based on olivine-hosted melt inclusions
51
52 483 indicates mixing of two distinct sources originated from the mantle, and the primary melt

1
2
3 484 generation starts from 75 km depth. However, according to Sölpüker (2007) Kula volcanism
4
5 485 originates from spinel peridotite with 7–9% degrees of fractional melting.
6
7
8 486 As can be seen in Figures 11b-c, Kula enclaves are separated from their host rocks due to
9
10 487 their relatively higher (Tb/Yb)n ratios (1.96-3.20), suggesting the presence of residual garnet
11
12 488 and melting in garnet stability field (Wang et al., 2002; Khudoley et al., 2012). Variations in
13
14 489 Sm/Yb, La/Yb Tb/Yb ratios in enclaves generally result from the melting of a garnet
15
16 490 peridotite. If this is the case, we should not expect any variation in La/Yb and Yb diagram
17
18 491 (Fig. 11d). However, the host rocks and enclaves have variation between La/Yb and Yb,
19
20
21 492 further suggesting the mixing between spinel and garnet peridotite sources. Moreover, the
22
23
24 493 presence of amphibole suggests the contribution of a spinel peridotite mantle source
25
26 494 (Worthing & Nasir, 2008; Tschegg et al., 2011; Moufti et al., 2012).
27
28 495
29
30
31 496 **9.2. Fractional Crystallisation and Crustal Contamination**

32
33 497 Various types of enclaves varying from wehrlite to gabbro, indicate that magma masses had
34
35 498 sufficient time for mineral settling to form cumulates. The melts reaching volatile saturation
36
37 499 contributed to the formation of ultramafic cumulates of different mineralogical composition.
38
39
40 500 For example, early-crystallized minerals such as spinel, olivine and clinopyroxenes
41
42 501 produced wehrlite with subsiding evolved melts and hydrous fluids could activate the
43
44 502 crystallisation of hornblende and phlogopite, producing hornblendites from primitive basaltic
45
46 503 magma with Na-alkaline affinity. The presence of nepheline and hauyne in the BII stage's
47
48 504 enclaves may indicate a magmatic evolution towards alkaline compositions.
49
50
51 505 The linear correlations between SiO₂ and some specific major and trace elements are
52
53 506 consistent with fractional crystallisation processes in the evolution of Kula host basalts and
54
55 507 enclaves. This could be explained by the presence of mafic microcrysts occurring in the
56
57 508 vesicular glass. Low Ni (<106 ppm) and Cr (<205 ppm) contents in host basalts also support
58
59 509 the arguments of fractional crystallization, as the decrease of Ni and Cr suggests olivine and

1
2
3 510 clinopyroxene fractionation, respectively ([Wilson, 1989](#); [Moufti et al., 2012](#)). Furthermore,
4
5 511 Ni and Cr contents of basalts (Ni: 7-106 ppm; Cr: 2-205 ppm) and enclaves (Ni: 0.5-91 ppm;
6
7 512 Cr: 7-301 ppm) are lower than the values commonly accepted for primary magmas (Ni=300-
8
9 513 400 ppm; Cr: 300-500 ppm; [Jung & Masberg, 1998](#)), possibly reflecting their fractionated
10
11 514 nature [with the exception of one sample, wehrlite, which has high Ni (598 ppm) and Cr
12
13 515 values (2331 ppm)]. For instance, the negative correlation between SiO₂ and MgO, Fe₂O₃,
14
15 516 TiO₂, and CaO, coupled with some specific elements such as Co, V and Sr are indicative of
16
17 517 olivine, clinopyroxene, Ca-plagioclase and Fe-Ti-oxides fractionation. P₂O₅ also has a clear
18
19 518 negative correlation with SiO₂, which is consistent with apatite removal. The increasing
20
21 519 trends between SiO₂ and K₂O, Na₂O and Rb also indicate fractional crystallisation processes
22
23 520 in the evolution of Kula host basalts.
24
25
26 521 [Haase et al. \(2000\)](#) argue that a high Nb/La (>1) ratio is the striking feature of
27
28 522 uncontaminated magmas from within-plate mantle sources. According to this criterion, it
29
30 523 suggests that the host basalts, having elevated Nb/La ratios (>1.3), were derived from
31
32 524 mantle sources with insignificant crustal contamination. Similarly, Nb/La ratios of the
33
34 525 enclaves (Nb/La: 1.2-2.4) also resemble those of their host rocks from within-plate settings.
35
36 526 Besides, Kula basalts and their enclaves have high Nb/Y ratios (>1.7), suggesting HFSE
37
38 527 enrichment commonly seen in lavas uncontaminated by crustal material from within-plate
39
40 528 mantle sources. This is a typical characteristic of uncontaminated alkaline ocean island
41
42 529 basalts ([Pearce & Cann, 1973](#)). [Alici et al. \(2002\)](#) illustrated in the OIB-normalised spider
43
44 528 diagram that the trace element patterns of Kula basalts are akin to OIB with considerable
45
46 530 enrichment in LILE (e.g. Sr, Rb, Ba, K) and HFSE (e.g. Nb, Th, U). This case can be ascribed
47
48 531 to mantle source enrichment during their genesis. The alkaline rocks studied here have
49
50 532 enriched incompatible element characteristic with high Nb/La and Nb/Y ratios, suggesting
51
52 533 derivation from a within-plate mantle source with an inconsequential crustal contamination.
53
54 534 Likewise, the Nb/U ratio of uncontaminated OIB is around 47±10 ([Hofmann et al., 1986](#)); the
55
56 535

1
2
3 536 range in Nb/U (31-58) of Kula basalts rule out the significant role of crustal contamination.
4
5 537 This argument is in agreement with the assessments of Güleç (1991) and Alıcı et al. (2002),
6
7 538 who suggested based on their isotopic data that Kula host rocks have not been subjected
8
9 539 to notable crustal contamination but have been treated by the effects of fractional
10 540 crystallization. Tokçaer et al. (2005) and Agostini et al. (2007) also suggest an OIB-like
11
12 541 asthenospheric mantle source for the KVF, without any contamination. The rapid ascent of
13
14 542 magma in Kula (Tokçaer et al., 2005) and short residence time in the crust (Georgatou &
15
16 543 Chiaradia, 2020) explain the negligible role of crustal contamination. This argument relates
17
18 544 to the residence duration of basaltic magmas in the continental crust. According to Holness
19
20 545 & Bunbury (2006), the co-genetic enclaves occur in the magma chamber emplaced beneath
21
22 546 the KVF but in the crust. However, Spera (1984); Aldanmaz et al. (2005); Demouchy et al.
23
24 547 (2006); Tang et al. (2006); Davis et al. (2007); Meng et al. (2015) and (Sun et al., 2018)
25
26 548 suggest that the presence of xenoliths and/or xenocrysts implies rapid ascent of magmas
27
28 549 without significant interaction with the crust. As the melts containing comagmatic enclaves
29
30 550 rise into the crust after extraction from the magma chambers in the lithospheric mantle, the
31
32 551 exsolution of volatiles increases, resulting in bulk magma volume expansion and the
33
34 552 demolition of the conduit wall-rock (Sun et al., 2018). This process explains the abundance
35
36 553 of the crustal xenoliths, such as granite, marble, schist, gneiss and migmatite, in the volcanic
37
38 554 deposits of the KVF. Crustal xenoliths having low-temperature minerals in the Kula lavas
39
40 555 and pyroclastics (Bayhan et al., 2002) suggest rapid ascent, thus avoiding remarkable
41
42 556 assimilation with crustal materials. These views are further supported by the presence of
43
44 557 embayed crystals indicating rapid changes in P-T conditions of magma batches. For
45
46 558 instance, embayed phlogopite, hornblende and olivine crystals are observed in Phl-
47
48 559 clinopyroxenite and wehrlite in Kula (Fig. 6). These embayed minerals may occur as a result
49
50 560 of partial melting of hydrous minerals due to decompression (Green et al., 1968; Francis,
51
52 561 1987; Grützner et al., 2013). In addition, the release of exsolved fluids from ascending

1
2
3 562 magma within the cumulate mush may also lead to reactions with pre-existing crystals and
4
5 563 producing hydrous phases such as phlogopite microcrysts mantling the olivine, observed in
6
7 564 BIII basalt. Furthermore, the presence of glass, including merged vesicles, implies that
8
9 565 enclaves experienced a decrease in pressure as the magma ascends rapidly to the surface.
10
11 566 Grützner et al. (2013) calculated the ascent rate of the magma from Moho to surface as 4–
12
13 567 11 days.
14
15
16
17 568
18
19 569

9.3.Thermobarometry

20
21 570 The textural properties indicate that the lava and enclaves may have a simple history of
22
23 571 cooling and heating before reaching the surface. Fresh and stable mineral assemblages
24
25 572 were selected, which were in equilibrium with the host magma. Clinopyroxene is ubiquitous
26
27 573 in both host rocks and enclaves. The crystallisation temperature and pressure of
28
29 574 clinopyroxene were estimated on the basis of Putirka (2008) equation 33, and Neave &
30
31 575 Putirka (2017), respectively. The whole rock and glass compositions were regarded as liquid
32
33 576 compositions, and the tests for equilibrium based on Putirka (1999) has been employed to
34
35 577 get more plausible estimates from Cpx-thermometer model (Fig. 12).
36
37
38 578 Therefore, only the Cpx compositions having $K_D^{(Fe-Mg)}$ values between 0.20 and 0.36 that fell
39
40 579 within the expected equilibrium range [$K_D^{(Fe-Mg)} = 0.28 \pm 0.08$] based on Putirka (2008), and
41
42 580 the values (the difference between predicted and observed DiHd) approaching zero, were
43
44 581 used. The diagram given here covers only predicted and observed DiHd
45
46 582 (diopside+heedenbergite) components, with the one-to-one line having an accepted deviation
47
48 583 of 10% (Mollo et al., 2015; Polo et al., 2017) (Suppl. Table 11).
49
50
51 584 Cpx-liquid (whole rock composition) thermobarometer yields the crystallisation temperature
52
53 585 and pressure for BI, BII and BIII lava flows at 1217–1231°C (average of 1227°C) and 9.5–
54
55 586 10.0 kbar (average of 9.8 kbar), 1130–1242°C (average of 1208°C) and 9.5–15.4 kbar
56
57
58
59
60

1
2
3 587 (average of 12.8 kbar) and 1149-1227°C (average of 1193°C) and 9.4-14.3 kbar (average
4 of 12.7 kbar), respectively ([Suppl. Table 11](#)).
5
6 588
7
8 589 Cpx-liquid thermobarometry was used for the enclaves, based on both Cpx-whole rock and
9
10 590 Cpx-co-existing glass pairs. Temperature and pressure estimates, based on the
11 compositions of Cpx and co-existing glass, give the following values: 1138-1200°C, 14.2-
12 591
13 592 18.8 kbar for wehrlite; 1148-1199°C, 25.2-27.6 kbar for Phl-clinopyroxenite; 1134-1206°C,
14
15 593 14.4-21.4 kbar for Cpx-hornblendite; and 1026-1034°C, 14.2-15.7 kbar for Hbl-gabbro.
16
17 593
18
19 594 However, estimates based on Cpx-whole rock composition yield higher temperatures but
20
21 595 lower pressures relative to the Cpx-glass composition pairs. In other words, temperature
22
23 and pressure estimates based on Cpx and co-existing glass compositions indicate the
24 596 different source regions. The inconsistency between the probable source characteristics
25
26 597 might originate from the analysed glasses, resulting from decompression-induced partial
27
28 598 melting of hydrous minerals such as amphibole and phlogopite ([Fig. 6f-h](#)).
29
30 599
31 600 BI basalts are the first products of the Kula volcanism, which developed as a result of crustal
32
33 600 thinning caused by mantle uplift in the Selendi basin on horst about 1.2 Ma ago. P-T
34
35 601 calculations indicate shallower sources (~ 30-36 km) for BI stage compared to other stages.
36
37 602
38 602 The BII and BIII stages have relatively the deeper origins. As the heat from the upwelling
39
40 603 asthenosphere rises ([Prelevic et al., 2012](#)), it might produce the initial melts of the spinel-
41
42 604 bearing BII and BIII basalts. Thus, the depth of the partial melting point may shift to a deeper
43
44 605 source from 30 to 50 km ([Fig. 12](#)). Most of the enclaves ranging from Phl-bearing wehrlite
45
46 606 to hornblendite are found in the base surge deposits of the M3 tuff ring (BII). In contrast to
47
48 607 lava flows of the BI and BIII stages, the P-T analyses of the Cpx minerals of a fusiform bomb
49
50 608 covering the wehrlite yield crystallisation temperatures of 1174-1260°C and pressures of 13-
51
52 609 19.5 kbar, which corresponds to depths of ~42-63 km in the lithosphere. These depths are
53
54 609
55 610 19.5 kbar, which corresponds to depths of ~42-63 km in the lithosphere. These depths are
56
57 611 generally compatible with the T-P conditions of the enclaves.
58
59 611
60

1
2
3 612 The ascending melts needs to stall at depths of the lithospheric mantle to form various
4 ultramafic enclaves. So, the alkaline basaltic melts, enriched with volatiles, migrate upwards
5 from the source region by percolating into the lithosphere to form a magma storage such as
6 small magma chambers and/or feeder dykes ([Grützner et al., 2013](#)) or lens-shaped masses
7
8 614 (i.e. "sill-like" [Hollnes & Bunbury, 2006](#)). According to P-T graph ([Fig. 12](#)), the magma
9 storage depths calculated from Cpx-liquid (whole rock composition) are between about 38-
10 615 59 km for hornblendite (BII), 46-50 km for Phl-clinopyroxenite (BII), 39-48 km for Cpx-
11
12 616 hornblendite (BII), and 36-42 km for Hbl-gabbro (BIII). The melting temperature notably
13 controls the MgO and Al₂O₃ content of a melt ([Pilet et al., 2010](#)). High TiO₂ (1.81-4.19 wt.%),
14
15 617 Al₂O₃ (14.6-18.2 wt.%) and low MgO (5.4-12.1 wt.%) contents point out the involvement of
16 a non-peridotite source, possibly an amphibole-bearing pyroxenite. Residual amphibole can
17
18 618 be attributed to melting near the asthenosphere-lithosphere boundary and/or under
19 619 lithospheric conditions ([Mayer et al., 2013](#)), since amphibole is not stable above ~100 km
20
21 620 (Pilet et al., 2008). The calculated pressures correspond to depths of approximately 36 to
22
23 621 63 km, suggesting the crystallisation under lithospheric mantle conditions.
24
25 622 In the light of the data, the evolution of Kula volcanism resulting from asthenospheric uplift
26
27 623 can be summarized as follows ([Fig. 13](#)):
28
29 624 I. Kula host basalts and enclaves most likely originated from a mixed garnet and spinel
30 peridotite source in the presence of amphibole and lesser phlogopite, indicating
31
32 625 metasomatic enrichment processes during their genesis.
33
34 626 II. The Kula Rift Volcanism is a sodic alkaline volcanism developed within the Gediz
35 Graben of the Western Anatolian Graben system. The first basaltic phase started to
36 produce lava flows about 1.2 Ma ago. These lava flows are cut by normal faults in the
37 form of staircases after settling and descending into the graben. Although [Richardson-](#)
38
39 633 [Bunbury \(1996\)](#) obtained Ar-Ar ages from the amphiboles of these lava flows, we did
40 634 not encounter any minerals indicating the presence of aqueous phases in these lavas
41
42 635
43
44 636
45
46 637

1
2
3 638 during our extensive sampling. Our clinopyroxene geobarometer calculations indicate
4
5 639 that the crystallization occurred at a depth of 30-36 km, which is the lower crust and
6
7 640 lithospheric mantle transition level. We did not encounter any basic or ultrabasic
8
9 641 enclaves in these basaltic lava flows that were formed during a dry phase. Therefore,
10
11 642 we accept that these lavas originated from sub-crustal magma settlements, which
12
13 643 probably also contributed to the uplift.
14
15 643
16

17 644 III. The petrographic and compositional study of the enclaves has shown that Kula
18
19 645 enclaves record multistage fractional crystallisation histories involving the migration of
20
21 646 melts and aqueous fluids from asthenosphere and/or lithosphere-asthenosphere
22
23 647 interaction levels. Wehrlite, Cpx-hornblendite, and hornblendite enclaves are abundant
24
25 648 in the second phase-basalts. According to geobarometer calculations, the
26
27 649 crystallization depths of these enclaves are between 40-55 km, while Cpx from host
28
29 649 basalts exhibits a wide range of crystallization depths, as 38-60 km. While Cpx-
30
31 650 hornblendite, hornblendite, and Hbl-gabbro enclaves are commonly encountered in the
32
33 651 third-stage basalts, the crystallization depths obtained from these enclaves indicate
34
35 652 shallower depths (35-43 km) compared to other stage enclaves.
36
37 653
38 653
39

40 654 IV. The most striking features of enclaves are that they are as fresh as the host rock, show
41
42 655 no deformation, and contain vesiculated interstitial glass. With these features, we can
43
44 656 say that enclaves and host basalts originated from the same source and rose rapidly
45
46 657 with the lava. As the phases progress from the second to the third stage, magma
47
48 658 chambers in the lithospheric mantle get closer to the surface.
49
50 658
51 659 V. The tectonic regime that created the rift is still active, and considering the very young
52
53 660 products of the third phase, we suggest that a volcanic eruption may occur in the near
54
55 661 future.
56
57
58 662
59
60 663

ACKNOWLEDGEMENTS

1
2
3 664 This research was supported by TÜBİTAK (Scientific and Technical Research Council of
4 Turkey), within the cadre of project YDABCAG-398, the Scientific Research Unit of
5
6 665 Hacettepe University (project T07 604 002) and by the French Embassy in Ankara (French
7
8 666 Ministere des Afaires Etrangères). Part of this research is compiled from the PhD thesis of
9
10 667 Erdal Şen. We are grateful to anonymous reviewers for their constructive comments which
11
12 668 greatly improved the manuscript. We extend our special appreciation to Editor Dr. Federico
13
14 669 Rossetti for his expertise and attention.
15
16
17 670
18
19 671
20
21 672
22
23
24 673
25
26 674
27
28
29 675
30
31 676
32
33 677
34
35 678
36
37
38 679
39
40 680
41
42 681
43
44
45 682
46
47 683
48
49 684
50
51 685
52
53
54 686
55
56 687
57
58 688
59
60 689

REFERENCES

- 1
2
3 690
4
5 691 Agostini S., Doglioni, C., Innocenti F., Manetti P., Tonarini S., Savaşçın M.Y. (2007) – The
6 transition from subduction-related to intraplate Neogene magmatism in the Western
7 Anatolia and Aegean area. In Beccaluva, L., Bianchini, G., and Wilson, M., eds., Cenozoic
8 Volcanism in the Mediterranean Area: Geological Society of America Special Paper 418,
9 1–15, [https://doi.org/10.1130/2007.2418\(01\)](https://doi.org/10.1130/2007.2418(01))
- 10 693
11
12 694
13
14 695
15
16
17 696 Aldanmaz E., Gourgaud A., Kaymakçı N. (2005) - Constraints on the composition and
18 thermal structure of the upper mantle beneath NW Turkey: Evidence from mantle
19 697 xenoliths and alkali primary melts. J. Geodyn., 39, 277-316.
20
21 698
22
23
24 699 <https://doi.org/10.1016/j.jog.2005.01.002>
25
26 700 Aldanmaz E., Pearce J. A., Thirlwall M.F., Mitchell J.G. (2000) - Petrogenetic evolution of
27 late Cenozoic, post-collision volcanism in western Anatolia, Turkey. J. Volcanol.
28
29 701
30
31 702 Geotherm., 102, 67-95.
32
33 703 Alıcı P., Temel A., Gourgaud A. (2002) - Pb-Nd-Sr isotope and trace element geochemistry
34
35 704 of Quaternary extension-related alkaline volcanism: a case study of Kula region (western
36 Anatolia, Turkey). J. Volcanol. Geotherm., 115, 487-510.
37
38 705
39
40 706 Alıcı P., Temel A., Gourgaud A., Kiefer G., Gündoðdu M.N. (1998) - Petrology and
41 geochemistry of potassic rocks in the Gölcük area (Isparta, SW Turkey): genesis of
42 707 enriched alkaline magmas. J. Volcanol. Geotherm., 85, 423–446.
43
44
45 708
46
47 709 Angelier J., Dumont J. F., Karamanderesi H., Poisson A., Simsek S., Uysal S. (1981) -
48 Analyses of fault mechanism an expansion of southwestern Anatolia since the Late
49 710 Miocene. Tectonophysics, 75, T1-T9.
50
51 711
52
53
54 712 Artemieva I.M. & Shulgin A. (2019) - Geodynamics of Anatolia: Lithosphere thermal structure
55 and thickness. Tectonics, 38, 4465-4487. <https://doi.org/10.1029/2019TC005594>
56
57
58
59
60

- 1
2
3 714 Baker J.A., Menzies M.A., Thirlwall M.F., Macpherson C.G. (1997) - Petrogenesis of
4
5 715 Quaternary intraplate volcanism, Sana'a, Yemen: implications for plume–lithosphere
6
7 716 interaction and polybaric melt hybridization. *J. Petrol.*, 38, 1359–1390.
8
9
10 717 Bayhan H., Aydar E., Şen E. Gourgaud A. (2006) - Melting of crustal xenoliths within
11
12 718 ascending basalt: Example from the Kula volcanic field, western Anatolia, Turkey. *C. R.
13
14
15 Geosci.*, 338/4, 237-243.
16
17 720 Bozkurt E. (2001) - Neotectonics of Turkey—a synthesis. *Geodin. Acta*, 14, 3–30.
18
19 721 Bozkurt E. (2003) - Origin of NE-trending basins in western Turkey, *Geodin. Acta*, 16, 2–6,
20
21 722 61-81. [https://doi.org/10.1016/S0985-3111\(03\)00002-0](https://doi.org/10.1016/S0985-3111(03)00002-0).
22
23
24 723 Bozkurt E. & Park R. (1997) - Microstructures of deformed grains in the augen gneisses of
25
26 724 southern Menderes Massif (western Turkey) and their tectonic significance. *Geol
27
28 Rundsch*, 86, 103–119. <https://doi.org/10.1007/s005310050125>
29
30
31 726 Bozkurt E. & Sözbilir H. (2004) - Tectonic evolution of the Gediz Graben: field evidence for
32
33 727 an episodic, two stage extension in western Turkey, *Geol. Mag.*, 141, 63-79.
34
35 728 Bozkurt E. & Mittwede S. (2005) - Introduction: Evolution of continental extensional tectonics
36
37
38 729 of western Turkey. *Geodin. Acta*, 18, 153-165. 10.3166/ga.18.153-165.
39
40 730 Bozkurt E. & Rojay B. (2005) - Episodic, two-stage Neogene extension and short-term
41
42 731 intervening compression in Western Turkey: field evidence from the Kiraz Basin and
43
44 732 Bozdağ Horst, *Geodin. Acta*, 18:3-4, 299-316, DOI: 10.3166/ga.18.299-316
45
46
47 733 Bunbury J.M.R. (1996) - The Kula Volcanic Field, western Turkey: the development of a
48
49 734 Holocene alkali basalt province and the adjacent normal-faulting graben. *Geol. Mag.*, 133
50
51 735 (3), 275-283
52
53
54 736 Bunbury J.M., Hall L., Anderson G.J., Stannard A. (2001) - The determination of fault
55
56 737 movement history from the interaction of local drainage with volcanic episodes. *Geol.
57
58
59 738 Mag.*, 138, 185-192
60

- 1
2
3 739 Cohen H.A., Dart C.J., Akyüz H.S., Barka A.A. (1995) - Syn-rift sedimentation and structural
4 development of the Gediz and Büyük Menderes grabens, western Turkey. *J. Geol. Soc.*,
5 740 London 152, 629-638.
6
7
8 741
9
10 742 Çiftçi B. & Bozkurt E. (2009) - Pattern of normal faulting in the Gediz Graben, SW Turkey.
11
12 743 *Tectonophysics*, 473, 234-260. <https://doi.org/10.1016/j.tecto.2008.05.036>
13
14 744 Çoban H., Karacık Z. Ece Ö.I. (2012) - Source contamination and tectonomagmatic signals
15 of overlapping Early to Middle Miocene orogenic magmas associated with shallow
16 continental subduction and asthenospheric mantle flows in Western Anatolia: A record
17 745
18
19 746 from Simav (Kütahya) region. *Lithos*, 140-141, 119-141.
20
21 747
22
23
24 748 Davis A.S., Clague D.A., Paduan J.B. (2007) - Diverse Origins of Xenoliths from Seamounts
25
26 749 at the Continental Margin, Offshore Central California. *J. Petrol.*, 48 (5), 829-852.
27
28 750 Demouchy S., Jacobsen S. D., Gaillard F., Stern C. R. (2006) - Rapid magma ascent
29 recorded by water diffusion profiles in mantle olivine. *Geology*, 34, 429–432.
30
31 751
32
33 752 Dewey J.F. & Şengör A.M.C. (1979) - Aegean and surrounding regions: complex multiplate
34 and continuum tectonics in a convergent zone. *Geol. Soc. Amer. Bull.*, 90, 84-92.
35 753
36
37 754 Doglioni C., Agostini S., Crespi M., Innocenti F., Manetti P., Riguzzi F., Savasçı Y. (2002) -
38
39 On the extension in western Anatolia and the Aegean Sea. *J. Virtual Explor.*, 8, 169-183.
40 755
41
42 756 <https://doi.org/10.3809/jvirtex.2002.00049>
43
44
45 757 Elkins L.J., Gaetani G.A., Sims K.W.W. (2008) - Partitioning of U and Th during garnet
46 pyroxenite partial melting: Constraints on the source of alkaline ocean island basalts,
47 758
48
49 759 *Earth Planet. Sci. Lett.*, 265, 1–2, 270-286. <https://doi.org/10.1016/j.epsl.2007.10.034>
50
51 760 Emre T. & Sözbilir H. (2007) - Tectonic evolution of the Kiraz Basin, Küçük Menderes
52
53 Graben: evidence for compression/uplift-related basin formation overprinted by
54 761
55 extensional tectonics in West Anatolia. *Turk. J. Earth Sci.*, 16, 441–470.
56 762
57
58 763 Ercan T., Dinçel A., Metin S., Türkcan A., Günay E. (1978) - Uşak yöresindeki Neojen
59
60 764 havzaların jeolojisi. *TJK Büll.*, c.21, 97-106.

- 1
2
3 765 Ercan T., Türkcan A., Dinçel A., Erdoğdu G. (1983) - Kula-Selendi (Manisa) Dolaylarının
4
5 766 Jeolojisi. Jeoloji Müh. Derg., 173-28.
6
7
8 767 Erkül F., Helvacı C., Sözbilir H. (2005) - Evidence for two episodes of volcanism in the
9
10 768 Bigadic borate basin and tectonic implications for western Turkey. Geol. J., 40, 545–570.
11
12 769 EROS (2018) - Shuttle Radar Topography Mission (SRTM) 1 Arc-Second Global. Earth
13
14 770 Resources Observation and Science Center (EROS). U.S. Geological Survey.
15
16
17 771 <https://doi.org/10.5066/F7PR7TFT>
18
19 772 Ersoy E.Y. (2013) - PETROMODELER (Petrological Modeler): A Microsoft® Excel©
20
21 773 spreadsheet program for modeling melting, mixing, crystallisation and assimilation
22
23
24 774 processes in magmatic systems. Turk. J. Earth Sci., 22, 115-125.
25
26 775 Ersoy Y. & Helvacı C. (2007) - Stratigraphy and geochemical features of the Early Miocene
27
28 776 bimodal (ultrapotassic and calc-alkaline) volcanic activity within the NE-trending Selendi
29
30
31 777 basin, western Anatolia, Turkey. Turk. J. Earth Sci., 16, 117-139.
32
33 778 Ersoy Y., Helvacı C., Sözbilir H. (2010) - Tectono-stratigraphic evolution of the NE–
34
35 779 SWtrending superimposed Selendi basin: implications for late Cenozoic crustal extension
36
37
38 780 in Western Anatolia. Tectonophysics, 488, 210–232.
39
40 781 Ersoy Y., Helvacı C., Palmer M.R. (2011) - Stratigraphic, structural and geochemical
41
42 782 features of the NE–SW trending Neogene volcano-sedimentary basins in western
43
44 783 Anatolia: Implications for associations of supra-detachment and transtensional strike-slip
45
46
47 784 basin formation in extensional tectonic setting. J. Asian Earth Sci., 41, 159–183.
48
49 785 Ersoy E.Y., Helvacı C., Palmer M.R. (2012) - Petrogenesis of the Neogene volcanic units in
50
51 786 the NE-SW-trending basins in western Anatolia, Turkey. Contrib. to Mineral. Petrol., 163,
52
53
54 787 379–401.
55
56 788 Ersoy Y., Helvacı C., Sözbilir H., Erkül F., Bozkurt E. (2008) - A geochemical approach to
57
58 789 Neogene–Quaternary volcanic activity of western Anatolia: an example of episodic
59
60 790 bimodal volcanism within the Selendi Basin, Turkey. Chem. Geol., 255, 265–282.

- 1
2
3 791 Foley S., Musselwhite D., van der Laan, S.R. (1999) - Melt compositions from ultramafic
4
5 792 vein assemblages in the lithospheric mantle: a comparison of cratonic and non-cratonic
6
7 793 settings. In J. J. Gurney (Ed.), Proceedings of the 7th International Kimberlite Conference
8
9
10 794 (Vol. 1, pp. 238-246). Red Roof Design.
11
12 795 Francis D. M. (1987) - Mantle-melt interaction recorded in spinel lherzolite xenoliths from the
13
14 796 Alligator Lake volcanic complex, Yukon, Canada, *J. Petrol.*, 28, 569 – 597.
15
16
17 797 Furman T. & Graham D. (1999) - Erosion of lithospheric mantle beneath the East African
18
19 798 Rift system: evidence from the Kivu volcanic province. *Lithos*, 48, 237-262.
20
21 799 Furman T., Bryce J. G., Karson J. Lotti A. (2004) - East African Rift System (EARS) Plume
22
23
24 800 Structure: Insights from Quaternary Mafic Lavas of Turkana, Kenya. *J. Petrol.*, 45 (5),
25
26 801 1069-1088.
27
28 802 Georgatou A.A. & Chiaradia M. (2020) – Magmatic sulphides in high-potassium calc-alkaline
29
30
31 803 to shoshonitic and alkaline rocks. *Solid Earth*, 11, 1-21, <https://doi.org/10.5194/se-11-1-2020>
32
33 804
34
35 805 Gessner, K., Markwitz, V., Güngör, T. (2018) - Crustal fluid flow in hot continental extension:
36
37
38 806 tectonic framework of geothermal areas and mineral deposits in western Anatolia.
39
40 807 Geological Society, London, Special Publications, 453 (1): 289-311.
41
42 808 <https://doi.org/10.1144/SP453.7>
43
44
45 809 Gessner, K., Gallardo, L.A., Markwitz, V., Ring, U., Thomson, S.N. (2013) - What caused
46
47 810 the denudation of the Menderes Massif: Review of crustal evolution, lithosphere structure,
48
49 811 and dynamic topography in southwest Turkey. *Gondwana Res.*, 24 (1), 243-274.
50
51 812 Gessner K., Ring U., Johnson C., Hetzel R., Passchier C. W., Güngör T. (2001) - An active
52
53
54 813 bivergent rolling-hinge detachment system: Central Menderes metamorphic core
55
56 814 complex in western Turkey. *Geology*, 29, 611-614.
57
58
59 815 Green D.H., Morgan J.W. Heier K. S. (1968) - Thorium, uranium and potassium abundances
60
816 in peridotite inclusions and their host basalts, *Earth Planet. Sci. Lett.*, 4, 155-166.

- 1
2
3 817 Grützner T., Prelevic D. Akal C. (2013) - Geochemistry and origin of ultramafic enclaves and
4
5 818 their basanitic host rock from Kula Volcano, Turkey. *Lithos* 180-181, 58-73.
6
7
8 819 Güleç N. (1991) - Crust-mantle interaction in Western Turkey: implications from Sr and Nd
9
10 820 isotope geochemistry of Tertiary and Quaternary volcanics. *Geol. Mag.*, 128 (5), 417-435.
11
12 821 Haase K.M., Mühe R. Stoffers P. (2000) - Magmatism during extension of the lithosphere:
13
14 822 geochemical constraints from lavas of the Shaban Deep, northern Red Sea. *Chem. Geol.*,
15
16 823 166, 225-239.
17
18
19 824 Hakyemez H. Y., Göktaş F., & Erkal T. (2013) - Quaternary Geology and Evolution of the
20
21 825 Gediz Graben. *Geol. Bull. of Turkey*, 56, 1-26.
22
23
24 826 Heineke C., Niedermann S., Hetzel R., Cüneyt Akal C. (2016) - Surface exposure dating of
25
26 827 Holocene basalt flows and cinder cones in the Kula volcanic field (Western Turkey) using
27
28 828 cosmogenic ^{3}He and ^{10}Be . *Quat. Geochronol.*, 34, 81-91.
29
30
31 829 <https://doi.org/10.1016/j.quageo.2016.04.004>
32
33 830 Helvacı C. (1995) - Stratigraphy, mineralogy, and genesis of the Bigadiç borate deposits,
34
35 831 western Turkey. *Econ. Geol.*, 90, 1237-1260.
36
37
38 832 Helvacı C. & Yağmurlu F. (1995) - Geological setting and economic potential of the lignite
39
40 833 and evaporite- bearing Neogene basins of Western Anatolia, Tur- key. *Isr. J. Earth Sci.*,
41
42 834 Vol. 44, 91-105.
43
44
45 835 Hetzel, R., H. Zwingmann, A. Mulch, K. Gessner, C. Akal, A. Hampel, T. Güngör, R.
46
47 836 Petschick, T. Mikes and F. Wedin (2013) - Spatiotemporal evolution of brittle normal
48
49 837 faulting and fluid infiltration in detachment fault systems: A case study from the Menderes
50
51 838 Massif, western Turkey, *Tectonics*, 32, 364–376, <https://doi.org/10.1002/tect.20031>
52
53
54 839 Hofmann A.W., Jochum K.P., Seufer M., White, W.M. (1986) - Nb and Pb in oceanic basalts:
55
56 840 new constraints on mantle evolution. *Earth Planet. Sci. lett.*, 79, 33-45.
57
58
59
60

- 1
2
3 841 Holness M.B. & Bunbury, J.M. (2006) - Insights into continental rift-related magma
4 chambers: Cognate nodules from the Kula Volcanic Province, Western Turkey. *J.*
5
6 842 *Volcanol. Geotherm.*, 153, 241-261.
7
8 843
9
10 844 Holness M.B., Cheadle M.J., Mckenzie D. (2005) - On the Use of Changes in Dihedral Angle
11
12 845 to Decode Late-stage Textural Evolution in Cumulates. *J. Petrol.*, 46, 8, 1565-1583.
13
14
15 846 Innocenti F., Agostini S., Di Vincenzo, G., Doglioni, C., Manetti, P., Savaşçın, M.Y. Tonarini,
16
17 847 S. (2005) - Neogene and Quaternary volcanism in Western Anatolia: magma sources and
18
19 848 geodynamic evolution. *Mar. Geol.*, 221, 397-421.
20
21 849 Ionov D.A., Griffin W.L., O'Reilly S.O. (1997) - Volatile-bearing minerals and lithophile trace
22
23 elements in the upper mantle. *Chem. Geol.* 141, 153–184.
24 850
25
26 851 Ionov D.A. & Hofmann A.W. (1995) - Nb-Ta-rich mantle amphiboles and micas: implications
27
28 852 for subduction-related metasomatic trace element fractionations. *Earth Planet. Sci. Lett.*,
29
30
31 853 131 (3–4), 341–356.
32
33 854 Işık V., Tekeli O., Seyitoğlu G. (2004) - The 40Ar/39Ar age of extensional ductile deformation
34
35 855 and granitoid intrusions in the northern Menderes core complex: Implications for the
36
37 initiation of extensional tectonics in western Turkey. *J. Asian Earth Sci.*, 23, 555-566.
38 856
39
40 857 Jolivet, L., Faccenna,C.et al. (2013) - Aegean tectonics: strain localisation, slab tearing and
41
42 858 trench retreat, *Tectonophysics*, 597, 1–33.
43
44
45 859 Jung S. & Masberg P. (1998) - Major-and trace-element systematics and isotope
46
47 860 geochemistry of Cenozoic mafic volcanic rocks from the Vogelsberg (central Germany):
48
49 861 Constraints on the origin of continental alkaline and tholeiitic basalts and their mantle
50
51 862 sources. *J. Volcanol. Geotherm.*, 86, 151-177.
52
53
54 863 Jung S., Vieten K., Romer R.L., Mezger K., Hoernes S., Satır M. (2012) - Petrogenesis of
55
56 864 Tertiary Alkaline Magmas in the Siebengebirge, Germany. *J. Petrol.*, 53 (11), 2381-2409,
57
58 865
59 <https://doi.org/10.1093/petrology/egs047>

- 1
2
3 866 Karaoğlu Ö., Helvacı C., Ersoy E.Y. (2010) - Petrogenesis and 40Ar/39Ar geochronology of
4
5 867 the volcanic rocks of the Usak–Güre basin, western Türkiye. *Lithos*, 119, 193–210.
6
7
8 868 Khudoley A.K., Prokopiev A.V., Chamberlain K.R., Ernst R.E., Jowitt S.M., Malyshev S.V.,
9
10 869 Zaitsev A.I., Kropachev A.P. Koroleva O.V. (2012) - Early Paleozoic mafic magmatic
11
12 870 events on the eastern margin of the Siberian Craton. *Lithos*, 174, 44–56.
13
14
15 871 Koçyiğit A. (2005) - The Denizli graben-horst system and the eastern limit of western
16
17 872 Anatolian continental extension: Basin fill, structure, deformational mode, throw amount
18
19 873 and episodic evolutionary history, SW Turkey. *Geodin. Acta – Geodin. Acta.* 18., 167–
20
21 874 208. <https://doi.org/10.3166/ga.18.167-208>
22
23
24 875 Langmuir C.H., Vocke R.D., Hanson G.N. Hart S.R. (1978) - A general mixing equation with
25
26 876 applications to Icelandic basalts. *Earth Planet. Sci. Lett.*, 37, 380–392.
27
28
29 877 Le Bas, M.J., Le Maitre, R.W., Streckeisen, A. Zanetti, B. (1986) - A chemical classification
30
31 878 of volcanic rock based on the total alkali - silica diagram. *J. Petrol.*, 27, 745–750.
32
33 879 Leake B.E., Woolley A.R., Arps C.E.S., Birch W.D., Gilbert M.C., Grice, J.D., Hawthorne,
34
35 880 F.C., Kato A., Kisch H.J., Krivovichev VG., Linthout K., Laird J., Mandarino J., Maresch,
36
37 881 W.V., Nickel, E.H., Rock N.M.S. Schumacher J.C., Smith D.C., Stephenson N.C.N.,
38
39 882 Ungaretti L., Whittaker E.J.W., Youzhi G. (1997) - Nomenclature of amphiboles; Report
40
41
42 883 of the Subcommittee on Amphiboles of the International Mineralogical Association
43
44 884 Commission on New Minerals and Mineral Names, *Eur. J. Mineral.*, 9, 623–651.
45
46
47 885 Lips A., Cassard D. Sözbilir H., Yılmaz H. Wijbrans J.R. (2001) - Multistage exhumation of
48
49 886 the Menderes Massif, Western Anatolia (Turkey). *Int. J. Earth Sci.*, 89, 781–792.
50
51 887 <https://doi.org/10.1007/s005310000101>
52
53
54 888 Maddy, D., Schreve, D., Demir, T., Veldkamp, A., Wijbrans, J.R., van Gorp, W., van
55
56 889 Hinsbergen, D.J.J., Dekkers, M.J., Scaife, R., Schoorl, J.M., Stemerdink, C., van der
57
58 890 Schriek, T., (2015) - The earliest securely-dated hominin artefact in Anatolia?, *Quat. Sci.*
59
60 891 Rev., 109, 68–75. <https://doi.org/10.1016/j.quascirev.2014.11.021>

- 1
2
3 892 Mahatsente R., Alemdar S., Çemen I. (2017) - "Effect of slab-tear on crustal structure in
4
5 893 Southwestern Anatolia: insight from gravity data modeling," in Neotectonics and
6
7 894 Earthquake Potential of the Eastern Mediterranean Region, Geophysical Monograph
8
9 10 895 Series, American Geophysical Union.
11
12 896 Mayer B., Jung S., Romer R.L., Stracke A., Haase K.M., Garbe-Schönberg, C.D. (2013)
13
14 15 897 Petrogenesis of Tertiary hornblende-bearing lavas in the Rhön, Germany, *J. Petro.*, 54,
16
17 18 898 2095-2123. <https://doi.org/10.1016/j.lithos.2021.106431>
19 899 McDonough W.F. (1990) - Constraints on the composition of the continental lithospheric
20
21 900 mantle. *Earth Planet. Sci. Lett.*, 101, 1-18.
22
23
24 901 McKenzie D. (2020) - The structure of the lithosphere and upper mantle beneath the Eastern
25
26 902 Mediterranean and Middle East. *Med. Geosc. Rev.*, 2, 311–326.
27
28 903 <https://doi.org/10.1007/s42990-020-00038-1>
29
30
31 904 McKenzie D.P. & O'Nions R.K. (1991) - Partial melt distributions from inversion of rare earth
32
33 905 element concentrations. *J. Petrol.*, 32, 1021-1091.
34
35 906 Meng F., Gao S., Niu Y., Liu Y. Wang X. (2015) - Mesozoic-Cenozoic mantle evolution
36
37 907 beneath the North China Craton: A new perspective from Hf–Nd isotopes of basalts.
38
39
40 908 *Gondwana Res.*, 27, 4, 1574-1585. <https://doi.org/10.1016/j.gr.2014.01.014>
41
42 909 Miyashiro A. (1978) - Nature of alkalic volcanic rock series. *Contrib. Mineral. Petrol.*, 66, 91-
43
44 910 104.
45
46
47 911 Mollo S., Giacomoni P.P., Coltorti M., Ferlito C., Lezzi G., Scarlato P. (2015) -
48
49 912 Reconstruction of magmatic variables governing recent Etnean eruptions: constraints
50
51 913 from mineral chemistry and P–T–fO₂–H₂O modeling. *Lithos*, 212–215, 311–320.
52
53
54 914 Morimoto N., Fabries J., Ferguson A., Ginzburg I., Roos M., Seifert F., Zussman J. (1988) -
55
56 915 Nomenclature of pyroxenes, *Bull. Mineral.*, 111, 535-550.
57
58
59
60

- 1
2
3 916 Moufti M.R., Moghazi A.M., Ali K.A. (2012) - Geochemistry and Sr–Nd–Pb isotopic
4 composition of the Harrat Al-Madinah Volcanic Field, Saudi Arabia, *Gondwana Res.*, 21,
5 917 670-689.
6
7
8 918 670-689.
9
10 919 Nakamura N. (1974) - Determination of REE, Ba, Fe, Mg, Na and K in carbonaceous and
11 ordinary chondrites. *Geochim. Cosmochim. Acta*, 38, 757-775.
12 920
13
14 921 Neave D. & Putirka K. (2017) - A new clinopyroxene-liquid barometer, and implications for
15 magma storage pressures under Icelandic rift zones. *Am. Min.*, 102: 777-794.
16
17 922
18
19 923 Nikogosian I.K., Bracco Gartner A.J.J., van Bergen M.J., Mason P.R.D., van Hinsbergen,
20 D.J.J. (2018) - Mantle sources of recent Anatolian intraplate magmatism: A regional
21 924 plume or local tectonic origin? *Tectonics*, 37, 4535–4566.
22
23
24 925
25
26 926 <https://doi.org/10.1029/2018TC005219>
27
28 927 Okay A.I., Zattin M, Cavazza W (2010) - Apatite fission-track data for Miocene Arabia-
29 Eurasia collision. *Geology* 38: 35-38
30
31 928
32
33 929 Pasquare G., Poli S., Vezzoli L., Zanchi A. (1988) - Continental Arc Volcanism and Tectonic
34 Setting In Central Anatolia, Turkey. *Tectonophysics*, 146, 1-4, 217-230.
35 930
36
37 931 Pearce J.A. & Cann J.R. (1973) - Tectonic setting of basic volcanic rocks determined using
38 trace element analysis. *Earth Planet. Sci. Lett.*, 19, 290-300.
39
40 932
41
42 933 Pearce J.A. (1983) - The role of subcontinental lithosphere in magma genesis at active
43 continental margins. In: *Continental basalt and Mantle xenoliths*, C. J. Hawkesworth and
44 934 M.J. Nory (eds) 230-249.
45
46
47 935
48
49 936 Pilet S., Baker, M.B., Stolper, E.M. (2008). Metasomatized lithosphere and the origin of
50 alkaline lavas. *Science*, 320, 916-919.
51
52 937
53
54 938 Pilet S., Ulmer P., Villiger, S. (2010) - Liquid line of descent of a basanitic liquid at 1·5 GPa:
55 constraints on the formation of metasomatic veins. *Contrib. to Mineral. Petrol.*, 159, 621-
56 939
57
58 940 643.
59
60

- 1
2
3 941 Polo L.A., Giordano D., Janasi V.A., Guimaraes L.F. (2017) - Effusive silicic volcanism in
4
5 942 Parana Magmatic Province, South Brazil: Physico-chemical conditions of storage and
6
7 943 eruption and considerations on the rheological behavior during emplacement. *J. Volcanol.*
8
9
10 944 *Geotherm.*, 355, 115-135. <https://dx.doi.org/10.1016/j.jvolgeores.2017.05.027>
11
12 945 Prelevic D., Akal C., Foley S.F., Romer R.L., Stracke A., Van Den Bogaard P. (2012) -
13
14 946 Ultrapotassic mafic rocks as geochemical proxies for post-collisional Dynamics of
15
16 947 orogenic lithospheric mantle: the case of southwestern Anatolia, Turkey. *J. Petrol.*, 53 (5),
17
18
19 948 1019–1055. <https://doi.org/10.1093/petrology/egs008>
20
21 949 Putirka K.D. (1999) - Clinopyroxene+liquid equilibrium to 100 kbar and 2450 K. *Contrib. to*
22
23
24 950 *Mineral. Petrol.*, 135, 151-163.
25
26 951 Putirka K.D. (2008) - Thermometers and barometers for volcanic systems. In: Putirka K,
27
28 952 Tepley F (eds) *Minerals, Inclusions and Volcanic Processes, Reviews in Mineralogy and*
29
30
31 953 *Geochemistry*, MSA, 69, 61-120.
32
33 954 Putirka K., Johnson M., Kinzler R., Longhi J., Walker D. (1996) - Thermobarometry of mafic
34
35 955 igneous rocks based on clinopyroxene-liquid equilibria, 0-30 kbar. *Contrib. to Mineral.*
36
37
38 956 *Petrol.*, 123, 92-108.
39
40 957 Purvis M. & Robertson A.H.F. (2004) - Neogene crustal extension in western (Aegean)
41
42 958 Turkey: evidence from the Alaşehir graben and the Selendi and Gördes basins.
43
44
45 959 *Tectonophysics* 391, 171–201.
46
47 960 Ring U. & Layer P. (2003) - High-pressure metamorphism in the Aegean, eastern
48
49 961 Mediterranean: Underplating and exhumation from the Late Cretaceous until the Miocene
50
51
52 962 to Recent above the retreating Hellenic subduction zone. *Tectonics*, 22, 3, 6(1-23).
53
54 963 <https://doi.org/10.1029/2001TC001350>
55
56 964 Rieder M., Cavazzini G., D'Yakonov Yu.S., Frank-Kamenetskii V.A., Gottardi G.,
57
58 965 Guggenheim S., Koval P.V., Müller G., Neiva A.M.R., Radoslovich E.W., Robert J.-L.,
59
60

- 1
2
3 966 Sassi F.P., Takeda H., Weiss Z., Wones D.R. (1998) - International Mineralogical
4
5 967 Association Report: Nomenclature of the micas, *Mineral. Mag.*, 63, 267-279.
6
7 968 Rojay B., Toprak V., Demirci C., Süzen, M. (2005) - Plio-Quaternary evolution of the Küçük
8
9 969 Menderes Graben Southwestern Anatolia, Turkey. *Geodin. Acta.*, 18, 317-331.
10
11 970 10.3166/ga.18.317-331.
12
13
14 971 Rollinson H.R. (1993) - Using geochemical data: evaluation, presentation, interpretation.
15
16
17 972 Longman Scientific and Technical, John Wiley and Sons, Inc., New York, 352p.
18
19 973 Salaün G., Pedersen H.A., Paul A., Farra V., Karabulut H., Hatzfeld D., Papazachos C.,
20
21 974 Childs D.M., Pequegnat C., SIMBAAD Team (2012) - High-resolution surface wave
22
23 975 tomography of the Aegean-Anatolia region: constraints on upper mantle structure,
24
25
26 976 *Geophys. J. Int.*, 190, 406–420. <https://doi.org/10.1111/j.1365-246X.2012.05483.x>
27
28 977 Saunders P., Priestley K., Taymaz T. (1998) - Variations in the crustal structure beneath
29
30 978 western Turkey. *Geophys. J. Int.*, 134, 373–389.
31
32
33 979 Seyitoğlu G. & Scott B.C. (1991) - Late Cenozoic crustal extension and basin formation in
34
35 980 west Turkey. *Geol. Mag.*, 128, 155-166.
36
37
38 981 Seyitoğlu G. & Scott B.C. (1992) - Late Cenozoic volcanic evolution of the NE Aegean
39
40 982 region. *J. Volcanol. Geotherm.*, 54, 157-176.
41
42 983 Seyitoğlu G. & Scott B. C. (1994) - Late Cenozoic basin development in west Turkey. Gordes
43
44 984 basin: tectonics and sedimentation. *Geol. Mag.*, 131, 631-637.
45
46
47 985 Seyitoğlu G. & Scott B.C. (1996) - The cause of N-S extensional tectonics in western Turkey:
48
49 986 Tectonic escape vs Back-arc spreading vs Orogenic collapse. *J. Geodyn.*, 22, 145-153.
50
51 987 Seyitoğlu G. (1997) - Late Cenozoic tectono-sedimentary development of Selendi and Uşak-
52
53 988 Güre basins: a contribution to the discussion on the development of east-west and north-
54
55 989 trending basins in western Turkey. *Geol. Mag.*, 134, 163-175.
56
57
58
59
60

- 1
2
3 990 Seyitoğlu G., Tekeli O., Çemen İ., Şen S., Işık V. (2002) - The role of the flexural
4 rotation/rolling hinge model in the tectonic evolution of the Alaşehir graben, western
5 Turkey. *Geol. Mag.*, 139, 15–26.
6
7
8 992
9
10 993 Seyitoğlu G., Aktuğ B., Esat K., Kaypak B. (2022) - Neotectonics of Turkey (Türkiye) and
11 surrounding regions: a new perspective with block modelling. *Geol. Acta*, 20.4, 1-21.
12 994
13
14 995
15 <https://doi.org/10.1344/GeologicaActa2022.20.4>
16
17 996 Shaw D.M. (1970) - Trace element fractionation during anatexis. *Geochim. Cosmochim.
18
19 997 Acta*, 34, 237-243.
20
21 998 Shaw J.E., Baker J.A., Menzies M.A., Thirlwall M.F., Ibrahim K.M. (2003) - Petrogenesis of
22 the Largest Intraplate Volcanic Field on the Arabian Plate (Jordan): a Mixed Lithosphere–
23
24 999 Asthenosphere Source Activated by Lithospheric Extension. *J. Petrol.*, 44 (9): 1657-1679.
25
26 1000
27
28 1001 Sözbilir H. (2002) - Geometry and origin of folding in the Neogene sediments of the Gediz
29
30 Graben, western Anatolia, Turkey. *Geodin. Acta*, 15, 277-288.
31 1002
32
33 1003 Sözbilir H. (2005) - Oligo-Miocene extension in the Lycian orogen: evidence from the Lycian
34 molasse basin, SW Turkey, *Geodin. Acta*, 18:3-4, 255-282.
35 1004
36
37 1005 <https://doi.org/10.3166/ga.18.255-282>
38
39
40 1006 Sölpüker U. (2007) - Petrology of Kula Volcanic Province, Western Turkey. Dissertation
41 University of Cincinnati (Available online at [http://etd.ohiolink.edu/view.cgi?
42 acc_num=ucin1187013478](http://etd.ohiolink.edu/view.cgi?acc_num=ucin1187013478)).
43
44
45
46
47 1009 Spera F. J. (1984) - Carbon dioxide in petrogenesis III: role of volatiles in the ascent of
48 alkaline magma with special reference to xenolith-bearing mafic lavas. *Contrib. Miner.
49 1010 Petrol.*, 88, 217–232.
50
51
52
53
54 1012 Streckeisen A. (1976) - To each plutonic rock its proper name. *Earth Sci. Rev.*, 12, 1-33.
55
56
57 1013 Sun P., Niu Y., Guo P., Cui H., Ye L. and Liu J. (2018) – The evolution and ascent paths of
58 mantle xenolith-bearing magma: Observations and insights from Cenozoic basalts in
59 Southeast China. *Lithos*, 310–311, 171–181. <https://doi.org/10.1016/j.lithos.2018.04.015>
60
61

- 1
2
3 1016 Şengör A.M.C. (1979) - The North Anatolian transform fault: its age, offset and tectonic
4
5 1017 significance. *J. Geol. Soc.*, 136, 269-282.
6
7 8 1018 Şengör A.M.C. & Yılmaz, Y. (1981) - Tethyan evolution of Turkey: a plate tectonic approach.
9
10 1019 *Tectonophysics*, 75, 181-241.
11
12 1020 Şengör A.M.C. & Yazıcı M. (2020) - The aetiology of the neotectonic evolution of Turkey.
13
14 1021 *Med. Geosc. Rev.*, 2, 327–339. <https://doi.org/10.1007/s42990-020-00039-0>
15
16 1022 Tang Y.J., Zhang H.F., Ying J.F. (2006) - Asthenosphere–lithospheric mantle interaction in
17
18 an extensional regime: Implication from the geochemistry of Cenozoic basalts from
19
20
21 1024 Taihang Mountains, North China Craton. *Chem. Geol.*, 233, 309-327.
22
23
24 1025 Thompson R.N. (1982) - Magmatism of the British Tertiary province. *Scott. J. Geol.*, 18,
25
26 1026 49-107
27
28 1027 Tokçaer M., Agostini S., Savaşçın M.Y. (2005) - Geotectonic setting and origin of the
29
30 youngest Kula volcanics (Western Anatolia), with a new emplacement model. *Turk. J.*
31
32
33 1029 *Earth Sci.* 14, 145–166.
34
35 1030 Tschech C., Ntaflos, T., Akinin V. (2011) - Polybaric petrogenesis of Neogene alkaline
36
37 magmas in an extensional tectonic environment: Viliga Volcanic Field, northeast Russia.
38
39
40 1032 *Lithos*, 122, 13-24.
41
42 1033 Ulusoy İ., Sarıkaya M.A., Schmitt A.K., Şen E., Danišík M., Gümüş E. (2019) - Volcanic
43
44 eruption eye-witnessed and recorded by prehistoric humans, *Quat. Sci. Rev.*, 212, 187-
45
46
47 1035 198. <https://doi.org/10.1016/j.quascirev.2019.03.030>.
48
49 1036 Wang K., Plank T., Walker J. D., Smith E. I. (2002) - A mantle melting profile across the
50
51 1037 Basin and Range, SW USA. *J. Geophys. Res.* 107 (10), 1029-2001.
52
53
54 1038 <https://doi.org/10.1029/2001JB000209>
55
56
57 1039 Wang K.L., Chung S.L., O'Reilly S., Sun S.S., Shinjo R., Chen C.H. (2004) - Geochemical
58
59 Constraints for the Genesis of Post-Collisional Magmatism and the Geodynamic
60
1041 Evolution of the Northern Taiwan Region. *J. Petrol.*, 45 (5), 975-1011.

- 1
2
3 1042 Watson B.E. (1980) - Apatite and phosphorus in mantle source regions: an experimental
4 study of apatite/melt equilibria at pressures to 25 kbar. *Earth Planet. Sci. Lett.*, 51, 322-
5 1043 335.
6
7
8 1044
9
10 045 Westaway R., Pringle M., Yurtmen S., Demir T., Bridgland D., Rowbotham G., Maddy D.
11
12 1046 (2004) - Pliocene and Quaternary regional uplift in western Turkey: The Gediz river
13 terrace staircase and the volcanism at Kula. *Tectonophysics*, 391, 121–169
14
15 1047
16
17 1048 Westaway R., Guillou H., Yurtmen S., Demir T., Scaillet S., Rowbotham G. (2005) -
18 Constraints on the timing and regional conditions at the start of the present phase of
19 1049 crustal extension in western Turkey, from observations in and around the Denizli region.
20
21 1050
22
23 1051 *Geodin. Acta*, 18, 209-238.
24
25
26 1052 Westaway R., Guillou H., Yurtmen S., Beck A., Bridgland D., Demir T., Scaillet, S.,
27
28 1053 Rowbotham G. (2006) - Late Cenozoic uplift of western Turkey: Improved dating of the
29
30 Kula Quaternary volcanic field and numerical modelling of the Gediz river terrace
31 1054
32
33 1055 staircase. *Glob. Planet. Change*, 51, 131–171
34
35 1056 Whitney, D.L. & Evans, B.W. (2010) - Abbreviations for Names of Rock-Forming Minerals.
36
37 1057 American Mineralogist, 95, 185-187. <http://dx.doi.org/10.2138/am.2010.3371>
38
39
40 1058 Wilson M. (1989) - Igneous petrogenesis, Unwin Hyman, London, 466p.
41
42 1059 Worthing M.A. & Nasir S. (2008) - Cambro-Ordovician potassic (alkaline) magmatism in
43
44 1060 Central Oman: Petrological and geochemical constraints on petrogenesis. *Lithos*, 106,
45
46
47 1061 25-38.
48
49 1062 Yaxley G. M., Crawford A.J., Green D.H. (1991) - Evidence for carbonatite metasomatism
50
51 1063 in spinel peridotite xenoliths from western Victoria, Australia. *Earth Planet. Sci. Lett.*, 107,
52
53
54 1064 305-317.
55
56 1065 Yaxley G.M., Kamenetsky V.S., Green D.H., Falloon T.J. (1997) - Glasses in mantle
57
58 1066 xenoliths from western Victoria, Australia, and their relevance to mantle processes, *Earth.*
59
60 1067 *Plan. Sci. Lett.*, 148, 433-446.

- 1
2
3 1068 Yılmaz Y; Saroğlu F; Güner Y. (1987) - Initiaton of the Neomagmatism in East Anatolia.
4
5 1069 Tectonophysics, 134, 1-3, 177-199.
6
7
8 1070 Yılmaz Y. (1989) - An approach to the origin of young volcanic rocks of western Turkey.
9
10 071 Tectonic Evolution of the Tethyan Region (Ed: A.M.C. Şengör), Kluwer Academic
11
12 1072 Publishers, Dordrecht, 159-189.
13
14
15 1073 Yılmaz Y. (1990) - Comparison of young volcanic associations of western and eastern
16
17 1074 Anatolia formed under a compressional regime: a review. J. Volcanol. Geotherm., 44, 69-
18
19 1075 77.
20
21
22 1076 Yılmaz Y., Genç S.C., Gürer O.F., Bozcu M., Yılmaz K. (2000) - When did the Western
23
24 077 Anatolian grabens begin to develop? In: Bozkurt E, Winchester JA, Piper JDA (editors),
25
26 1078 Tectonics and Magmatism in Turkey and the Surrounding Area. Geol. Soc. Special
27
28 1079 Publication, London 173: 353-384.
29
30
31 1080 Zhu L., Mitchell B.J., Akyol N., Cemen I., Kekovalı K. (2006) - Crustal thickness variations
32
33 1081 in the Aegean region and implications for the extension of continental crust, J. Geophys.
34
35 1082 Res. Sol. Earth, 1978–2012, 111(B1). <https://doi.org/10.1029/2005JB003770>
36
37
38 1083
39
40 1084
41
42 1085
43
44
45 1086
46
47 1087
48
49 1088
50
51 1089
52
53
54 1090
55
56 1091
57
58 1092
59
60

FIGURE CAPTIONS

Figure 1. a) Geodynamical sketch map of Anatolian block, locations of major faults and study area shown on Digital Elevation Model (DEM) of Anatolia. (AEZ: Aegean Extension Zone; NAF: North Anatolian Fault; EAF: East Anatolian Fault; EF: Ecemis Fault; TGF: Tuz Gölü Fault and OF: Ovacık Fault. Big arrows indicate the sense of plate motion and half arrows show the relative motion direction on the faults). b) Map showing hillshade topography of the western Anatolia. Faults and graben boundaries are taken from Karaoğlu et al. (2010) and Ersoy et al. (2011, 2012). The pale yellow-coloured dashed line refers to the Menderes Massif (Gessner et al., 2018). GG: Gediz graben, SG: Simav graben, KmG: Küçük Menderes graben, BmG: Büyük Menderes graben, GöB: Gördes basin, DB: Demirci basin, SB: Selendi basin, GüB: Güre basin, NMM: Northern Menderes Massif, CMCC: Central Menderes Core Complex, ÇS: Çine Submassif.

Figure 2. Geological map of the Kula Volcanic Field (modified from Ercan et al., 1978) and published age data. [1]: Westaway et al., 2006, [2]: Westaway et al., 2004, [3]: Maddy et al., 2015, [4]: Bunbury, 2001, [5]: Heineke et al., 2016, [6]: Ulusoy et al., 2019 (Age data is only for Çakallar Divlit Tepe cone and lava flows near Demirköprü Dam). M1-3: tuff ring, M4: maar, Gm: groundmass, Amp: amphibole, ZDD: Zircon double-dating, Cosm: cosmogenic. Geological map draped over SRTM 1 Arc-Second Global DEM hillshade (EROS, 2018); Coord. Sys: UTM, datum: ED1950.

Figure 3. Field photographs: a) Base surge deposits of Kızıl Tepe tuff ring (M3). Olivine bearing ultramafic enclaves are dominant in lithic-rich layers. Hammer is 30 cm long. b) Small cinder cones having basal diameter and height of 100-150 m and 20-30 m, respectively (northern side of Divlit Tepe near Kula). c) Bağ Tepe, a breached cinder cone, with lava extrusions ceased its activity. It is rich in hornblendite (hammer is 30 cm long). d) Enclaves marked by red arrows in M3 tuff ring deposits (BII) varying in size

1
2
3 1118 from <3 to 16 cm, inset images; macro and thin section view. e) and f) Rounded and sub-
4 rounded hornblendite enclaves (marked by red arrows) in the lava flow erupted from Bağ
5 1119 Tepe cinder cone (BIII). Hammer is 30 cm long, inset image; broken sample. g) Wehrlite
6
7 8 1120 sample (K97-10a2, BII) from M3 tuff ring. Notice the broken and unbroken vesicles. Inset
9
10 1121 image; macro view. Cpx: clinopyroxene, Ol: olivine, Phl: phlogopite.
11
12 1122
13
14
15
16 1123 **Figure 4.** Photomicrographs of the host rock in the KVF (plane-polarized). a) Skeletal olivine
17 phenocryst. Groundmass; microphenocryst to fine microlite and microcryst (BI). b) Olivine
18 phenocryst and euhedral spinel inclusions (BIII). c) Sub-rounded olivine, fresh hornblende
19 phenocrysts and leucites in the groundmass (BII). d) Hornblende and euhedral spinel
20 1125 microphenocrysts (BIII). e) Green-coloured, relict clinopyroxene core is mantled by
21
22 1126 another clinopyroxene showing a distinct pleochroism. Note the glass inclusions at the
23 reaction zone (BII). Micro-enclaves containing quenched interstitial glass: (f) hornblendite
24
25 1127 (BIII), (g) Phl-Cpx-hornblendite (BIII) and (h) clinopyroxenite (BII). Ol: olivine, Cpx:
26
27 1128 clinopyroxene, Hbl: hornblende, Pl: plagioclase, Lct: leucite, Nph: nepheline, Spl: spinel,
28
29 1129 G: glass and V: vesicle.
30
31
32 1130
33
34 1131
35
36 1132
37
38
39
40 1133 **Figure 5.** Classification of the enclaves according to their modal mineralogy ([Streckeisen, 1976](#)).
41
42 1134
43
44
45 1135 **Figure 6.** Photomicrographs of the enclaves containing glass (G) and vesicle (V), plane-
46 polarized: a) Hornblendite (BII); prismatic hornblende (Hbl) aggregates in very pale brown
47
48 1136 coloured vesicular glass. b) Hornblendite (BIII); euhedral hornblende and clinopyroxene
49
50 1137 (Cpx) in brown coloured vesicular glass. Apatite (Ap) is not only observed as inclusion in
51
52 1138 Hbl and Cpx, but also in the glass. c) Same sample as (b). Note some apatites showing
53
54 1139 an elongation from towards the glass. d) Cpx-hornblendite (BII); euhedral and embayed
55
56 1140 hauyne (Hyn) containing glass inclusions. Some are clear and embayed. The colour of
57
58 1141 the glass is changing from dark brown to light brown. It is darker in colour towards to
59
60
1142

1
2
3 1143 hornblende and clinopyroxene in contrast to hauyne crystal. e) Pl-bearing Phl-Cpx-
4
5 1144 hornblendite (BII); plagioclase (Pl) showing sieve texture. It is enclosing euhedral apatite
6
7 8 1145 crystals. Note the clinopyroxene microcryst in the glass (arrowed), lining up around the
9
10 146 hornblende crystals. f) Phl-clinopyroxenite (BIII); clinopyroxene and embayed phlogopite
11
12 147 (Phl) crystals. Detached phlogopite pieces and main crystal show optically continuity.
13
14
15 148 Note the clinopyroxene microcrysts in the black coloured glass. g) Wehrlite (BII);
16
17 149 clinopyroxene, embayed olivines with inclusion of spinel (Spl) and embayed hornblende
18
19 150 crystals in a Gp. Hornblende has ragged edge formed by partial melting. h) Wehrlite (BII);
20
21 151 poikilitic hornblende enclosing olivine and clinopyroxene. Note the curved marks inside
22
23 the hornblende, (BII). i) Hornblendite (BIII); oriented long prismatic hornblendes with Gim
24
25 (interstitial vesicular glass). j) Hbl-clinopyroxenite (BII); inter-granular dark coloured Gp
26
27 (glass pockets). k) Ol-Hbl-clinopyroxenite (BII); replacements of clinopyroxene by
28
29 hornblende along cleavage planes and alteration of olivine to iddingsite along rims and
30
31 155 cracks. l) Hbl-gabbro (BIII); dusty rimmed plagioclase enclosing clinopyroxenes and
32
33 156 apatite. m) Hbl-gabbro (BIII); fine-grained phlogopites formed around the relict olivine. n)
34
35 157 Wehrlite (BII); glass associated with inter-granular minerals of sub-hedral olivines,
36
37 158 clinopyroxenes and hornblendes.
38
39
40 159
41
42
43 160 **Figure 7.** Composition of clinopyroxenes from host rock and enclaves plotted in the ternary
44
45 system Wo-En-Fs, with fields from [Morimoto et al. \(1988\)](#).
46
47
48
49 162 **Figure 8.** Total Alkali Silica classification diagram ([Le Bas et al., 1986](#)) for the host rock and
50
51 163 glass in enclaves. The dashed line separates alkali and subalkaline fields, after [Miyashiro](#)
52
53 164 ([1978](#)). Small circle symbols of host rocks are from [Alici et al. \(2002\)](#). Phl: phlogopite,
54
55
56 165 Cpx: clinopyroxene, Hbl: hornblende
57
58
59 166 **Figure 9.** Major (wt.%) and trace (ppm) element abundances versus SiO₂ for host rock and
60
61 enclaves.
62
63
64
65
66
67

1
2
3 1168 **Figure 10.** a) and b) MORB-normalised ([Pearce, 1983](#)) incompatible trace element patterns
4
5 1169 of host rocks and enclaves. c) and d) Chondrite-normalised ([Nakamura, 1974](#)) REE
6
7 1170 patterns of host rocks and enclaves.
8
9
10

11 1171 **Figure 11.** a) Ba/Rb versus Rb/Sr diagram ([Furman & Graham 1999](#)) of host rocks and
12
13 1172 enclaves. SCLM: Sub-continental lithospheric mantle. b) and c) Sm/Yb – La/Yb and
14
15 1173 (Tb/Yb)n – (La/Yb)n non-modal batch melting ([Shaw, 1970](#)) diagrams showing the melt
16
17 1174 curves of spinel ($\text{Ol}_{0.62/0.40} + \text{Opx}_{0.24/0.30} + \text{Cpx}_{0.12/0.90} + \text{Spinel}_{0.02/0.20}$) and garnet-peridotite
18
19 1175 ($\text{Ol}_{0.66/0.1} + \text{Opx}_{0.27/0.18} + \text{Cpx}_{0.03/0.3} + \text{garnet}_{0.04/0.42}$) and binary mixing line between spinel
20
21 1176 and garnet peridotite melting curves. Normalisation values are from [Thompson \(1982\)](#).
22
23
24 1177 The horizontal black dashed line separates the melting fields of garnet and spinel-
25
26 1178 peridotite ([Wang et al., 2002](#)). d) Yb-La/Yb diagram showing spinel and garnet non-modal
27
28 1179 batch melting curves. Initial concentrations for La, Sm, Yb and Tb are from [McDonough](#)
29
30 1180 ([1990](#)). Subscripts of spinel and garnet-peridotite mineral compositions refer source
31
32 1181 mode/melts modes during non-modal batch melting. Source and melt modes of spinel
33
34 1182 and garnet peridotites are from [McDonough \(1990\)](#) and [Wang et al. \(2004\)](#), respectively.
35
36 1183 Partial melting coefficients are compiled from [McKenzie & O'Nions \(1991\)](#); [Rollinson](#)
37
38 1184 ([1993](#)) and [Elkins et al. \(2008\)](#).
39
40
41
42
43

44 1185 **Figure 12.** Pressure-temperature diagram illustrating the potential source region for host
45
46 1186 rocks and enclaves from the KVF (adopted from [Jung et al., 2012](#) and references therein).
47
48
49 1187 Cpx pressure and temperature estimates based on [Neave & Putirka \(2017\)](#) and [Putirka](#)
50
51 1188 ([2008](#); eqn. 33), respectively. The average Moho depth is accepted as ~30 km from
52
53
54 1189 [Saunders et al. \(1998\)](#), [Zhu et al. \(2006\)](#), [Mahatsente et al. \(2017\)](#) and [Artemieva &](#)
55
56 1190 [Shulgin \(2019\)](#).
57
58

59 1191 **Figure 13.** Schematic illustration showing the evolution and probable conduits of the Kula
60
61
62
63
64
65
66
67
68
69
70
71
72
73
74
75
76
77
78
79
80
81
82
83
84
85
86
87
88
89
90
91
92
93
94
95
96
97
98
99
100
101
102
103
104
105
106
107
108
109
110
111
112
113
114
115
116
117
118
119
120
121
122
123
124
125
126
127
128
129
130
131
132
133
134
135
136
137
138
139
140
141
142
143
144
145
146
147
148
149
150
151
152
153
154
155
156
157
158
159
160
161
162
163
164
165
166
167
168
169
170
171
172
173
174
175
176
177
178
179
180
181
182
183
184
185
186
187
188
189
190
191
192
193
194
195
196
197
198
199
200
201
202
203
204
205
206
207
208
209
210
211
212
213
214
215
216
217
218
219
220
221
222
223
224
225
226
227
228
229
230
231
232
233
234
235
236
237
238
239
240
241
242
243
244
245
246
247
248
249
250
251
252
253
254
255
256
257
258
259
260
261
262
263
264
265
266
267
268
269
270
271
272
273
274
275
276
277
278
279
280
281
282
283
284
285
286
287
288
289
290
291
292
293
294
295
296
297
298
299
300
301
302
303
304
305
306
307
308
309
310
311
312
313
314
315
316
317
318
319
320
321
322
323
324
325
326
327
328
329
330
331
332
333
334
335
336
337
338
339
340
341
342
343
344
345
346
347
348
349
350
351
352
353
354
355
356
357
358
359
360
361
362
363
364
365
366
367
368
369
370
371
372
373
374
375
376
377
378
379
380
381
382
383
384
385
386
387
388
389
390
391
392
393
394
395
396
397
398
399
400
401
402
403
404
405
406
407
408
409
410
411
412
413
414
415
416
417
418
419
420
421
422
423
424
425
426
427
428
429
430
431
432
433
434
435
436
437
438
439
440
441
442
443
444
445
446
447
448
449
450
451
452
453
454
455
456
457
458
459
460
461
462
463
464
465
466
467
468
469
470
471
472
473
474
475
476
477
478
479
480
481
482
483
484
485
486
487
488
489
490
491
492
493
494
495
496
497
498
499
500
501
502
503
504
505
506
507
508
509
510
511
512
513
514
515
516
517
518
519
520
521
522
523
524
525
526
527
528
529
530
531
532
533
534
535
536
537
538
539
540
541
542
543
544
545
546
547
548
549
550
551
552
553
554
555
556
557
558
559
5510
5511
5512
5513
5514
5515
5516
5517
5518
5519
5520
5521
5522
5523
5524
5525
5526
5527
5528
5529
5530
5531
5532
5533
5534
5535
5536
5537
5538
5539
55310
55311
55312
55313
55314
55315
55316
55317
55318
55319
55320
55321
55322
55323
55324
55325
55326
55327
55328
55329
55330
55331
55332
55333
55334
55335
55336
55337
55338
55339
55340
55341
55342
55343
55344
55345
55346
55347
55348
55349
55350
55351
55352
55353
55354
55355
55356
55357
55358
55359
55360
55361
55362
55363
55364
55365
55366
55367
55368
55369
55370
55371
55372
55373
55374
55375
55376
55377
55378
55379
55380
55381
55382
55383
55384
55385
55386
55387
55388
55389
55390
55391
55392
55393
55394
55395
55396
55397
55398
55399
553100
553101
553102
553103
553104
553105
553106
553107
553108
553109
553110
553111
553112
553113
553114
553115
553116
553117
553118
553119
553120
553121
553122
553123
553124
553125
553126
553127
553128
553129
553130
553131
553132
553133
553134
553135
553136
553137
553138
553139
553140
553141
553142
553143
553144
553145
553146
553147
553148
553149
553150
553151
553152
553153
553154
553155
553156
553157
553158
553159
553160
553161
553162
553163
553164
553165
553166
553167
553168
553169
553170
553171
553172
553173
553174
553175
553176
553177
553178
553179
553180
553181
553182
553183
553184
553185
553186
553187
553188
553189
553190
553191
553192
553193
553194
553195
553196
553197
553198
553199
553200
553201
553202
553203
553204
553205
553206
553207
553208
553209
553210
553211
553212
553213
553214
553215
553216
553217
553218
553219
553220
553221
553222
553223
553224
553225
553226
553227
553228
553229
553230
553231
553232
553233
553234
553235
553236
553237
553238
553239
553240
553241
553242
553243
553244
553245
553246
553247
553248
553249
553250
553251
553252
553253
553254
553255
553256
553257
553258
553259
553260
553261
553262
553263
553264
553265
553266
553267
553268
553269
553270
553271
553272
553273
553274
553275
553276
553277
553278
553279
553280
553281
553282
553283
553284
553285
553286
553287
553288
553289
553290
553291
553292
553293
553294
553295
553296
553297
553298
553299
553300
553301
553302
553303
553304
553305
553306
553307
553308
553309
553310
553311
553312
553313
553314
553315
553316
553317
553318
553319
553320
553321
553322
553323
553324
553325
553326
553327
553328
553329
553330
553331
553332
553333
553334
553335
553336
553337
553338
553339
553340
553341
553342
553343
553344
553345
553346
553347
553348
553349
553350
553351
553352
553353
553354
553355
553356
553357
553358
553359
553360
553361
553362
553363
553364
553365
553366
553367
553368
553369
553370
553371
553372
553373
553374
553375
553376
553377
553378
553379
553380
553381
553382
553383
553384
553385
553386
553387
553388
553389
553390
553391
553392
553393
553394
553395
553396
553397
553398
553399
553400
553401
553402
553403
553404
553405
553406
553407
553408
553409
553410
553411
553412
553413
553414
553415
553416
553417
553418
553419
553420
553421
553422
553423
553424
553425
553426
553427
553428
553429
553430
553431
553432
553433
553434
553435
553436
553437
553438
553439
553440
553441
553442
553443
553444
553445
553446
553447
553448
553449
553450
553451
553452
553453
553454
553455
553456
553457
553458
553459
553460
553461
553462
553463
553464
553465
553466
553467
553468
553469
553470
553471
553472
553473
553474
553475
553476
553477
553478
553479
553480
553481
553482
553483
553484
553485
553486
553487
553488
553489
553490
553491
553492
553493
553494
553495
553496
553497
553498
553499
553500
553501
553502
553503
553504
553505
553506
553507
553508
553509
553510
553511
553512
553513
553514
553515
553516
553517
553518
553519
553520
553521
553522
553523
553524
553525
553526
553527
553528
553529
553530
553531
553532
553533
553534
553535
553536
553537
553538
553539
553540
553541
553542
553543
553544
553545
553546
553547
553548
553549
553550
553551
553552
553553
553554
553555
553556
553557
553558
553559
553560
553561
553562
553563
553564
553565
553566
553567
553568
553569
553570
553571
553572
553573
553574
553575
553576
553577
553578
553579
553580
553581
553582
553583
553584
553585
553586
553587
553588
553589
553590
553591
553592
553593
553594
553595
553596
553597
553598
553599
553600
553601
553602
553603
553604
553605
553606
553607
553608
553609
553610
553611
553612
553613
553614
553615
553616
553617
553618
553619
553620
553621
553622
553623
553624
553625
553626
553627
553628
553629
553630
553631
553632
553633
553634
553635
553636
553637
553638
553639
553640
553641
553642
553643
553644
553645
553646
553647
553648
553649
553650
553651
553652
553653
553654
553655
553656
553657
553658
553659
553660
553661
553662
553663
553664
553665
553666
553667
553668
553669
553670
553671
553672
553673
553674
553675
553676
553677
553678
553679
553680
553681
553682
553683
553684
553685
553686
553687
553688
553689
553690
553691
553692
553693
553694
553695
553696
553697
553698
553699
553700
553701
553702
553703
553704
553705
553706
553707
553708
553709
553710
553711
553712
553713
553714
553715
553716
553717
553718
553719
553720
553721
553722
553723
553724
553725
553726
553727
553728
553729
553730
553731
553732
553733
553734
553735
553736
553737
553738
553739
5537340
5537341
5537342
5537343
5537344
5537345
5537346
5537347
5537348
5537349
5537350
5537351
5537352
5537353
5537354
5537355
5537356
5537357
5537358
5537359
5537360
5537361
5537362
5537363
5537364
5537365
5537366
5537367
5537368
5537369
5537370
5537371
5537372
5537373
5537374
5537375
5537376
5537377
5537378
5537379
5537380
5537381
5537382
5537383
5537384
5537385
5537386
5537387
5537388
5537389
5537390
5537391
5537392
5537393
5537394
5537395
5537396
5537397
5537398
5537399
5537400
5537401
5537402
5537403
5537404
5537405
5537406
5537407
5537408
5537409
55374010
55374011
55374012
55374013
55374014
55374015
55374016
55374017
55374018
55374019
55374020
55374021
55374022
55374023
55374024
55374025
55374026
55374027
55374028
55374029
55374030
55374031
55374032
55374033
55374034
55374035
55374036
55374037
55374038
55374039
55374040
55374041
55374042
55374043
55374044
55374045
55374046
55374047
55374048
55374049
55374050
55374051
55374052
55374053
55374054
55374055
55374056
55374057
55374058
55374059
55374060
55374061
55374062
55374063
55374064
55374065
55374066
55374067
55374068
55374069
55374070
55374071
55374072
55374073
55374074
55374075
55374076
55374077
55374078
55374079
55374080
55374081
55374082
55374083
55374084<br

1
2
3 1193 accepted as ca. 80 km from [Salaün et al. \(2012\)](#), [Mahatsente et al. \(2017\)](#) and [Artemieva](#)
4
5 1194 & [Shulgin \(2019\)](#). However, it is thought that the depth of the LAB decreases from 80 km
6
7 1195 in the northwest and 105 km in the southeast (brown-coloured arrows) to ca. 60 km
8
9 1196 beneath the Kula volcanic field (i.e. [Artemieva & Shulgin, 2019](#)) based on calculated P-T
10
11 1197 values. The depth of the lens-shaped magma chambers including ultramafic cumulates
12
13 1198 resulting from fractional crystallisation (FC) is calculated using the Cpx-melt
14
15 1199 thermobarometers.
16
17
18
19
20
21
22
23
24
25
26
27
28
29
30
31
32
33
34
35
36
37
38
39
40
41
42
43
44
45
46
47
48
49
50
51
52
53
54
55
56
57
58
59
60

TABLE CAPTIONS

Supplementary Table 1. Modal mineralogy of the glass bearing enclaves.

Supplementary Table 2. Selected microprobe analyses of olivines from the host rocks and enclaves.

Supplementary Table 3. Selected microprobe analyses of clinopyroxenes from the host rocks and enclaves. Nomenclature after [Morimoto et al. \(1988\)](#).

Supplementary Table 4. Selected microprobe analyses of hornblendes from the host rocks and enclaves. Nomenclature after [Leake et al. \(1997\)](#).

Supplementary Table 5. Representative microprobe analyses of phlogopites.

Supplementary Table 6. Selected microprobe analyses of plagioclases.

Supplementary Table 7. Selected microprobe analyses of feldspathoids.

Supplementary Table 8. Microprobe analyses of oxides.

Supplementary Table 9. Microprobe analyses of the glasses from enclaves.

Supplementary Table 10. Major and trace-element analyses for the KVF.

Supplementary Table 11. Minimum and maximum T-P values from the clinopyroxene thermometer of [Neave & Putirka \(2007\)](#) and [Putirka \(2008, eqn. 33\)](#). Cpx-liquid test between the predicted and observed Diopside-Hedenbergite (DiHd) components, calculated by [Putirka et al. \(1996\)](#) and [Putirka \(1999\)](#). Blue lines are the equilibrium range accepted as 10% deviation to one-to-one line.

Supplementary Data 1. T-P calculation Excel spreadsheet.

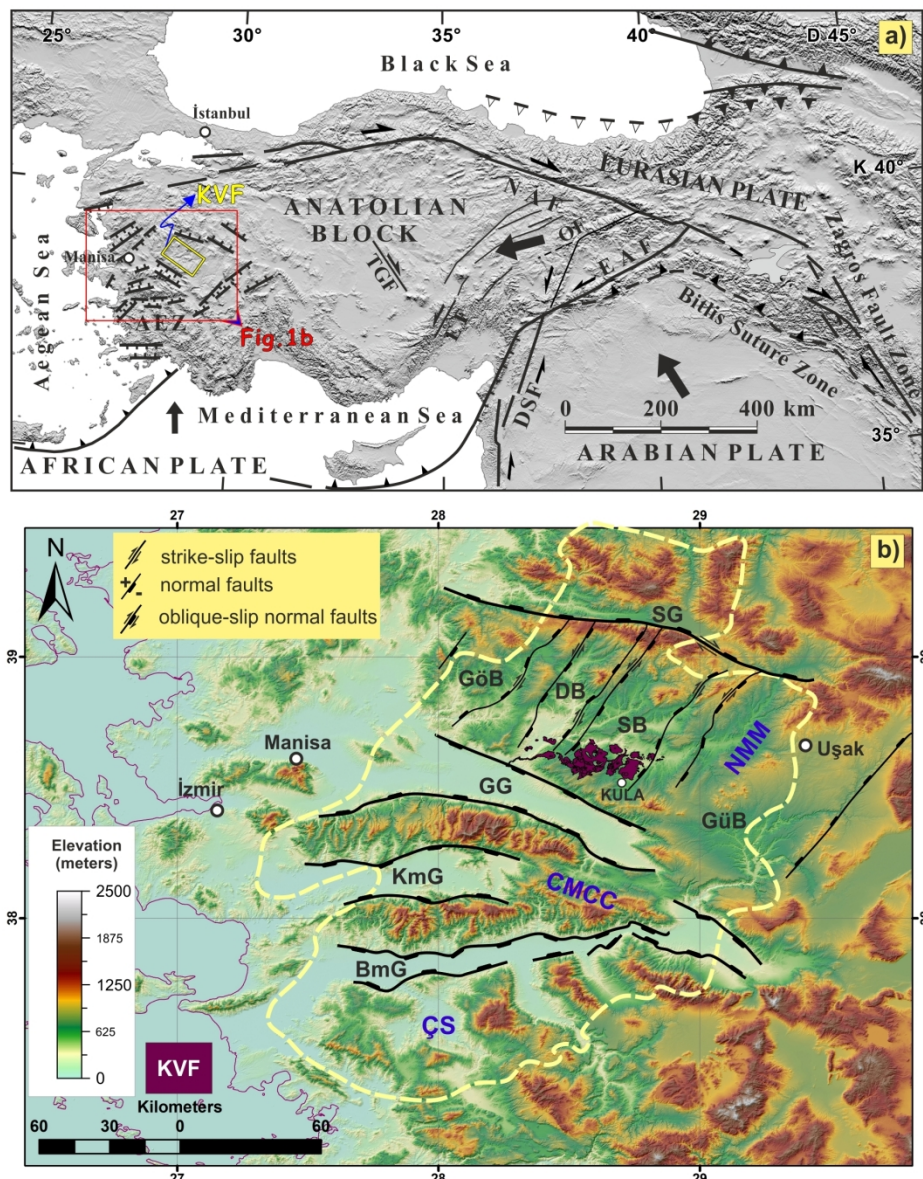


Figure 1

163x208mm (300 x 300 DPI)

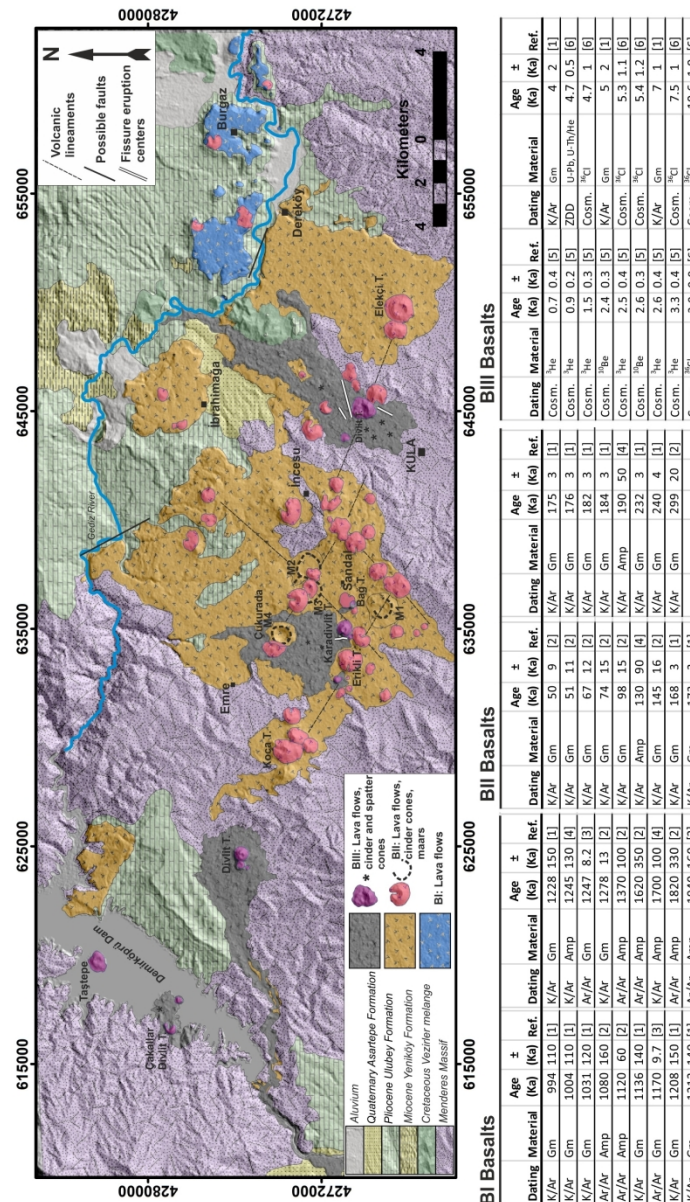


Figure 2

158x272mm (300 x 300 DPI)

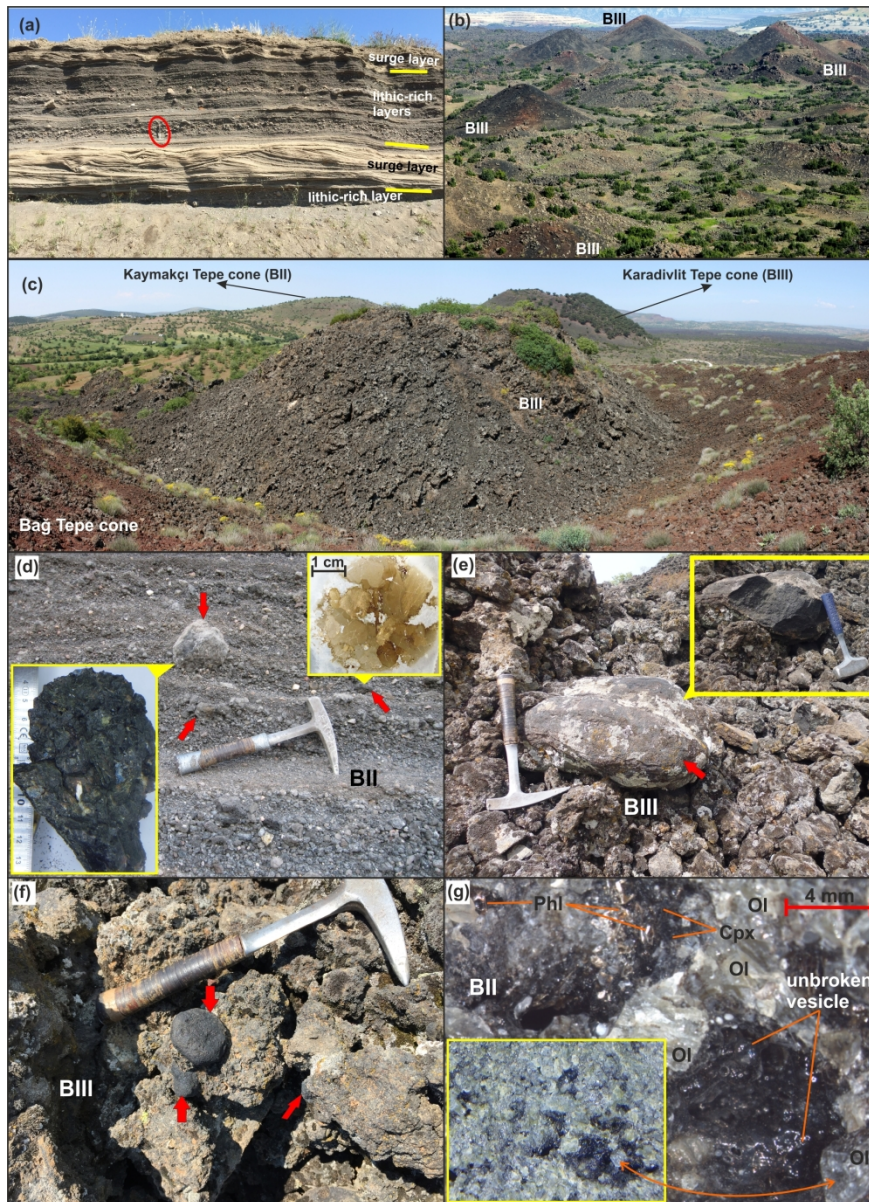


Figure 3

195x268mm (300 x 300 DPI)

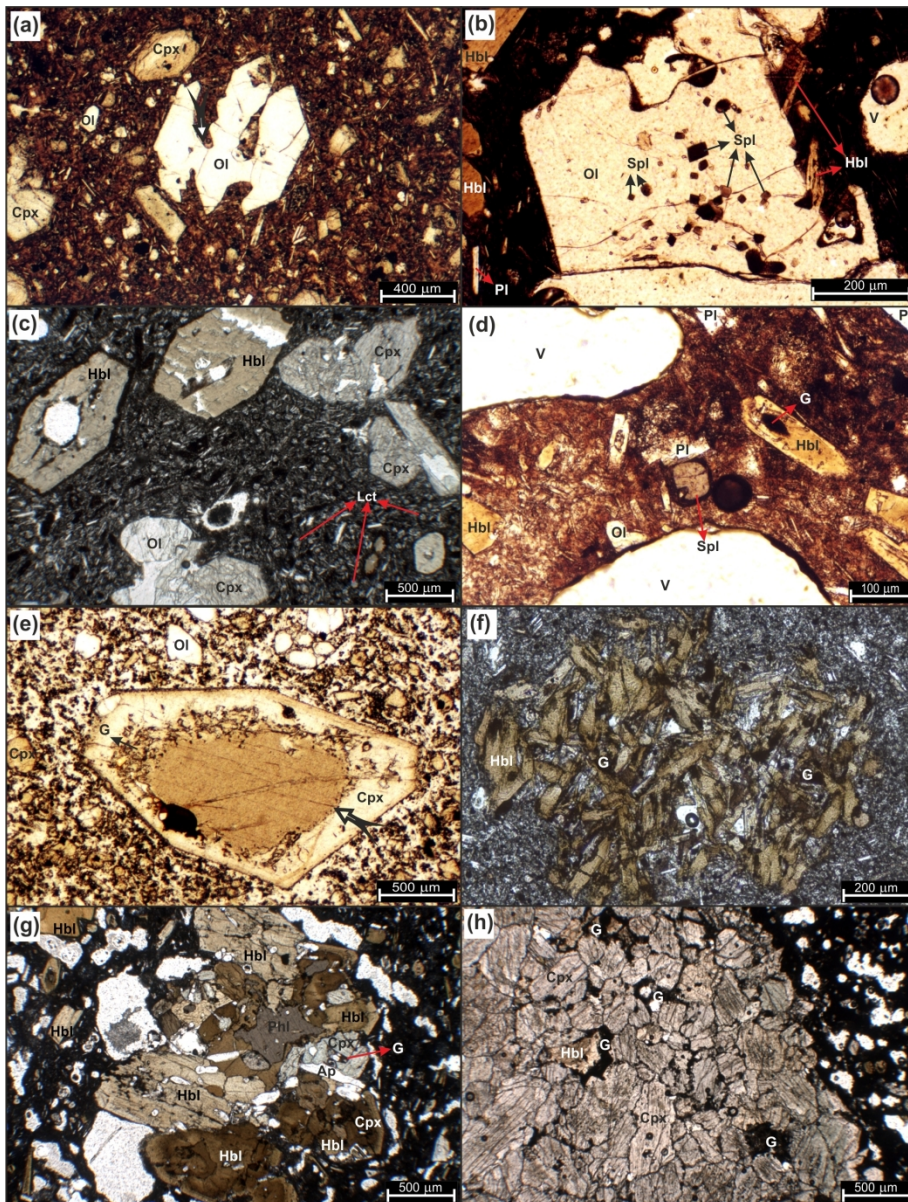


Figure 4

182x240mm (300 x 300 DPI)

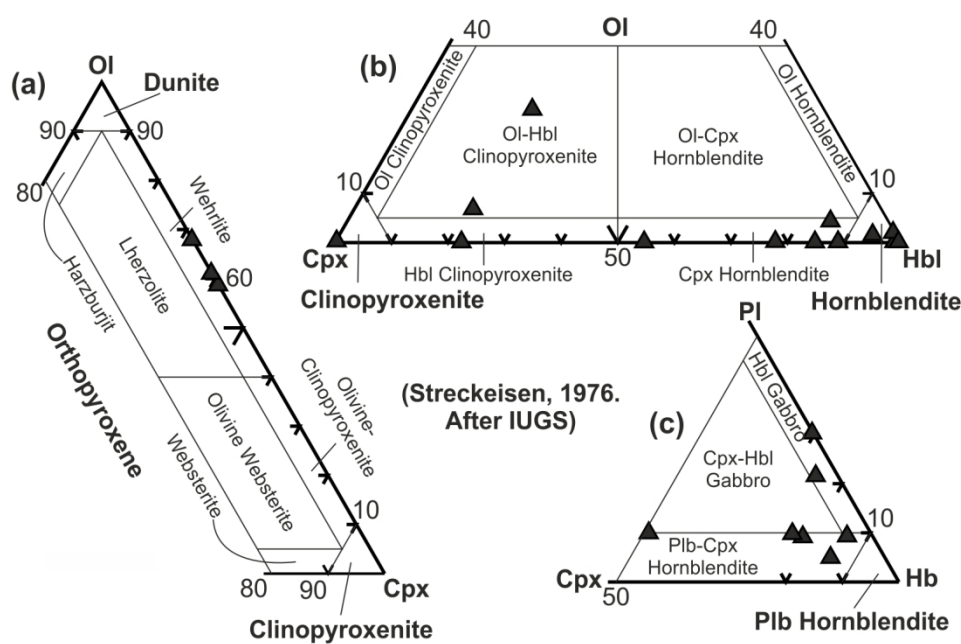


Figure 5

144x93mm (300 x 300 DPI)

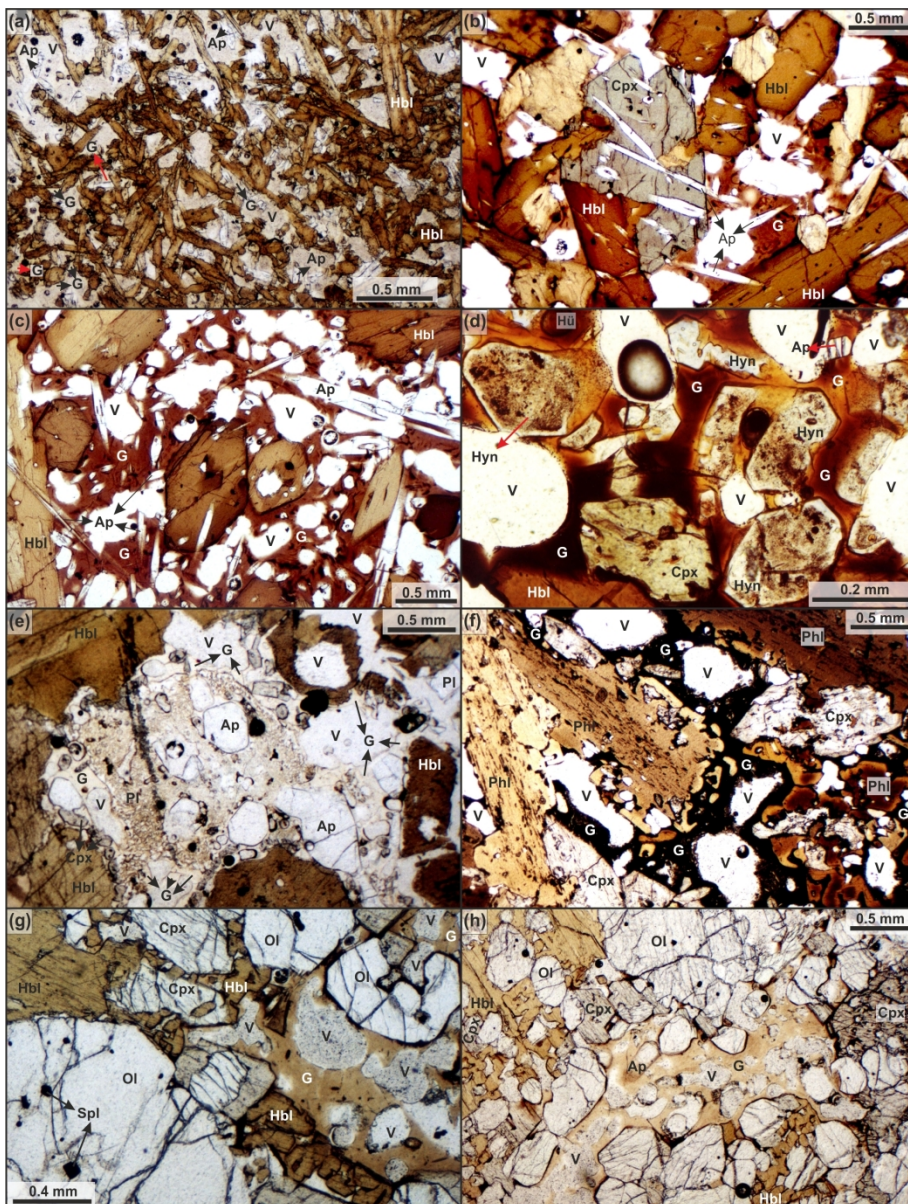


Figure 6

182x240mm (300 x 300 DPI)

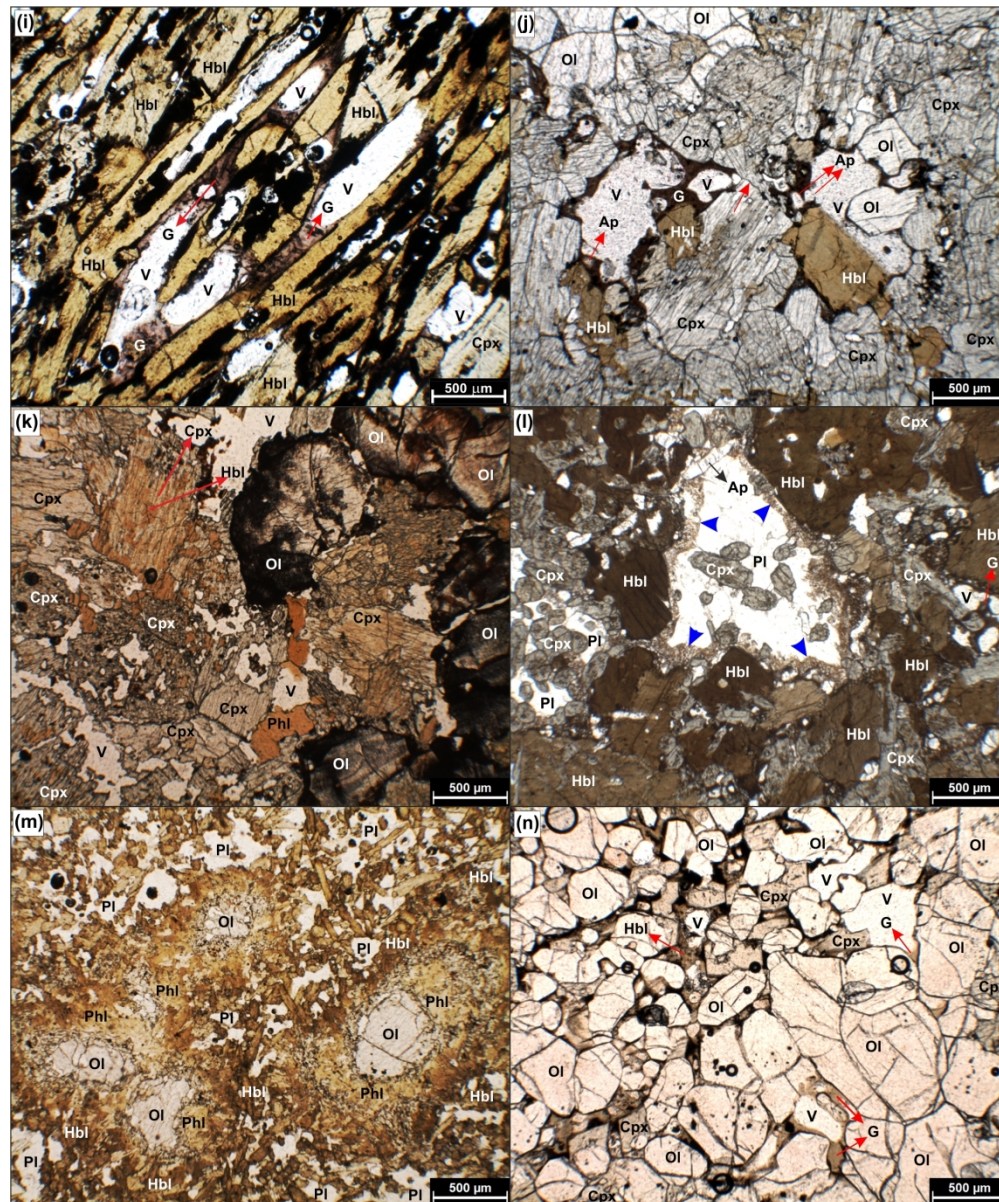


Figure 6 continued

191x229mm (300 x 300 DPI)

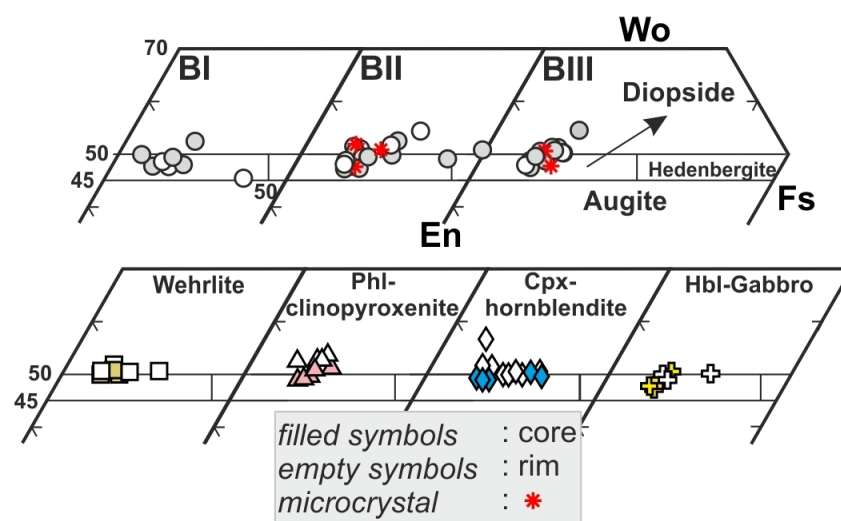


Figure 7

105x57mm (300 x 300 DPI)

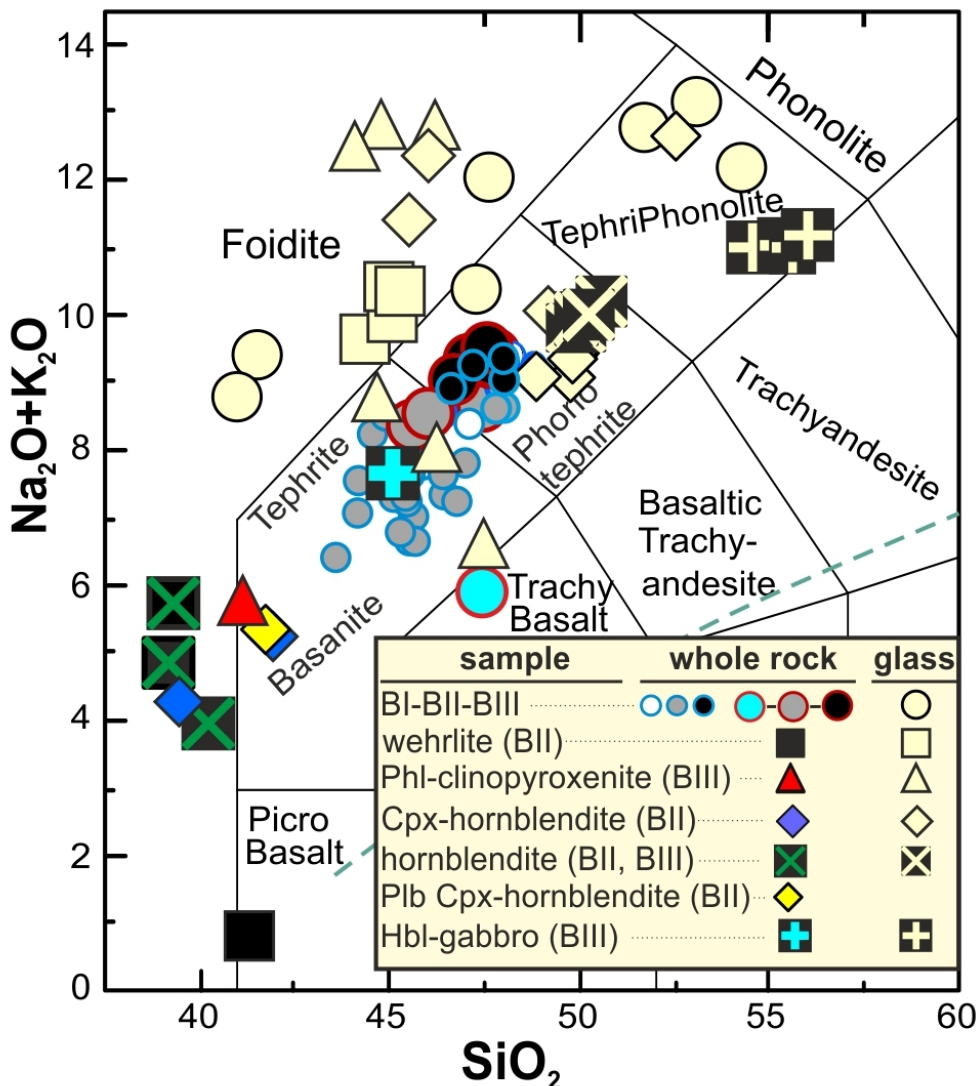


Figure 8

82x91mm (300 x 300 DPI)

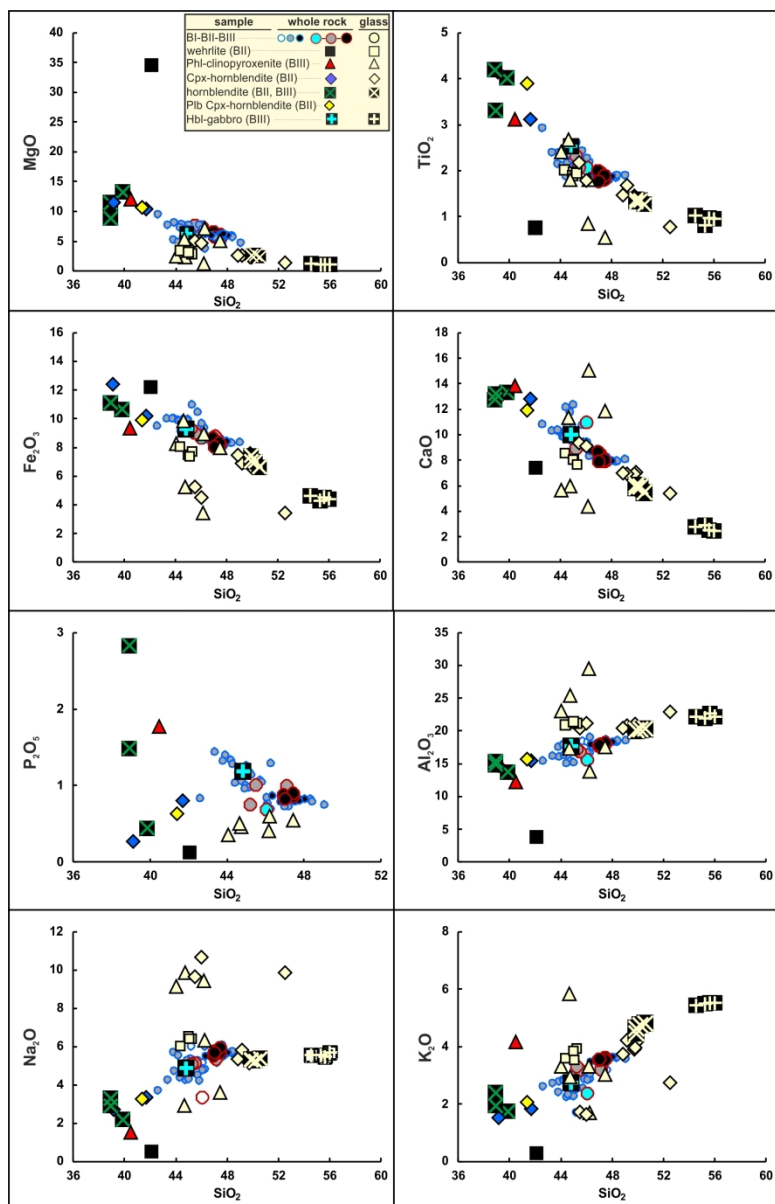


Figure 9

182x282mm (300 x 300 DPI)

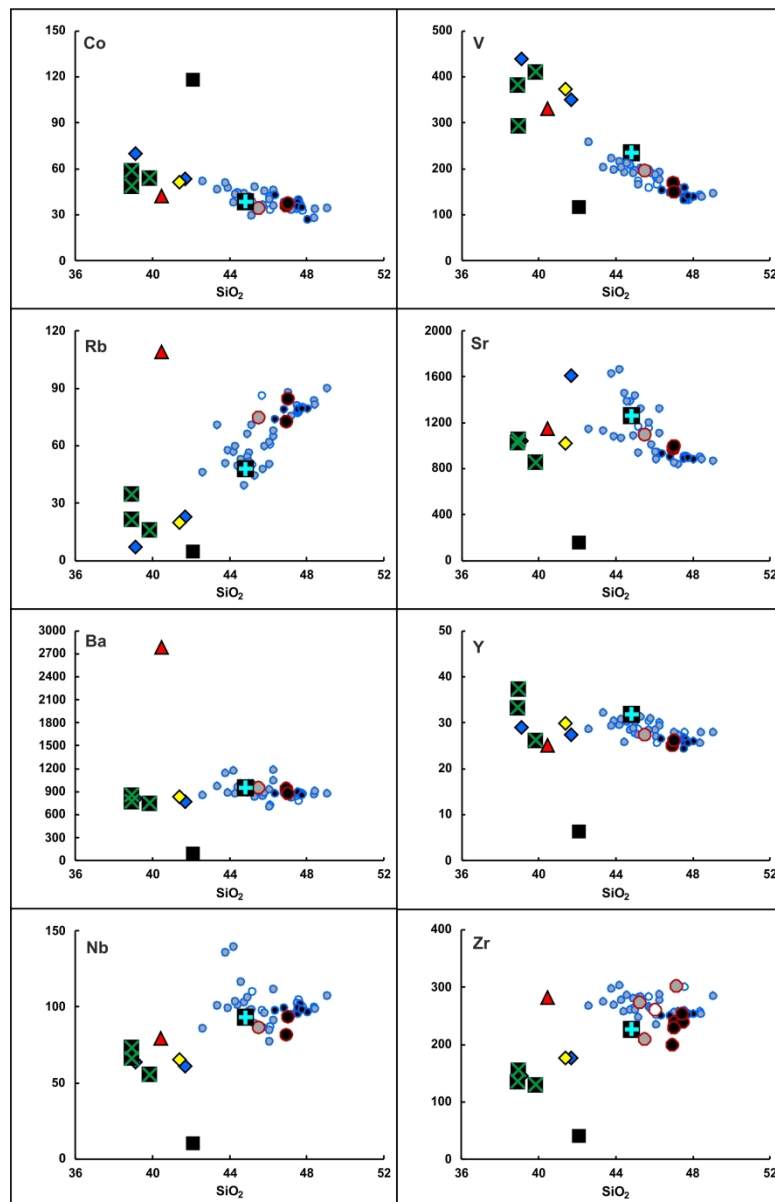


Figure 9 continued

182x281mm (300 x 300 DPI)

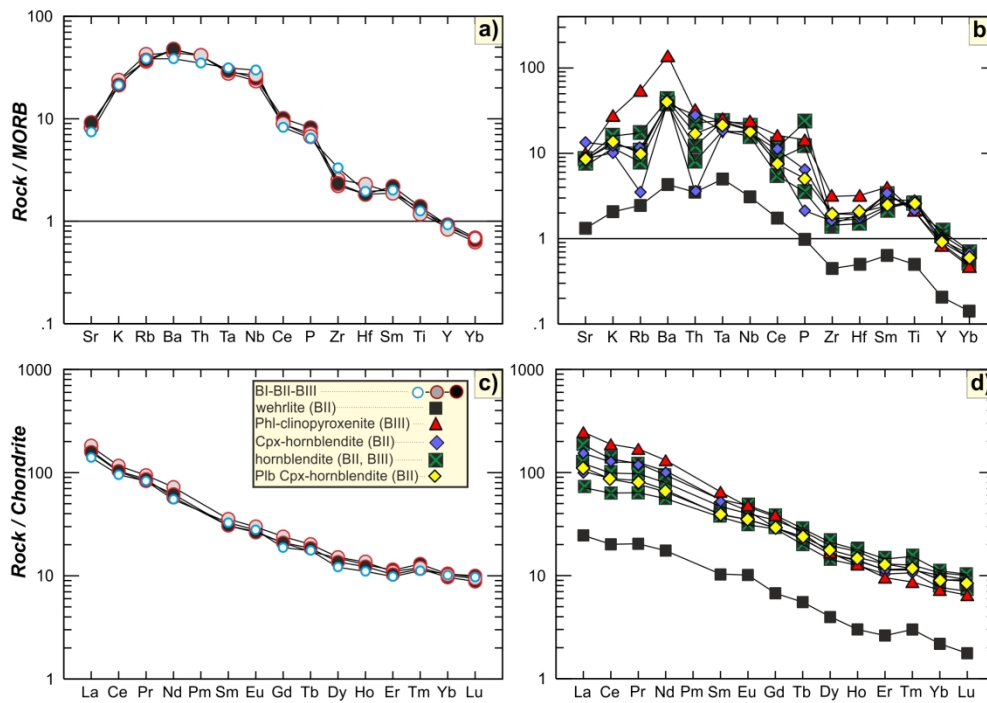


Figure 10

187x130mm (300 x 300 DPI)

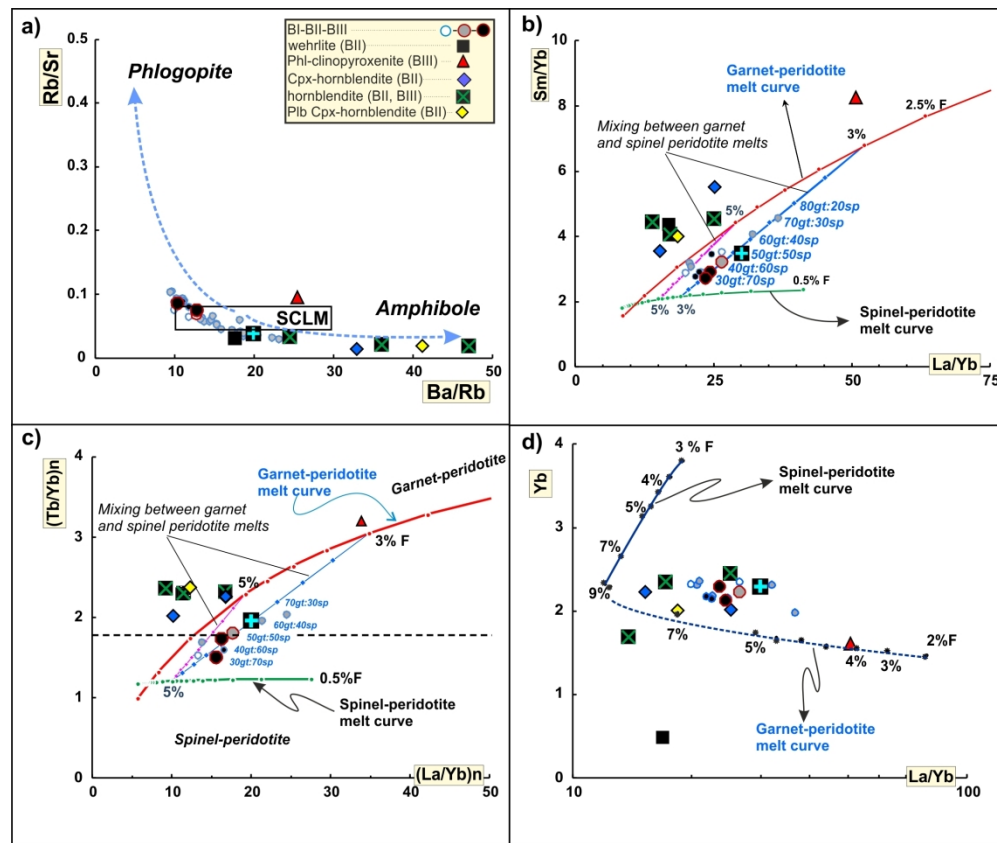


Figure 11

192x161mm (300 x 300 DPI)

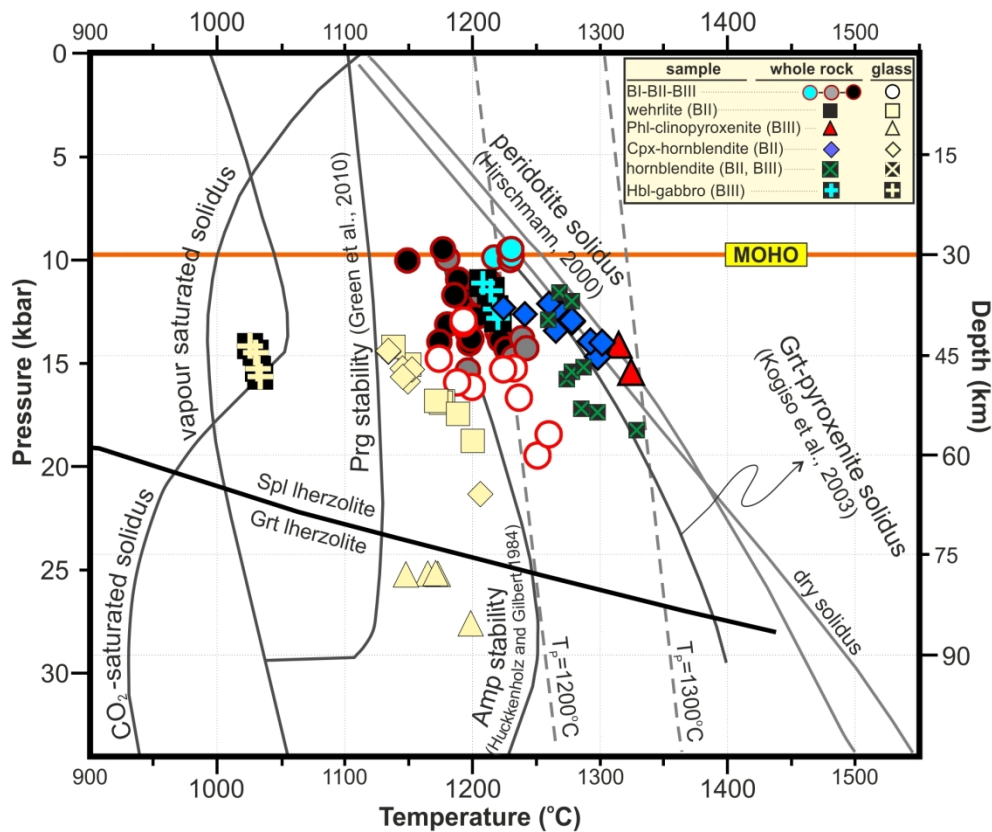


Figure 12

166x143mm (300 x 300 DPI)

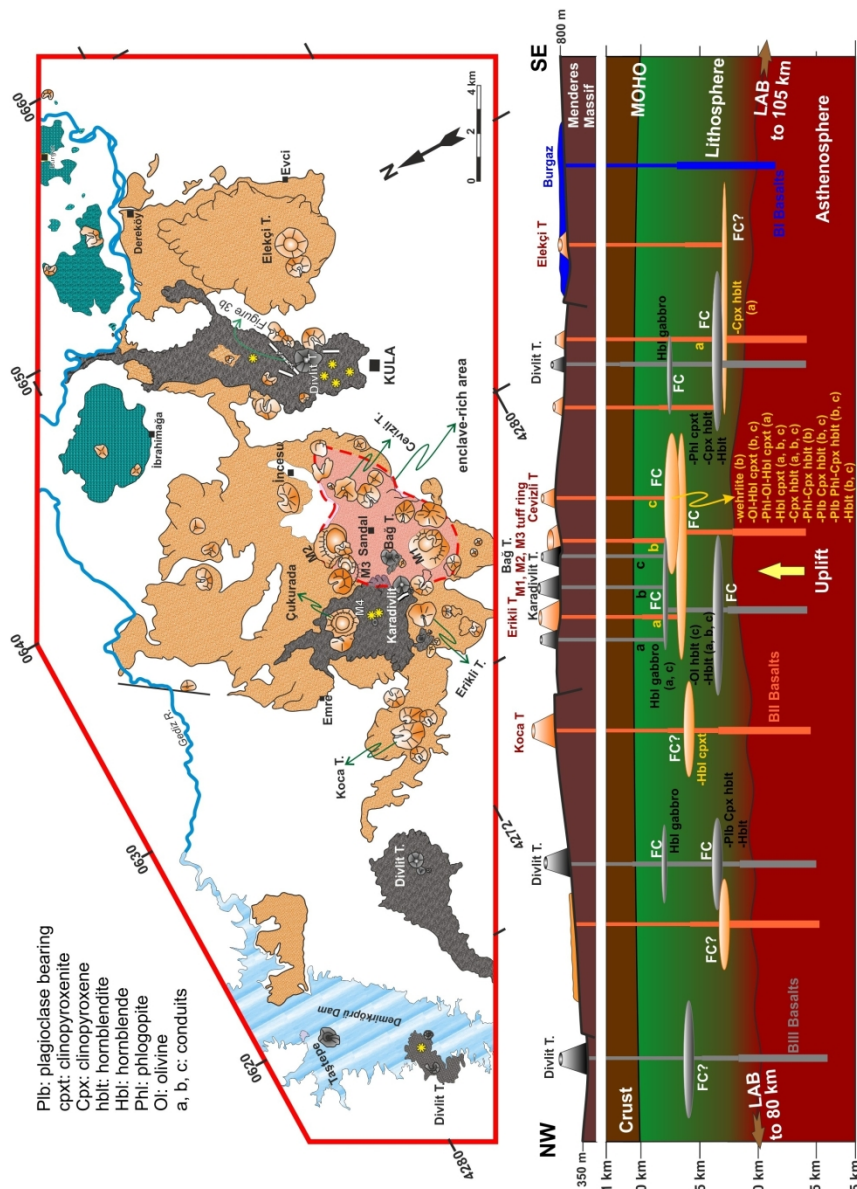


Figure 13

173x242mm (300 x 300 DPI)

1	UTM coordinates (WGS84, E / N)	637447 / 4272874			645204 / 4270729	635889 / 4269521	637447 / 4272874	639387 / 4271146	634570 / 4268 542	637447 / 4272874	634570 / 4268542	637447 / 4272874	
2	Sample No: K97-	10a2(BII)	10a15(BII)	10a9(BII)	10a17(BII)	70a2(BIII)	49a3(BII)	10a16(BII)	30a(BII)	48a2(BII)	10a1(BII)	48a1(BII)	10a10(BII)
3	# of points	3000	3000	2890	2759	3000	2391	1000	3000	3151	1000	2061	2000
4	Sample	Wehrlite	Wehrlite	Wehrlite	Hbl-Cpxt	Phl-Cpxt	OI-Hbl- Cpxt	Cpx-Hblt	Cpx-Hblt	Cpx-Hblt	Cpx-Hblt	Cpx- Hblt	Plb-Cpx- Hblt
5	Olivine	56,9	54,8	50,3	-	-	6,7	-	-	-	-	3,25	-
6	Clinopyroxene	26,83	38,5	32	74	33	70,4	13,2	12,03	40,24	9,2	7,52	7,9
7	Hornblende	5,64	3,7	16,9	21,5	-	20,7	75,2	42,83	48,87	75,5	63,9	55,1
8	Phlogopite	-	-	0,3	0,2	38,5	-	-	-	-	2,1	-	18,1
9	Plagioclase	-	-	-	-	-	-	-	1,14	0,2	-	-	7
10	Nepheline	-	-	-	-	-	-	-	-	-	-	-	-
11	Haüyne	-	-	-	-	-	-	-	1,33	-	-	-	-
12	Apatite	-	-	-	-	1	0,1	3	1,67	0,06	-	-	6,5
13	Sphene	-	-	-	-	-	-	-	-	0,48	1,1	-	1,5
14	Calcite	-	0,5	-	-	-	-	-	-	-	-	-	-
15	Oxides	1,27	0,8	0,1	-	0,2	-	-	-	-	-	-	-
16	Total	90,64	98,3	99,6	95,7	75,4	97,9	91,4	59	89,85	87,9	74,67	96,1
17	Glass	5,8	0,6	0,3	3,2	13,9	1,3	5	19,03	6,09	4,1	11,45	1,8
18	Vesicle	3,56	1,1	0,1	1,1	10,7	0,8	3,6	21,97	4,06	8	13,88	2,1
19	Total	9,36	1,7	0,4	4,3	24,6	2,1	8,6	41	10,15	12,1	25,33	3,9
20	UTM coordinates (WGS84, E / N)	631879 / 4270995	644710 / 4269654	635889 / 4269521	634570 / 4268542	639684 / 4269941	624717 / 4275318	624717 / 4275318	637447 / 4272874	636125 / 4270660	632680 / 4271325		
21	Sample No: K97-	37a4(BII)	17a2(BIII)	49a1(BII)	14a(BIII)	33a(BII)	44a(BIII)	46a(BIII)	10a18(BII)	10a8(BII)	42a2(BIII)	39a1(BIII)	
22	# of points	2006	3000	1077	2635	1000	2211	3300	2587	2000	2000	1000	
23	Sample	Phl-Ol-Hbl Cpxt	Hblt	Hblt	Hblt	Hblt	Plb Cpx Hblt	Plb Cpx Hblt	Plb Phl-Cpx Hblt	Plb Phl-Cpx Hblt	Hbl Gabbro	Hbl Gabbro	
24	Olivine	22,9	-	0,8	-	1,2	0,5	-	-	-	0,8	-	
25	Clinopyroxene	43,5	-	2	0,5	-	31,4	9	8,1	3,5	2,8	-	
26	Hornblende	18,2	73,5	47,4	58,4	58,1	40,7	61,24	72,1	67,2	53,4	32,3	
27	Phlogopite	13,2	-	-	-	1,9	1,2	-	6,4	6,9	0,8	-	
28	Plagioclase	-	-	-	-	-	7,9	7,37	4,1	7,2	15,4	14	
29	Apatite	0,4	3	1,4	7,1	4	0,7	1,21	0,5	4,9	2,6	3,7	
30	Sphene	-	-	-	-	-	-	-	1,3	1,5	-	-	
31	Total	98,2	76,5	51,6	66	65,2	82,4	78,82	92,5	91,2	75,8	50	
32	Glass	1,1	11,5	17,9	17,7	14	9,4	11,57	4,3	4,1	11,3	29	
33	Vesicle	0,7	12	30,5	16,3	20,8	8,2	9,61	3,2	4,7	12,9	21	
34	Total	1,8	23,5	48,4	34	34,8	17,6	21,18	7,5	8,8	24,2	50	

Ol: olivine, Cpx: clinopyroxene, Hbl: hornblende, Phl: phlogopite, Plb: plagioclase bearing, Cpxt: clinopyroxenite , Hblt: hornblendite

		Host rock												Enclave											
Olivine	Sample	BI			BII			BIII			Wehrlite (BII)						Hornblende Gabbro (BIII)								
		K97-58	10	31	48	42	70	10a2	42a2	c	r	mc	c	r	mc	c	r	c	r	c	r	c	r	c	r
wt.%	#	c	r	mc	c	r	mc	c	r	c	r	mc	c	r	mc	c	r	c	r	c	r	c	r	c	r
SiO ₂	39,20	36,92	37,65	39,45	39,29	39,08	39,46	38,80	38,16	39,40	38,92	39,28	39,43	38,96	39,65	39,86	39,44	39,12	39,19	39,28	40,24	38,63	38,08	39,32	38,97
Al ₂ O ₃	0,04	0,00	0,08	0,04	0,03	0,03	0,06	0,02	0,04	0,09	0,01	0,05	0,03	0,06	0,05	0,03	0,03	0,01	0,03	0,02	0,05	0,00	0,04	0,03	0,04
FeOt	14,92	25,74	26,75	12,34	12,77	13,62	12,87	14,20	18,47	15,72	17,49	14,16	14,34	14,28	13,63	13,07	14,79	14,98	14,70	14,30	13,90	18,29	19,81	14,50	15,38
MgO	46,21	37,38	35,19	47,35	46,87	46,01	47,39	45,87	42,03	44,90	43,42	46,27	45,86	45,81	47,62	47,22	45,80	46,07	45,81	45,79	46,10	42,29	40,65	46,11	45,09
CaO	0,29	0,40	0,39	0,21	0,25	0,25	0,22	0,25	0,28	0,25	0,29	0,22	0,22	0,27	0,24	0,18	0,08	0,09	0,15	0,25	0,21	0,21	0,23	0,11	
Na ₂ O	0,00	0,04	0,02	0,03	0,03	0,02	0,01	0,00	0,00	0,04	0,00	0,00	0,00	0,02	0,03	0,00	0,01	0,02	0,04	0,02	0,00	0,01	0,01	0,01	
K ₂ O	0,01	0,00	0,06	0,01	0,03	0,00	0,00	0,01	0,01	0,02	0,00	0,00	0,03	0,00	0,01	0,00	0,00	0,02	0,03	0,00	0,01	0,00	0,02	0,00	
TiO ₂	0,01	0,02	0,05	0,02	0,08	0,00	0,00	0,00	0,04	0,09	0,05	0,05	0,05	0,00	0,00	0,00	0,01	0,03	0,04	0,03	0,00	0,04	0,01	0,00	0,09
MnO	0,20	0,48	0,58	0,19	0,24	0,17	0,25	0,29	0,36	0,24	0,26	0,22	0,20	0,29	0,21	0,13	0,24	0,25	0,25	0,19	0,21	0,50	0,55	0,26	0,29
Cr ₂ O ₃	0,05	0,00	0,00	0,03	0,04	0,03	0,00	0,02	0,02	0,03	0,00	0,02	0,00	0,05	0,00	0,01	0,02	0,00	0,01	0,00	0,00	0,00	0,00	0,03	0,11
NiO	0,05	0,03	0,00	0,19	0,18	0,14	0,13	0,14	0,06	0,08	0,08	0,09	0,12	0,11	0,05	0,14	0,11	0,09	0,14	0,13	0,11	0,09	0,09	0,15	0,10
Total	100,98	100,99	100,77	99,86	99,81	99,34	100,38	99,58	99,48	100,86	100,51	100,35	100,23	99,84	101,48	100,64	100,55	100,69	100,27	99,93	100,92	100,02	99,43	100,66	100,19
Calculation based on O=4 APFU																									
Si	0,977	0,972	0,995	0,983	0,982	0,985	0,981	0,979	0,983	0,986	0,986	0,982	0,987	0,980	0,978	0,987	0,986	0,979	0,983	0,987	0,997	0,988	0,988	0,982	0,982
Al	0,001	-	0,002	0,001	0,001	0,001	0,002	-	0,001	0,003	-	0,001	0,001	0,002	0,001	0,001	0,001	0,001	-	0,001	0,001	0,001	-	0,001	0,001
Fe	0,311	0,566	0,591	0,257	0,267	0,287	0,267	0,300	0,398	0,329	0,371	0,296	0,300	0,301	0,281	0,271	0,309	0,313	0,308	0,300	0,288	0,391	0,430	0,303	0,324
Mg	1,717	1,466	1,387	1,759	1,746	1,728	1,755	1,725	1,614	1,675	1,640	1,724	1,711	1,718	1,749	1,743	1,706	1,717	1,712	1,714	1,702	1,613	1,572	1,716	1,693
Ca	0,008	0,011	0,011	0,006	0,007	0,007	0,006	0,007	0,008	0,007	0,008	0,006	0,006	0,007	0,006	0,005	0,002	0,002	0,004	0,007	0,006	0,006	0,006	0,003	
Na	-	0,002	0,001	0,001	0,002	0,001	0,001	-	-	0,002	-	-	0,001	0,001	-	-	0,001	0,002	0,002	0,001	-	0,001	0,001	-	
K	-	-	0,002	-	0,001	-	-	-	-	0,001	-	-	0,001	-	-	-	-	-	0,001	-	0,001	-	-	0,001	
Ti	-	-	0,001	-	0,002	-	-	-	-	0,001	0,002	0,001	0,001	0,001	-	-	-	-	0,001	0,001	0,001	-	-	-	0,002
Mn	0,004	0,011	0,013	0,004	0,005	0,004	0,005	0,006	0,008	0,005	0,006	0,005	0,004	0,006	0,004	0,003	0,005	0,005	0,005	0,004	0,011	0,012	0,005	0,006	
Cr	0,001	-	-	0,001	0,001	0,001	-	-	-	0,001	-	-	0,001	-	-	-	-	-	-	-	-	0,001	0,002		
Ni	0,001	0,001	-	0,004	0,004	0,003	0,003	0,003	0,001	0,002	0,002	0,002	0,002	0,001	0,003	0,002	0,002	0,003	0,003	0,002	0,002	0,002	0,003	0,002	
Total	3,021	3,029	3,004	3,016	3,017	3,015	3,019	3,021	3,015	3,012	3,013	3,016	3,013	3,019	3,023	3,012	3,013	3,022	3,017	3,015	3,002	3,012	3,012	3,018	3,015
Mg#	85	72	70	87	87	86	87	85	80	84	82	85	85	85	86	87	85,00	85,00	85,00	85,00	86,00	80,00	79,00	85,00	84,00
Fo	84,7	72,1	70,1	87,2	86,7	85,8	86,8	85,2	80,2	83,6	81,6	85,3	85,1	85,1	86,2	86,6	84,7	84,6	84,7	85,1	85,5	80,5	78,5	85,0	83,9

c: core, r: rim, mc: microcrystal

Cpx	Host rock										Enclave										Hbl-gabbro (BIII)				Phl-clinopyroxenite				
	BI		BII		BIII		Wehrlite (BII)		Cpx-hornblendite (BII)				42a2		70a2		42a2		70a2		42a2		70a2		42a2		70a2		
	Sample	K97-58	10	31	42	70	10a2	30a	48a	42a2	70a2																		
	wt.%	c #13	r #14	c #80	r #81	c #90	r #91	mc #99	mc #21	c #45	r #46	c #56	r #57	mc #67	c #57	c in g #67	c #95	c in g #5	c #14	c #132	r #133	c in g #133	c #152	r #65	c #66	r #6	c #7	r #7	
SiO₂	52,18	49,32	44,57	47,74	45,83	48,74	47,86	50,13	48,82	49,37	40,85	46,37	45,66	47,39	43,69	46,41	45,62	45,95	46,41	45,80	49,42	49,44	48,97	51,90	44,90				
Al₂O₃	0,66	2,82	7,25	5,37	9,26	6,49	6,44	3,19	5,62	4,91	12,92	7,71	8,88	6,28	9,83	9,39	8,97	9,52	8,98	8,71	6,07	5,78	6,17	4,10	9,62				
FeO	2,49	13,51	15,94	6,19	8,38	4,89	4,82	13,14	5,25	5,03	7,51	7,50	5,65	3,85	8,77	5,49	6,27	7,46	5,06	5,55	6,18	5,09	9,11	5,50	6,73				
MgO	16,96	10,58	5,98	13,97	11,13	14,43	13,52	8,91	14,71	15,06	10,09	11,95	12,90	14,69	10,49	12,89	12,54	11,83	12,98	12,64	12,64	14,83	10,38	13,59	11,32				
CaO	25,52	21,07	20,99	22,95	21,72	22,45	24,12	19,30	22,99	22,66	23,73	22,58	22,77	23,53	22,08	22,47	22,69	22,50	22,32	23,01	23,65	22,12	21,77	22,94	23,55				
Na₂O	0,17	0,70	1,78	0,53	1,07	0,72	0,77	2,94	0,49	0,54	0,66	0,81	0,76	0,56	0,87	0,72	0,80	0,89	0,88	0,73	1,07	0,59	1,53	1,42	0,87				
K₂O	0,01	0,02	0,00	0,01	0,02	0,00	0,00	0,00	0,01	0,01	0,00	0,03	0,03	0,02	0,04	0,02	0,01	0,01	0,03	0,04	0,00	0,00	0,01	0,02	0,01				
TiO₂	0,12	1,13	1,92	1,98	2,33	1,77	1,74	0,46	1,79	1,42	3,04	1,89	2,43	1,72	3,00	2,80	2,19	2,04	2,34	2,63	1,12	1,62	1,57	0,69	3,25				
MnO	0,38	0,41	0,59	0,11	0,12	0,08	0,10	0,35	0,08	0,13	0,08	0,15	0,04	0,05	0,44	0,09	0,12	0,13	0,12	0,12	0,14	0,12	0,24	0,14	0,17				
Cr₂O₃	0,00	0,00	0,00	0,00	0,02	0,32	0,11	0,05	0,04	0,34	0,02	0,07	0,16	0,47	0,00	0,35	0,00	0,03	0,62	0,49	0,08	0,22	0,04	0,07	0,04				
Total	98,50	99,57	99,02	98,85	99,87	99,88	99,49	98,47	99,80	99,48	98,91	99,05	99,30	98,56	99,20	100,63	99,21	100,36	99,75	99,71	100,37	99,81	99,79	100,37	100,44				
Calculation based on O=6 APFU																													
Si	1,93	1,88	1,73	1,78	1,70	1,79	1,77	1,91	1,80	1,82	1,54	1,74	1,69	1,76	1,65	1,70	1,69	1,69	1,71	1,70	1,81	1,82	1,83	1,89	1,66				
Mg	0,94	0,60	0,35	0,78	0,62	0,79	0,74	0,51	0,81	0,83	0,57	0,67	0,71	0,81	0,59	0,70	0,69	0,65	0,71	0,70	0,69	0,81	0,58	0,74	0,62				
Ca	1,01	0,86	0,87	0,92	0,87	0,88	0,95	0,79	0,91	0,89	0,96	0,91	0,90	0,94	0,89	0,88	0,90	0,89	0,88	0,91	0,93	0,87	0,90	0,93					
Na	0,01	0,05	0,13	0,04	0,08	0,05	0,06	0,22	0,04	0,04	0,05	0,06	0,06	0,04	0,06	0,05	0,06	0,06	0,06	0,05	0,08	0,04	0,11	0,10	0,06				
K	0,00	0,00	0,00	0,00	0,00	0,00	0,00	0,00	0,00	0,00	0,00	0,00	0,00	0,00	0,00	0,00	0,00	0,00	0,00	0,00	0,00	0,00	0,00	0,00	0,00	0,00	0,00		
Ti	0,00	0,03	0,06	0,06	0,07	0,05	0,05	0,01	0,05	0,04	0,09	0,05	0,07	0,05	0,09	0,08	0,06	0,06	0,07	0,07	0,03	0,05	0,04	0,02	0,09				
Mn	0,01	0,01	0,02	0,00	0,00	0,00	0,01	0,00	0,00	0,01	0,00	0,01	0,00	0,01	0,00	0,00	0,00	0,00	0,00	0,00	0,00	0,00	0,01	0,00	0,01	0,00	0,01		
Cr	0,00	0,00	0,00	0,00	0,00	0,01	0,00	0,00	0,01	0,00	0,00	0,01	0,01	0,01	0,00	0,00	0,02	0,01	0,00	0,01	0,00	0,00	0,00	0,00	0,00	0,00	0,00		
Fe³⁺	0,08	0,10	0,23	0,13	0,13	0,09	0,14	0,23	0,10	0,10	0,23	0,14	0,15	0,12	0,17	0,08	0,16	0,15	0,11	0,12	0,12	0,07	0,09	0,10	0,15				
Fe²⁺	0,00	0,33	0,29	0,06	0,13	0,06	0,00	0,19	0,06	0,05	0,01	0,09	0,03	0,00	0,11	0,08	0,04	0,08	0,05	0,05	0,07	0,09	0,19	0,07	0,06				
Al_{IV}	0,03	0,12	0,27	0,22	0,30	0,21	0,24	0,09	0,21	0,18	0,47	0,27	0,31	0,24	0,36	0,30	0,31	0,31	0,29	0,31	0,19	0,19	0,17	0,11	0,34				
Al_{VI}	0,00	0,01	0,06	0,02	0,11	0,07	0,05	0,05	0,04	0,03	0,11	0,08	0,08	0,04	0,08	0,10	0,09	0,11	0,10	0,07	0,08	0,07	0,10	0,07	0,08				
Total	4,02	4,00	4,00	4,00	4,00	4,00	4,00	4,00	4,00	4,00	4,00	4,00	4,00	4,01	4,00	4,00	4,00	4,00	4,00	4,00	4,00	4,00	4,00	4,00	4,00	4,00	4,00		
Fe₂O₃	2,77	3,41	7,94	4,66	4,70	3,22	5,21	8,05	3,68	3,62	8,13	5,03	5,21	4,28	5,93	3,06	5,53	5,32	3,83	4,42	4,41	2,40	3,27	3,56	5,21				
FeO	0,00	10,44	8,80	2,00	4,15	1,98	0,13	5,90	1,94	1,76	0,20	2,98	0,97	0,00	3,43	2,74	1,29	2,67	1,61	1,57	2,21	2,94	6,17	2,29	2,04				
Wo	49,97	45,47	50,26	48,60	49,65	48,46	51,66	45,99	48,35	47,67	54,39	50,12	50,46	50,09	50,73	50,28	50,40	50,24	50,35	51,23	51,34	47,35	50,24	49,72	52,87				
En	46,21	31,77	19,93	41,16	35,40	43,31	40,29	29,56	43,03	44,08	32,17	36,88	39,77	43,51	33,54	40,12	38,73	36,76	40,74	39,14	38,19	44,15	33,34	40,98	35,34				
Fs	3,81	22,76	29,81	10,24	14,95	8,23	8,05	24,45	8,62	8,25	13,44	13,00	9,77	6,40	15,73	9,60	10,87	13,00	8,91	9,63	10,48	8,51	16,41	9,30	11,79				
Mg*	92	58	40	80	70	84	83	55	83	84	71	74	80	87	68	81	78	74	82	80	78	84	67	82	75				

c: core, r: rim, mc: microcrystal, g: glass, Hbl: hornblend, Cpx: clinopyroxene, Phl: phlogopite

1
2
3 **(BIII)**
4
5 r
6 #11
7 42,14
8 12,32
9 6,80
10 10,80
11 24,29
12 0,49
13 0,01
14 3,12
15 0,10
16 0,04
17 100,08
18
19
20 1,56
21 0,60
22 0,97
23 0,04
24 0,00
25 0,09
26 0,00
27 0,00
28 0,20
29 0,02
30 0,44
31 0,10
32
33 4,00
34 6,98
35 0,52
36 54,45
37 33,66
38 11,89
39 74
40
41
42
43
44
45
46

		Host rock																		Enclave																							
		BII									BIII									Wehrlite (BII)						Hornblendite (BIII)						Clinopyroxene hornblendite (BII)						Hbl-Gabbro (BIII)					
Hbl	BII	Sample	K97-10	c	r	m	c	m	m	c	r	c	m	c	r	c	r	c	inc	c	r	inc	c in g	c	c	r	c	c	c in g	c													
		wt.%	#92	#93	#96	#1	#12	#21	#34b	#35b	#39b	#59	#47b	#48b	#64	#65	#34	#35	#40	#18	#19	#20	#103	#107	#129	#130	#147	#42	#54	#58													
SiO ₂	38,71	37,90	37,21	38,28	40,48	40,96	38,98	38,04	39,24	39,33	37,94	38,45	38,74	39,18	39,74	39,03	38,60	37,65	38,64	37,93	38,98	40,57	38,83	39,44	39,40	39,75	38,83	38,11															
Al ₂ O ₃	13,86	14,30	14,49	14,80	11,92	10,85	14,73	14,59	14,58	14,21	14,07	14,49	14,82	14,09	14,55	14,03	14,05	14,34	14,52	15,09	14,94	14,54	14,59	15,07	14,71	14,18	14,54	15,35															
FeOt	11,06	11,11	16,21	8,04	7,40	9,52	8,17	8,74	8,39	9,92	16,97	10,10	13,91	8,25	8,19	11,14	14,32	11,70	9,12	14,59	8,74	8,14	7,86	10,06	7,82	7,89	9,51	13,75															
MgO	13,20	12,41	8,88	14,03	10,36	9,21	14,23	13,85	13,93	13,44	8,43	12,77	10,78	14,65	13,92	12,39	10,73	12,13	13,33	10,25	13,97	14,41	14,25	13,49	14,62	13,94	12,90	10,39															
CaO	12,22	11,99	11,45	12,27	22,18	21,55	12,39	11,86	12,28	11,98	11,74	11,90	11,16	12,19	11,84	12,13	11,61	11,77	11,89	11,78	11,84	12,23	12,07	12,17	12,21	11,50	11,83	11,70															
Na ₂ O	2,49	2,27	2,61	2,09	0,86	1,02	2,24	2,20	2,43	2,46	2,34	2,24	2,49	2,34	2,44	2,50	2,46	2,86	2,84	2,71	3,02	2,45	2,59	2,46	2,46	2,92	2,69	2,70															
K ₂ O	1,78	1,49	1,77	2,07	0,05	0,03	1,81	1,88	1,73	1,69	1,78	1,64	2,03	1,75	1,73	1,89	1,72	1,62	1,55	1,63	1,33	1,53	1,82	2,07	1,71	1,53	1,50	1,44															
TiO ₂	4,37	5,46	4,71	5,27	4,34	3,66	5,15	5,30	5,35	4,19	3,95	4,78	3,05	4,53	5,38	4,42	4,24	3,83	4,27	3,58	4,42	4,31	4,78	2,30	5,12	5,49	5,26	3,70															
MnO	0,20	0,10	0,31	0,04	0,11	0,18	0,10	0,10	0,07	0,12	0,25	0,15	0,21	0,06	0,07	0,10	0,19	0,18	0,13	0,27	0,13	0,15	0,10	0,09	0,08	0,10	0,16	0,23															
Cr ₂ O ₃	0,03	0,00	0,00	0,04	0,02	0,08	0,00	0,00	0,00	0,02	0,00	0,00	0,03	0,08	0,02	0,00	0,03	0,02	0,03	0,00	0,00	0,09	0,10	0,03	0,13	0,01	0,04																
Tot	97,91	97,02	97,65	96,92	97,70	97,05	97,78	96,56	98,00	97,36	97,46	96,53	97,22	97,10	97,87	97,64	97,96	96,09	96,32	97,82	97,37	98,33	96,97	97,24	98,15	97,41	97,24	97,40															
Calculation based on O=23 APFU																																											
Si	5,77	5,69	5,70	5,69	6,01	6,17	5,73	5,68	5,76	5,84	5,83	5,77	5,87	5,80	5,82	5,83	5,82	5,74	5,79	5,74	5,76	5,90	5,75	5,87	5,75	5,84	5,77	5,76															
Mg	2,93	2,78	2,03	3,11	2,29	2,07	3,12	3,09	3,05	2,98	1,93	2,86	2,43	3,23	3,04	2,76	2,41	2,76	2,98	2,31	3,07	3,12	3,15	2,99	3,18	3,05	2,86	2,34															
Ca	1,95	1,93	1,88	1,95	3,53	3,48	1,95	1,90	1,93	1,91	1,93	1,91	1,81	1,93	1,86	1,94	1,88	1,92	1,91	1,91	1,87	1,90	1,92	1,94	1,91	1,81	1,88	1,89															
Na	0,72	0,66	0,78	0,60	0,25	0,30	0,64	0,64	0,69	0,71	0,70	0,65	0,73	0,67	0,69	0,72	0,72	0,84	0,83	0,80	0,86	0,69	0,74	0,71	0,70	0,83	0,77	0,79															
K	0,34	0,29	0,35	0,39	0,01	0,01	0,34	0,36	0,32	0,32	0,35	0,31	0,39	0,33	0,32	0,36	0,33	0,32	0,30	0,31	0,25	0,28	0,34	0,39	0,32	0,29	0,28	0,28															
Ti	0,49	0,62	0,54	0,59	0,48	0,41	0,57	0,60	0,59	0,47	0,46	0,54	0,35	0,50	0,59	0,50	0,48	0,44	0,48	0,41	0,49	0,47	0,53	0,26	0,56	0,61	0,59	0,42															
Mn	0,03	0,01	0,04	0,00	0,01	0,02	0,01	0,01	0,01	0,01	0,03	0,02	0,03	0,01	0,01	0,02	0,02	0,03	0,02	0,02	0,03	0,02	0,02	0,01	0,01	0,01	0,02	0,03															
Cr	0,00	0,00	0,00	0,00	0,00	0,01	0,00	0,00	0,00	0,00	0,00	0,00	0,00	0,01	0,00	0,00	0,00	0,00	0,00	0,00	0,00	0,00	0,01	0,01	0,00	0,01	0,00	0,00	0,00														
Fe 3+	0,13	0,09	0,02	0,00	0,00	0,00	0,14	0,00	0,08	0,00	0,05	0,31	0,11	0,00	0,00	0,16	0,11	0,00	0,13	0,07	0,00	0,00	0,17	0,00	0,00	0,00	0,00	0,09	0,09														
Fe2+	1,25	1,31	2,05	1,00	0,92	1,20	1,00	0,95	1,03	1,15	2,18	1,22	1,45	0,91	1,00	1,39	1,65	1,39	1,14	1,71	1,01	0,99	0,97	1,09	0,96	0,97	1,18	1,65															
Aliv	2,25	2,32	2,30	2,30	1,38	1,21	2,26	2,33	2,22	2,17	2,16	2,24	2,17	2,21	2,17	2,15	2,20	2,27	2,20	2,27	2,25	2,10	2,24	2,15	2,25	2,14	2,21	2,25															
Alvi	0,18	0,21	0,31	0,29	0,91	0,91	0,29	0,23	0,31	0,32	0,39	0,32	0,46	0,24	0,35	0,33	0,29	0,30	0,37	0,41	0,35	0,39	0,32	0,49	0,29	0,33	0,34	0,48															
Tot	16,04	15,89	16,01	15,93	15,80	15,79	15,92	15,92	15,91	15,95	15,96	15,89	16,00	15,96	15,85	15,99	15,96	16,11	16,01	16,05	16,00	15,87	15,98	16,08	15,92	15,89	15,91	15,98															
Mg#	68	66	49	76	71	63	75	74	75	70	47	69	58	76	75	66	57	65	72	55	74	76	70	77	76	70	57																
Naming	Prg	Krs	Krs	Krs	Prg	Prg	Krs	Krs	Prg	Prg	Krs	Prg	Krs	Prg	Krs	Prg	Prg	Krs	Prg	Prg	Krs	Prg	Prg	Krs	Prg	Krs	Prg	Krs	Prg	Krs	Prg												

c: core, r: rim, mc: microcrystal, g: glass, inc: inclusion, Prg: pargasite, Krs: kaersutite, Hbl: hornblend

Phl	Phl-clinopyroxenite (BIII)				Hbl-Gabbro (BIII)	
	Sample	K97-70a2		42a2		
wt.%	c #4	r #5	c #12	r #13	mc #48	mc #60
SiO₂	36,44	35,63	36,27	36,38	38,45	37,40
Al₂O₃	17,17	16,95	15,81	17,21	14,69	15,78
FeOt	11,82	10,23	12,21	9,64	7,73	9,67
MgO	16,84	17,60	17,06	18,44	21,41	18,86
CaO	0,03	0,10	0,00	0,05	0,06	0,07
Na₂O	0,46	0,46	0,51	0,61	0,86	0,96
K₂O	9,67	9,67	9,56	9,34	9,06	9,02
TiO₂	3,95	4,33	2,58	3,33	2,96	3,27
MnO	0,19	0,14	0,17	0,14	0,11	0,12
Total	96,57	95,11	94,17	95,15	95,33	95,14
Calculation based on O=22 APFU						
Si	5,73	5,66	5,83	5,73	6,05	5,95
Al	3,18	3,17	2,99	3,19	2,73	2,96
Fe³⁺	0,49	0,59	0,85	0,64	0,77	0,65
Fe²⁺	1,07	0,77	0,79	0,63	0,23	0,62
Mg	3,95	4,16	4,09	4,33	5,02	4,47
Ca	0,01	0,02	0,00	0,01	0,01	0,01
Na	0,14	0,14	0,16	0,19	0,26	0,30
K	1,94	1,96	1,96	1,88	1,82	1,83
Ti	0,47	0,52	0,31	0,39	0,35	0,39
Mn	0,03	0,02	0,02	0,02	0,01	0,02
Fe	1,56	1,36	1,64	1,27	1,02	1,29
Total	17,00	17,00	17,00	17,00	17,26	17,22
Fe₂O₃	4,13	4,91	7,04	5,36	6,62	5,49
FeO	8,11	5,82	5,87	4,82	1,77	4,73
Mg/Fe	2,54	3,07	2,49	3,41	4,94	3,47
Fe#	0,28	0,25	0,29	0,23	0,17	0,22

c: core, r: rim, mc: microcrystal

PI	Host rock										Enclave										
	BI			BII			BIII				Hornblende gabbro (BIII)					Cpx-hornblendite (BII)					
Sample	K97-58			31		48		42		70		K97-42a2					K97-48a				
	c	r	m	m	m	m	m	m	m	m	c	r	c	m	m	m	c	c	c	r	
wt.%	#10b	#11b	#2b	#14	#23	#37b	#40b	#70	#82	#42b	#43b	#43	#55	#67	#70	#140	#141	#142			
SiO₂	53,54	52,89	50,95	54,12	51,45	53,71	52,12	53,02	54,17	55,85	54,95	55,83	55,78	56,42	57,50	44,36	51,50	43,70			
Al₂O₃	28,94	29,29	30,08	27,11	29,13	28,36	30,02	28,32	25,90	28,19	28,66	27,10	27,04	26,96	26,70	34,09	29,21	35,06			
FeOt	0,38	0,34	0,69	0,49	0,46	0,68	0,63	0,55	1,25	0,21	0,32	0,29	0,23	0,27	0,25	0,18	0,56	0,23			
MgO	0,03	0,05	0,07	0,03	0,01	0,04	0,05	0,14	0,62	0,01	0,03	0,03	0,01	0,02	0,00	0,03	0,03	0,00			
CaO	11,47	11,73	12,93	9,31	11,86	10,53	11,88	11,04	9,87	9,59	10,58	9,47	9,35	8,73	8,54	17,96	12,05	18,70			
Na₂O	4,67	4,50	3,88	5,94	4,68	5,28	4,38	4,95	6,13	5,62	5,31	5,89	5,94	6,19	6,16	1,17	4,55	0,69			
K₂O	0,64	0,61	0,45	0,61	0,26	0,43	0,46	0,61	0,89	0,65	0,58	0,58	0,69	0,66	0,66	0,06	0,26	0,04			
TiO₂	0,08	0,09	0,16	0,11	0,20	0,17	0,12	0,08	0,53	0,05	0,00	0,03	0,03	0,04	0,04	0,03	0,20	0,07			
Total	99,74	99,49	99,20	97,71	98,04	99,18	99,66	98,71	99,36	100,16	100,43	99,21	99,06	99,27	99,84	97,88	98,35	98,49			
Calculation based on O=32 APFU																					
Si	9,74	9,65	9,37	10,01	9,54	9,81	9,51	9,75	9,96	10,04	9,89	10,14	10,15	10,22	10,33	8,37	9,53	8,20			
Al	6,20	6,30	6,53	5,91	6,37	6,11	6,46	6,14	5,61	5,97	6,08	5,80	5,80	5,76	5,66	7,58	6,37	7,76			
Fe	0,06	0,05	0,11	0,08	0,07	0,10	0,10	0,08	0,19	0,03	0,05	0,05	0,04	0,04	0,04	0,03	0,09	0,04			
Mg	0,01	0,01	0,02	0,01	0,00	0,01	0,01	0,04	0,17	0,00	0,01	0,01	0,00	0,01	0,00	0,01	0,01	0,00			
Ca	2,23	2,29	2,55	1,84	2,36	2,06	2,32	2,18	1,94	1,85	2,04	1,84	1,82	1,70	1,64	3,63	2,39	3,76			
Na	1,64	1,59	1,38	2,13	1,68	1,87	1,55	1,77	2,19	1,96	1,85	2,07	2,09	2,18	2,15	0,43	1,63	0,25			
K	0,15	0,14	0,11	0,15	0,06	0,10	0,11	0,14	0,21	0,15	0,13	0,13	0,16	0,15	0,15	0,01	0,06	0,01			
Ti	0,01	0,01	0,02	0,02	0,03	0,02	0,02	0,01	0,07	0,01	0,00	0,00	0,00	0,01	0,01	0,01	0,03	0,01			
Total	20,04	20,05	20,08	20,14	20,12	20,08	20,07	20,12	20,35	20,01	20,05	20,05	20,07	20,05	19,98	20,06	20,10	20,03			
An	56,8	58,3	64,4	46,1	58,8	52,6	59,7	54,6	46,2	48,1	52,0	46,9	46,1	43,5	43,0	89,7	59,9	93,9			
Ab	39,4	38,1	32,9	50,2	39,6	44,9	37,6	41,8	48,9	48,0	44,5	49,7	49,9	52,6	53,0	10,0	38,5	5,9			
Or	3,8	3,6	2,7	3,6	1,6	2,5	2,7	3,6	5,0	3,9	3,4	3,4	4,0	3,9	4,0	0,3	1,5	0,2			

c: core, r: rim, m: microlite

Nepheline

Sample	K97-31	48		BIII	Hbl-clinopyroxenite (BII)			
	m	m	c	r	c	c	c	c
wt.%	#13	#15b	#17b	#18b	#83	#33	#38	#45
SiO₂	43,37	43,98	44,07	43,05	52,76	43,31	43,11	42,85
Al₂O₃	28,18	33,85	33,86	34,12	25,85	34,23	34,19	33,50
FeOt	3,29	0,58	0,20	0,23	2,56	0,15	0,14	0,14
MgO	1,17	0,00	0,04	0,02	0,28	0,02	0,01	0,00
CaO	4,79	1,48	1,80	1,25	0,54	2,58	2,73	2,04
Na₂O	14,23	15,43	15,82	16,21	13,24	15,75	15,94	16,03
K₂O	2,39	4,04	4,16	4,37	1,67	4,35	3,84	4,37
TiO₂	1,45	0,07	0,00	0,00	0,77	0,00	0,01	0,00
Total	98,85	99,43	99,95	99,24	97,67	100,40	99,97	98,93

Calculation based on O=32 APFU

Si	8,48	8,40	8,39	8,27	9,96	8,24	8,23	8,28
Al	6,49	7,62	7,60	7,73	5,75	7,68	7,69	7,63
Fe	0,54	0,09	0,03	0,04	0,40	0,03	0,02	0,02
Mg	0,34	0,00	0,01	0,01	0,08	0,00	0,00	0,00
Ca	1,00	0,30	0,37	0,26	0,11	0,53	0,56	0,42
Na	5,39	5,72	5,84	6,04	4,85	5,81	5,90	6,01
K	0,60	0,98	1,01	1,07	0,40	1,06	0,94	1,08
Ti	0,21	0,01	0,00	0,00	0,11	0,00	0,00	0,00
Total	23,06	23,13	23,24	23,42	21,68	23,35	23,34	23,44

Leucite**Hauyne**

Sample	56	48	42	70	Cpx-hornblendite (BII)			
	c	c	m	c	c	c	c	c
wt.%	16	#28	#30	#81	#2	#3	#12	#105
SiO₂	54,87	54,39	55,04	54,40	34,37	35,68	34,11	34,02
Al₂O₃	22,94	23,10	24,26	23,51	28,12	26,78	27,29	28,13
FeOt	0,42	0,27	0,23	0,29	0,23	0,57	0,21	0,80
MgO	0,01	0,00	0,00	0,01	0,23	0,25	0,16	0,22
CaO	0,00	0,00	0,06	0,04	7,57	6,78	7,59	7,71
Na₂O	0,09	0,29	0,50	0,10	10,35	7,26	8,07	8,36
K₂O	21,20	21,11	19,49	21,32	4,29	5,40	5,28	6,30
TiO₂	0,12	0,16	0,00	0,24	0,02	0,00	0,06	0,00
Total	99,76	99,32	99,57	99,92	85,17	82,71	82,75	85,55
Calc. based on O=32 APFU					Calc. based on O=21 APFU			
Si	2,00	1,99	1,99	1,98	5,16	5,46	5,26	5,13
Al	0,99	1,00	1,03	1,01	4,97	4,83	4,95	5,00
Fe	0,01	0,01	0,01	0,01	0,03	0,07	0,03	0,10
Mg	0,00	0,00	0,00	0,00	0,05	0,06	0,04	0,05
Ca	0,00	0,00	0,00	0,00	1,22	1,11	1,25	1,25
Na	0,01	0,02	0,04	0,01	3,01	2,15	2,41	2,44
K	0,99	0,99	0,90	0,99	0,82	1,05	1,04	1,21
Ti	0,00	0,00	0,00	0,01	0,00	0,00	0,01	0,00
Total	4,00	4,01	3,96	4,01	15,27	14,73	14,98	15,19

c: core, r: rim, m: microlite

Oxides	Host rock						Enclave						Cpx-hornblendite	
	BI			BIII			Wehrlite (BII)							
	Sample	K97-58		70		10a2				48a				
wt.%	Titanomagnetite			Spinel			Chromian spinel						Magnesian ilmenite	
	mc #5	mc #6	mc #7	inc #66	inc #78	inc #79	mp #86	inc #50	inc #51	inc #54	inc #55	inc #56	c #155	c #156
SiO₂	0,10	0,10	0,07	0,05	0,12	0,11	0,02	0,05	0,02	0,00	0,00	0,03	0,24	0,42
Al₂O₃	4,10	4,09	3,68	55,08	59,64	59,65	61,19	38,13	37,98	32,42	32,39	36,52	0,41	0,24
FeOt	65,78	64,87	65,64	27,54	19,19	19,54	28,64	25,50	25,70	24,33	25,05	25,23	33,28	33,15
MgO	4,21	3,95	3,85	16,19	20,08	19,88	9,60	14,89	14,59	13,85	13,72	13,70	8,42	8,46
CaO	0,16	0,24	0,14	0,02	0,04	0,00	0,04	0,00	0,04	0,02	0,00	0,01	0,02	0,16
Na₂O	23,14	23,05	22,23	1,04	0,95	1,17	0,31	1,41	1,42	0,86	0,90	0,87	53,74	53,46
MnO	0,69	0,72	0,76	0,27	0,06	0,07	0,26	0,15	0,13	0,07	0,06	0,16	0,49	0,39
Cr₂O₃	0,09	0,04	0,02	0,05	0,01	0,04	0,00	18,97	19,03	27,21	26,89	22,33	0,02	0,05
Total	98,28	97,07	96,38	100,25	100,10	100,46	100,06	99,10	98,91	98,76	99,00	98,84	96,61	96,32
Calculation based on O=32 APFU													O=6 APFU	
Si	0,03	0,03	0,02	0,01	0,03	0,02	0,01	0,01	0,00	0,00	0,00	0,01	0,01	0,02
Al	1,37	1,39	1,26	13,76	14,39	14,38	15,61	10,30	10,30	9,04	9,02	10,02	0,02	0,01
Fe³⁺	4,65	4,55	4,98	1,87	1,26	1,21	0,28	1,75	1,74	1,56	1,64	1,55	0,01	0,01
Fe²⁺	10,98	11,08	10,98	3,01	2,02	2,13	4,90	3,14	3,21	3,25	3,32	3,37	1,35	1,35
Mg	1,78	1,69	1,67	5,12	6,13	6,06	3,10	5,09	5,01	4,89	4,83	4,76	0,61	0,62
Ca	0,05	0,07	0,04	0,00	0,01	0,00	0,01	0,00	0,01	0,01	0,00	0,00	0,00	0,01
Ti	4,95	5,00	4,86	0,17	0,15	0,18	0,05	0,24	0,25	0,15	0,16	0,15	1,97	1,97
Mn	0,17	0,17	0,19	0,05	0,01	0,01	0,05	0,03	0,02	0,01	0,01	0,03	0,02	0,02
Cr	0,02	0,01	0,00	0,01	0,00	0,01	0,00	3,44	3,46	5,09	5,02	4,11	0,00	0,00
Total	24,00	24,00	24,00	24,00	24,00	24,00	24,00	24,00	24,00	24,00	24,00	24,00	4,00	4,00
Fe²O³	21,76	20,98	22,75	11,75	8,20	7,89	1,74	10,15	10,02	8,79	9,20	8,82	0,20	0,26
FeO	46,20	45,99	45,16	16,96	11,81	12,44	27,08	16,37	16,69	16,42	16,77	17,28	33,10	32,91
Mg#	10	10	9	51	65	64	37	51	50	50	49	49	31	31
Cr#=Cr/(Cr+Al)	0,015	0,007	0,003	0,001	0,000	0,000	0,000	0,250	0,252	0,360	0,358	0,291	0,024	0,117
Fe²⁺/(Mg+Fe²⁺)	0,860	0,867	0,868	0,370	0,248	0,260	0,613	0,382	0,391	0,399	0,407	0,414	0,688	0,686
Fe³⁺/(Cr+Al+Fe³⁺)	0,769	0,765	0,798	0,120	0,081	0,078	0,018	0,113	0,112	0,100	0,104	0,099	0,233	0,377

c: core, mc: microcrystal, mp: microphenocryst, inc: inclusion

1
2 (BII)
3 _____
4 ite
5 c
6 #160
7 0,02
8 0,35
9 33,97
10 7,93
11 0,01
12 52,94
13 0,40
14 0,05
15 95,67
16 _____
17 J
18 0,00
19 0,02
20 0,04
21 1,37
22 0,59
23 0,00
24 1,98
25 0,02
26 0,00
27 4,01
28 _____
29 0,98
30 33,08
31 _____
32 29
33 0,088
34 0,700
35 0,618
36
37
38
39
40
41
42
43
44
45
46
47
48
49
50
51
52
53
54
55
56
57
58
59
60

Glass	Wehrlite (BII)				Phl-clinopyroxenite				Cpx-hornblendite (BII)								Hornblendite (BIII)				Hbl-Gabbro (BIII)							
	Sample	K97-10a2		70a2						48a2				30a								17a2		42a2				
		Gim	Gim	Gp	Gp	Gim	Gim	Gim	Gim	Gp	Gp	Gim	Gim	Gim	Gim	Gim	inc (Hyn)	Gp	Gp	Gim	Gim	Gim	Gim	Gp	inc (Pl)			
wt.%		#62	#63	#66	#74	#8	#9	#14	#19	#24	#25	#138	#144	#153	#6	#11	#15	#24	#102	#106	#27	#29	#36	#41	#44	#53	#56	#71
SiO₂	44,33	45,04	44,96	45,25	46,18	44,75	47,46	44,64	44,05	46,22	45,49	46,00	52,54	49,91	49,76	49,81	49,17	49,20	48,86	50,58	49,91	49,91	50,24	55,31	55,63	54,58	56,04	
TiO₂	2,02	1,96	1,89	1,94	0,85	1,81	0,55	2,67	2,40	1,80	2,18	1,79	0,77	1,33	1,44	1,43	1,68	1,53	1,46	1,27	1,32	1,37	1,34	0,81	0,95	1,01	0,94	
Al₂O₃	20,86	21,12	21,25	21,09	29,38	25,27	17,51	17,22	22,97	13,67	20,31	21,04	22,85	20,42	20,68	20,93	20,63	20,68	20,29	20,18	20,00	19,98	20,08	21,88	22,57	22,08	22,09	
Fe₂O₃	8,06	7,33	7,47	7,67	3,35	5,22	7,91	9,77	8,20	8,87	5,22	4,46	3,37	6,64	7,42	7,54	6,82	7,23	7,42	6,58	7,38	6,98	7,00	4,25	4,46	4,62	4,38	
MnO	0,18	0,19	0,16	0,13	0,16	0,21	0,26	0,26	0,26	0,28	0,21	0,14	0,00	0,17	0,17	0,17	0,14	0,17	0,20	0,15	0,18	0,17	0,16	0,15	0,13	0,14	0,10	
MgO	3,48	3,33	3,11	2,94	1,25	2,40	5,13	5,31	2,48	7,19	5,01	4,59	1,42	2,32	2,48	2,35	2,58	2,11	2,65	2,32	2,63	2,57	2,76	1,08	0,98	1,11	1,03	
CaO	8,55	8,11	8,00	7,65	4,30	5,92	11,81	11,26	5,60	15,00	9,27	9,07	5,36	6,99	6,89	5,66	6,86	5,93	6,95	5,40	6,00	5,81	5,86	2,88	2,51	2,72	2,43	
Na₂O	6,04	6,41	6,55	6,41	9,46	9,86	3,59	2,94	9,17	6,33	9,67	10,70	9,88	5,27	5,15	5,37	5,84	4,44	5,34	5,38	5,33	5,28	5,23	5,53	5,46	5,54	5,66	
K₂O	3,58	3,55	3,86	3,93	3,33	2,93	3,03	5,84	3,31	1,71	1,72	1,64	2,74	4,17	3,92	3,97	4,21	3,49	3,74	4,81	4,47	4,65	4,76	5,49	5,52	5,44	5,51	
P₂O₅					0,40	0,45	0,54	0,49	0,35	0,59																		
Total	97,1	97,0	97,2	97,0	98,7	98,8	97,8	100,4	98,8	101,6	99,1	99,4	98,9	97,2	97,9	97,2	97,9	94,8	96,9	96,7	97,2	96,7	97,4	97,4	98,2	97,2	98,2	
FeO_t	7,3	6,6	6,7	6,9	3,0	4,7	7,1	8,8	7,4	8,0	4,7	4,0	3,0	6,0	6,7	6,8	6,1	6,5	6,7	5,9	6,6	6,3	6,3	3,8	4,0	4,2	3,9	
Mg#	44	45	43	41	40	45	54	49	35	59	63	65	43	38	37	36	40	34	39	39	39	40	41	31	28	30	30	

Gp: glass pockets, Gim: glass associated with intergranular minerals, inc: inclusion, Hyn: hauyne, Pl: plagioclase. Hbl: hornblend, Cpx: clinopyroxene, Phl: phlogopite

	Equation (13) Putirka RiMG '08	Equation (14) Putirka RiMG '08	Equation (15) Putirka RiMG '08	Equation (16) Putirka RiMG '08	Thornber '87 Mg-thermometer	
	T(C) 1	1086	1143	1169	1163	1084
2	1086	1143	1180	1187	1084	
3	1086	1143	1180	1187	1084	
4	1086	1143	1180	1187	1084	
5	1082	1140	1166	1147	1081	
6	1082	1140	1178	1170	1081	
7	1082	1140	1178	1170	1081	
8	1082	1140	1178	1170	1081	
9	1076	1139	1161	1142	1077	
10	1076	1139	1173	1166	1077	
11	1076	1139	1173	1166	1077	
12	1076	1139	1173	1166	1077	
13	1072	1131	1154	1131	1073	
14	1072	1131	1166	1155	1073	
15	1072	1131	1166	1155	1073	
16	1072	1131	1166	1155	1073	
17						
18						
19						
20						
21						
22						
23						
24						
25						

1 Helz &
2 Thornber '87
3 Ca-thermometer
4 T(C)

5 1110

6 1110

7 1110

8 1110

9 1103

10 1103

11 1103

12 1103

13 1103

14 1103

15 1103

16 1101

17 1101

18 1101

19 1101

20 1095

21 1095

22 1095

23 1095

24 1095

25 1095

For Review Only

Sample-K97-	Host rock											Italian Journal of Geosciences									
	BII				BIII							Wehrlite		Phl-Cpxt		Cpx-Hornblendite		Hornblendite		Plb Cpx-Hblt	
	wt.%	58	30	31	48	14	17	42	46	70	10a2	70a2	30a	48a2	14a	17a2	46a	42a2			
SiO ₂	46,04	47,12	45,49	45,22	47,05	47,45	46,94	47,44	47,01	42,05	40,45	41,69	39,12	38,94	38,92	41,39	44,83				
Al ₂ O ₃	15,59	17,54	16,81	17,19	17,92	17,89	17,69	18,18	17,84	3,82	12,1	15,32	14,6	15,25	14,8	15,55	17,66				
Fe ₂ O ₃	8,69	8,76	8,98	9,31	8,5	8,21	8,65	8,31	8,01	12,16	9,3	10,13	12,34	11,1	11,05	9,83	9,24				
MnO	0,13	0,16	0,16	0,17	0,15	0,14	0,15	0,16	0,14	0,17	0,15	0,14	0,21	0,15	0,13	0,13	0,16				
MgO	7,22	5,78	7,7	6,07	5,94	6,1	6,52	5,4	5,71	34,63	12,1	10,4	11,57	8,8	11,38	10,66	6,34				
CaO	10,95	8,48	9,24	8,89	8,31	7,88	8,65	8,01	7,89	7,35	13,76	12,72	12,77	13,15	12,69	11,88	9,95				
Na ₂ O	3,36	5,37	5,15	5,09	5,77	5,68	5,53	5,93	5,69	0,53	1,53	3,37	2,73	3,3	2,89	3,25	4,87				
K ₂ O	2,37	3,21	3,19	3,3	3,55	3,62	3,55	3,55	3,57	0,31	4,16	1,85	1,52	2,39	1,94	2,06	2,74				
TiO ₂	2,05	1,96	2,07	2,32	1,9	1,81	1,99	1,89	1,77	0,75	3,12	3,11	4,14	3,3	4,19	3,89	2,53				
P ₂ O ₅	0,69	0,99	1	0,75	0,85	0,86	0,88	0,9	0,82	0,12	1,76	0,79	0,26	2,82	1,48	0,62	1,18				
LOI	1,93	0,42	0,2	1,05	-0,03	0,58	-0,18	0,06	0,19	-0,41	1,95	0,73	0,49	0,51	0,47	0,62	0,32				
TOTAL	99,02	99,79	99,99	99,36	99,91	100,22	100,37	99,83	98,64	101,48	100,38	100,25	99,75	99,71	99,94	99,88	99,82				
(ppm)																					
Sr		1101								980	998	159	1149	1609	1041	1049	1022	1019	1256		
Ba		956								940	881	86	2771	761	804	852	768	819	951		
Rb		74,7								72,9	84,5	4,9	109	23,1	7	34,7	21,3	19,9	47,9		
Ni		69								55	50	598	91	23	13	< .5	39	39	18		
Co		34,2								35,9	37,2	117,8	41,5	53	69,5	48,5	58,6	50,7	38,2		
Cr	182	141	167	94	113	68	78	68	59	2331	301	96	34	7	42	94	68				
V		195								169	149	115	329	349	437	293	382	372	234		
Zr	260	301	230	273	239	239	242	254	227	35	303	261	193	205	189	228	252				
Y		27,4								25,1	26,2	6,2	24,9	27,3	28,8	37,2	33,2	29,8	31,7		
Nb		86,8								81,9	93,8	10,8	79,2	61	63,5	73,1	66,2	65,2	93,1		
Ga		20,7								20,6	22,8	6	18,5	17,9	19,1	18,3	17,2	17,7	20,7		
Cs		1,1								1,2	1,4	< .1	1,3	0,2	< .1	0,4	0,2	0,3	0,7		
Hf		4,4								4,4	5,5	1,2	7,7	4,6	4,1	4,3	4,6	4,9	5,2		
Ta		5,3								5	5,1	0,9	4,2	3,3	3,2	4,4	4,3	4,1	5,5		
Th		8,2								8,3	8,3	0,7	6	5,6	0,7	4,5	2,4	3,4	6,9		
Tl		0,3								0,1	< .1	0,4	0,2	0,2	0,1	0,2	0,4	0,1	0,3		
U		2,8								1,8	2,8	0,5	1,1	2	0,1	1,6	0,6	0,9	2,6		
Zr		209,8								199,8	229,5	40,2	280,8	175,7	144,4	154	134,4	175,2	226,2		
La		59								52,1	53,9	8,1	81,2	50,7	33,9	61,5	40,3	37	68,8		
Ce		100,7								88,3	89,5	17,4	162,5	109,5	75,5	117,1	85,4	74,6	117,3		
Pr		10,55								9,2	9,68	2,28	18,98	14	9,37	13,69	10,88	8,64	12,26		
Nd		45,5								38,8	36,2	11	82,8	65,2	42,7	59,6	50,1	40,9	49		
Sm		7,2								6,2	6,2	2,1	13,2	11,1	7,9	11,1	9,5	8	8		
Eu		2,29								2,03	2,07	0,78	3,58	3,26	2,7	3,69	3,08	2,68	2,69		
Gd		6,62								5,78	5,74	1,86	10,22	8,05	8,03	10,63	9,52	8,03	7,98		
Tb		0,95								0,87	0,81	0,26	1,21	1,07	1,06	1,34	1,27	1,12	1,06		
Dy		5,19								4,66	5,08	1,37	5,73	5,54	5,56	7,23	6,72	6,1	6,09		
Ho		0,95								0,86	0,9	0,21	0,89	0,97	0,99	1,25	1,2	1,05	1,07		
Er		2,47								2,32	2,55	0,59	2,15	2,58	2,55	3,26	2,92	2,92	2,88		
Tm		0,36								0,35	0,39	0,09	0,26	0,35	0,34	0,46	0,38	0,35	0,36		
Yb		2,23								2,13	2,29	0,48	1,6	2,01	2,22	2,45	2,34	2	2,29		
Lu		0,32								0,3	0,34	0,06	0,22	0,3	0,31	0,35	0,34	0,31	0,37		
Pb		2								3	4	< 2	< 2	3	< 2	< 2	< 2	< 2	3		

For Review Only

			T°C		P(kbar)	
			min	max	min	max
Host rocks	B I		1217	1231	9,5	10,0
	B II	<i>Cpx-whole rock</i>	1130	1242	10,0	15,4
	B III		1149	1227	9,5	14,3
Enclaves	Bomb in M3 (BII)	<i>Cpx-coexisting glass</i>	1174	1260	13,0	19,5
	Wehrlite (BII)	<i>Cpx-coexisting glass</i>	1138	1200	14,2	18,8
	Hornblendite (BII)	<i>Cpx-whole rock</i>	1259	1329	11,6	18,3
	Phlogopite clinopyroxenite (BIII)	<i>Cpx-whole rock</i>	1314	1324	14,1	15,5
	Clinopyroxenite hornblendite (BII)	<i>Cpx-coexisting glass</i>	1148	1199	25,2	27,6
	Clinopyroxenite hornblendite (BII)	<i>Cpx-whole rock</i>	1221	1266	12,1	13,4
	Clinopyroxenite hornblendite (BII)	<i>Cpx-coexisting glass</i>	1134	1206	14,4	21,4
	Hornblende gabbro (BIII)	<i>Cpx-whole rock</i>	1208	1220	11,1	12,8
	Hornblende gabbro (BIII)	<i>Cpx-coexisting glass</i>	1026	1034	14,2	15,7

